EXPERIMENTAL STUDY OF PHASE RELATIONSHIPS IN PART OF THE SYSTEM Mg-Fe-Ca-Ti-Si-O AT 1300°C, 1atm, AND VARIOUS OXYGEN FUGACITIES, WITH APPLICATIONS TO REDOX PARTIAL MELTING

PING SHI

Ph.D.

University of Edinburgh

1989

To my parents and homeland

ACKNOWLEDGEMENT

This work was carried out during the tenure of a Huo Yingdong studentship from Hongkong, and a TC award from the British Council. I thank the Edinburgh Grant Institute of Geology for providing facilities and expertise.

I am particularly grateful to Dr. Ben Harte, for his influence on the interest of mantle processes, especially the redox state of the mantle and redox reaction in kimberlite magmatism. His encouragement on applying the experimental results to kimberlites, have prompted further elaboration on data interpretation; and his thorough proof reading and criticism have helped greatly with the improvement of the final manuscript.

Dr. Gordon M. Biggar is also specially thanked for his patience in instructing experimental techniques and repairing equipment that I damaged (not on purpose!). He is also thanked for careful and speedy proof reading.

Ben, Gordon and Dr. Roy Gill (my combined supervisors) are also thanked for their help in preparing lectures.

I must admit that working with the Edinburgh microprobe unit in the institute is a great pleasure. I certainly should not forget the guidance and help from Drs. Peter Hill, Douglas Russell, John Craven and Stuart Kearns. With characteristic understatement they would describe their readiness to take any trouble at any time is "almost admirable".

Thanks to many of my fellow postgrads, whose friendship has been an important psychological support for my prolonged stay in the UK. I am indebted to many people for their help with English, especially, Dr. Mark Welch, and Stuart Kearns.

ABSTRACT

Phase relationships in part of the system Mg-Fe-Ca-Ti-Si-O were experimentally determined at 1 atmosphere and 1300°C. The effects of change in oxygen fugacity on the compositions of coexisting phases in assemblages of IL+USP+LQ, and IL+USP+OL+LQ in the system Mg-Fe-Ti-Si-O, and assemblages of IL+USP+OL+LQ and IL+USP+OL+PEROV+LQ in the system Mg-Fe-Ca-Ti-Si-O were systematically characterized. Amongst the above assemblages, the assemblage IL+USP+OL+LQ in the system Mg-Fe-Ti-Si-O and IL+USP+OL+PEROV+LQ in Mg-Fe-Ca-Ti-Si-O are invariant at fixed P, T and oxygen fugacity, and therefore, the mineral and liquid compositions are fixed. At a given P and T, the composition of each phase as a function of oxygen fugacity has been determined. For example, in the system Mg-Fe-Ti-Si-O, for a change of log fO_2 from -10.0 to -5.3, olivine changes from FO_{62} to FO_{78}, and ilmenite from $IL_{73}GK_{27}$ to $IL_{50}GK_{23}HM_{27}$ (ilmenite-geikielite-haematite).

Using the geothermometer of O'Neill and Wall (1988), with Mg-Fe^{2+} partitioning data between OL and USP as input, the expected equilibrium temperatures were calculated. The calculated results show reasonable agreement with the experimentally controlled temperature. However, the calculated temperature from the geothermometer of Andersen and Lindsley (1981) for OL+IL pairs show significant deviations from the experimentally controlled temperature for ferric rich compositions. Thus, a serious recalibration of this geothermometer may be needed.

Given the experimentally determined compositional information, it is possible to calculate the effects of oxygen fugacity on the melting of bulk compositions analogous to natural peridotites. With known phase compositions and a specific bulk composition (selected to satisfy the invariant assemblage, and to be analogous to peridotite), mass-balance calculations have been performed, and the relative quantities of the constituent phases (expressed as the sum of mole% of oxides) calculated as functions of oxygen fugacity at constant P and T.

The degree of partial melting is strongly influenced by the redox state. For example, in the assemblage IL+USP+OL+LQ in the system Mg-Fe-Ti-Si-O, for an olivine rich bulk composition, a variation of up to 32% partial melting occurs. The maximum degree of partial melting leading to the most "infertile" solid residue occurs at about 0.5 log fO_2 unit above NNO. The maximum melt productivity for unit increase in log fO_2 exists at about 0.5 log fO_2 unit below NNO, ie. near QFM. In fact up to 63% of the melt possibly generated by oxidation is produced within ± 1 log fO_2 unit of QFM.

The coincidence of the oxygen fugacity value (near QFM) of the maximum melt productivity with those of the most voluminous basalts on the ocean floor and continents suggests that redox state has an important control over basic melt production. Hence, the typical oxygen fugacity of tholeiites is not merely a function of mantle redox state, but is a product of redox control over the conditions of melt formation and extraction. The importance of redox control on melting deep in the mantle is further supported by the evidence of olivine and ilmenite macrocrysts and phenocrysts in kimberlites and melilitites. These show marked compositional variations indicative of different redox states, which might result from redox melting of more reduced and oxidized (subducted) mantle components. In the generation of island arc magmas in subduction zones, the conjunction of highly oxidized subducted oceanic crust with normal mantle is expected to have a major effect on the progress of melt production and its variation with time. Thus, subduction related redox reaction and partial melting is possibly a major mechanism and control for magma generation during tectonic cycles.

TABLE OF CONTENTS

LIST OF FIGURES

LIST OF TABLES

CHAPTER 1

INTRODUCTION

1.1. About redox melting

Oxygen fugacity has been understood to play an important role in crystal fractionation, eg. the apparent iron enrichment and silica enrichment in evolution of different basaltic magmas. The importance of oxygen fugacity during partial melting, however, has only recently been recognized during the debate over the oxidation state of the earth's upper mantle.

Two effects of the changing oxidation states can be rationalized. Firstly, the redox state controls, or is controlled by, the composition of any volatile phase in the C-O-H system which is believed to exist in the upper mantle; and the composition of the coexisting volatile phase affects the volatile-induced partial melting (eg. Yoder and Tilley 1962; Wyllie, 1978, 1979; Taylor and Green, 1988). Secondly, the redox state controls, or is controlled by, the Fe^{3+}/Fe^{2+} ratio of any given source rock. If we accept that partial melting is due to particular changes in P,T and X_i, changes in Fe^{3+}/Fe^{2+} ratio should not be neglected in the search for the relevant melting mechanisms. At least, the relative abundance of iron, which is one of the most important major components in the mantle peridotite and subducted oceanic crust (if recycling is considered) is better known, and in the situation that there has not been a reliable estimation about the absolute abundance of C-O-H species, it is possible that the control of the Fe^{3+}/Fe^{2+} ratio on partial melting is of no less importance than that of gas species.

In their experiments, Taylor and Green (1988) demonstrated that, at relatively reducing conditions, the initial melting of a `fertile peridotite` `saturated with $H_2O$-$CH_4$ dominated fluids` occurred `at temperatures well above stable continental geotherm, even under quite $H_2O$ rich conditions`. Although their result does not

conclude that a H_2O-CO_2 dominated fluid phase decreases the solidus of a fertile peridotite well below the continental geotherm, it does suggest that a more oxidizing condition is a possible solution (redox melting). Even if it is true, the whole picture is still blurred by the fact that increase in oxygen fugacity is accompanied by the simultaneous increase in both the CO_2 and H_2O in the fluid phase and the Fe^{3+}/Fe^{2+} ratio in the source rock. Therefore, redox melting involves both the redox-volatile induced melting and the redox-transition-metal induced melting, and the two mechanisms should be distinguished. Unfortunately, there has been a tendency to attribute more credit to the role of the volatiles, despite the successful interpretation of the effect of Fe^{3+}/Fe^{2+} ratio (oxygen fugacity) on the relationship of silicates-oxides-liquid during crystal fractionation.

The role of Fe^{3+}/Fe^{2+} ratio on partial melting is not less comprehensible than that of volatiles, and can be illustrated with the simple system FeO-Fe_2O_3-SiO_2 (Osborn and Muan, 1960) (***Fig. 1.1***). The fayalite-magnetite cotectic in this system represents a thermal trough, and, the liquidus of the system is sensitive to oxygen fugacity, hence, the possibility of redox-transition-metal induced partial melting exists. A detailed explanation of the melting processes in the system FeO-Fe_2O_3-SiO_2 is illustrated in ***Fig. 1.2*** with a composition of fixed Si/Fe ratio along the line ABCD at a temperature of about 1170^0C. In principle, such a redox melting mechanism should be applicable to natural rock system: Therefore, the effects of change in redox state on partial melting are important no matter whether there is or is not a volatile phase present in the magma source region.

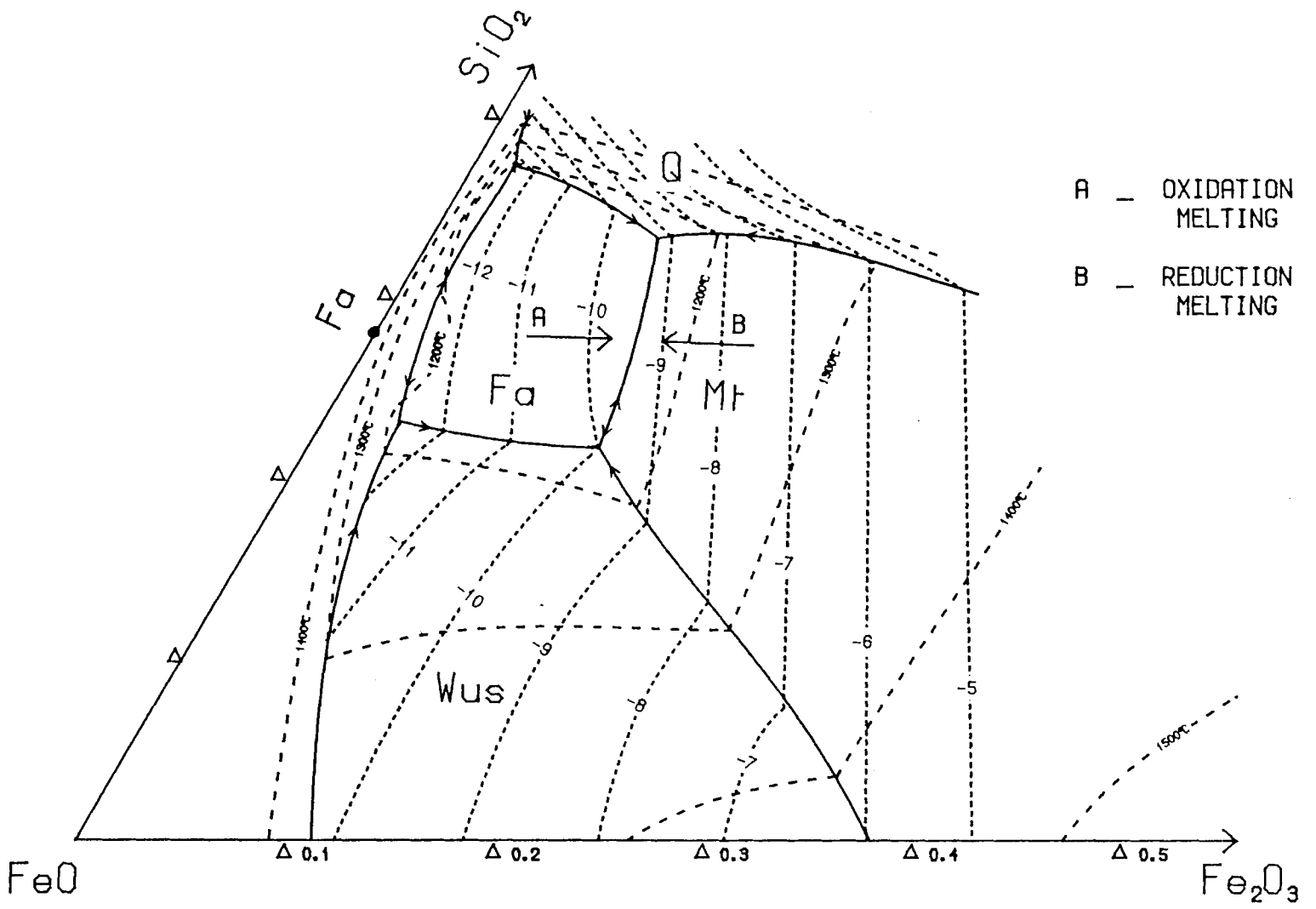

Fig. 1.1 *liquidus of the system* FeO-Fe_2O_3-SiO_2 *(modified from Osborn and Muan, 1960). Components in wt%. Dotted lines, oxygen isobars (in* $logfO_2$*). Dashed lines, isotherms. Arrows A and B represent the direction of change in* Fe^{3+}/Fe^{2+} *ratio. Change of oxygen fugacity results in change in bulk composition along A-B. The fayalite-magnetite cotectic represents a thermal trough which locates the lowest liquidus temperature along A-B.*

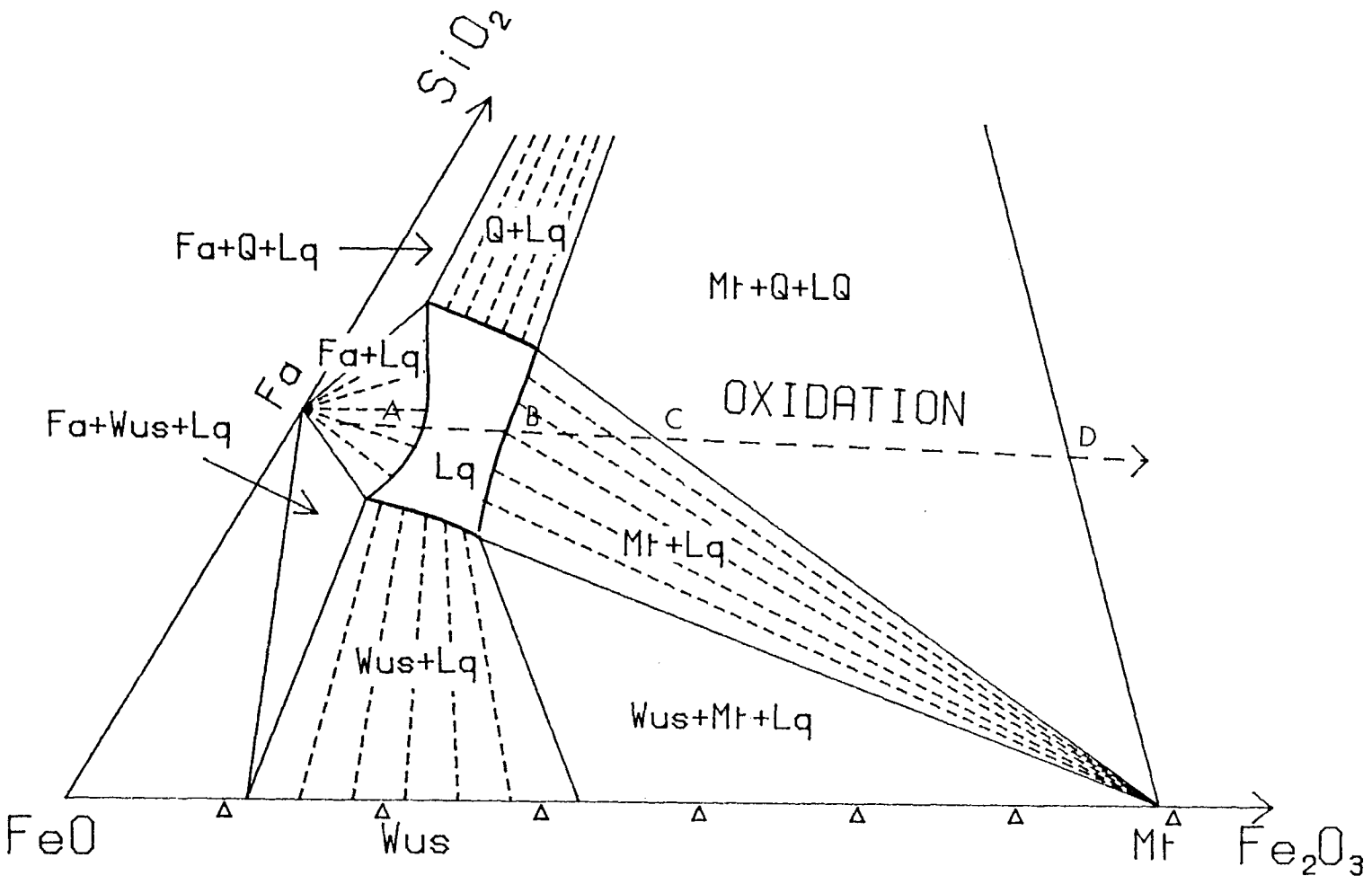

Fig. 1.2 *Schematic isothermal section (derived from Osborn and Muan, 1960) at about 1170°C. Line ABCD represents the effect of increasing oxygen content on bulk composition with fixed Fe/Si atomic ratio. With increasing oxygen content (fO_2), fayalite in the fayalite+liquid assemblage dissolves till it vanishes, and the bulk composition moves in to the one phase assemblage (liquid). With further increase in oxygen content (fO_2), the bulk composition enters the magnetite+liquid stability field, and magnetite precipitates. As more oxygen is added to the system, the bulk composition moves into the magnetite+tridymite+liquid three phase stability field, and the fO_2 is buffered. Introducing oxygen to this buffering assemblage causes increase in magnetite and tridymite at the expense of the liquid, and eventually drives the bulk composition into the subsolidus. Therefore, with the bulk composition represented by the line ABCD, increasing oxygen content, for portion A, results in melting, whilst proceeding through B, C and D results in progressive increase in solid and loss of melt.*

There has been general consensus that the initial redox characteristics of the earth's mantle was reduced, analogous to that of the Moon (Arculus and Delano 1987). Although there has been no conclusive agreement on the present oxidation state of the Earth's upper mantle (Arculus 1985; Arculus and Delano 1987; Chrislie, *et al.*, 1986; Haggerty and Tompkins 1983; Mattioli and Wood 1987; O'Neill and Wall 1987; Ulmer, *et al.*, 1987), `There does seem to be limited data suggestive of a secular trend towards oxidation of the upper mantle, especially in the subcontinental lithospheric portion (Arculus and Delano 1987).` If the relatively reduced primary mantle is subsequently subject to oxidation, either through differential degassing or introduction of subducted highly oxidized oceanic crust, more melt may be generated. On the contrary, relatively oxidized material such as oceanic crust may yield more melt during subduction if reduction occurs. In fact, redox reactions can never happen independently, and the redox reaction associated with the subducted oceanic crust is possibly an important mechanism for magmatic activity during tectonic cycles.

Such a mechanism may not be completely restricted to arc or active continental margin volcanism. The possible progressive oxidation of the mantle wedge underlying a volcanic arc or active continental margin may result in the prevention of further reduction of the highly oxidized oceanic crust, thus, enabling the oxidized material to be transported deeper into mantle region. Therefore, some deep source volcanism may also be subduction related.

In this study, systems of Mg-Fe-Ti-Si-O and Mg-Fe-Ca-Ti-Si-O were chosen as simplified analogues to basic-ultrabasic natural rock systems. Phase relationships were partially determined at 1300°C with various controlled oxygen fugacities, and key assemblages, such as the assemblage USP+IL+OL+LQ in the Ca-free system, were carefully monitored. Due to its invariant character at fixed P (1atm), T (1300°) and oxygen fugacity, this assemblage is ideal for study of effects of oxygen fugacity on phase compositions without involving experimental problems associated with a small degree of partial melting. The acquired compositional data of the coexisting phases can

then be used to calculate particular bulk compositions of the selected systems analogous to that of natural rock, and the relative quantity of each phase in them. The results shed light on the understanding of the effects of oxygen fugacity on the chemical reactions involved in partial melting and residue depletion in a relevant oxide bearing system. Although all the experiments were carried out at 1 atm, the general oxide-silicate-melt relationships are thought to be applicable to high pressure conditions.

1.2. Previous work

Due to the low solubility of Si in the Ti-bearing ore minerals , many researchers have treated the Ti-bearing oxides as a subsystem for convenience. Research on these separated subsystems has revealed beneficial results on the understanding in relationships amongst oxide minerals. After the pioneering work of Lindsley (1963) and Buddington and Lindsley (1964) on the geothermometry and oxygen barometry in the system Fe-Ti-O, considerable effort was added to determine the magnesium influence on this system (Speidel, 1970; Woermann *et al.*, 1969a, 1969b). In a study of the relationship of these Ti-bearing oxides with silicates, Speidel (1964), Woermann and Lamprecht (1970) added SiO_2 into the system Fe-Mg-Ti-O and characterized the subsolidus phase relations. With the interest of geothermometry, some researchers performed Mg-Fe partitioning experiments between oxides and silicates, dominantly under the subsolidus conditions (Andersen and Lindsley, 1979; Bishop, 1980; Rowson and Irvine, 1980).

In early studies on the effect of oxygen fugacity on basaltic and andesitic magmatism, most synthetic experiments were carried out within a simplified system of Fe-Mg-Ca-Si-Al-O (eg. Osborn, 1959; Presnall, 1966; Roeder and Osborn, 1966). These studies together with those on natural rock system (eg. Kennedy, 1955; Hamilton *et al.*, 1964) were reviewed by Hamilton and Anderson (1967). Although these early works combined with more recent studies (Biggar, 1974; Hill and Roeder, 1974; Thompson,

1975) helped understanding of the role of oxygen fugacity during the crystallization of an iron-bearing silicate melt, little has been done on the effect of oxygen fugacity on partial melting; probably due to the emphasis on the effects of temperature and pressure perturbations on melt production, as well as difficulties of oxygen fugacity control at high pressure.

Recent research on partial melting at either `dry` or fluid-bearing conditions is extensive, and the literature concerning melting studies is abundant (eg. Basaltic volcanism study project, 1981, Scarfe and Brearley, 1987; Wyllie, 1987). Most of these studies emphasize pressure, temperature and H_2O-CO_2 dominant fluids as the dominant factors in partial melting processes; and oxygen fugacity is regarded as an important intensive variable only from the viewpoint of its influence on fluid phase compositions (eg. $H_2O/CO_2/CH_4$ ratio) (Foley, 1988; Taylor and Green, 1988; Wyllie, 1987).

1.3. General experimental problems

Melting experiments of iron-bearing systems encounter several general problems which affect the quality of experimental results.

BULK COMPOSITION CONTROL: This problem is not only the oxygen content control, but also, probably equally severe, the iron content control. Platinum, palladium, rhodium and their alloys are notorious for alloying the iron (eg. Nehru and Wyllie, 1975; Biggar, 1977; Johannes and Bode, 1978). Application of other capsule material is restricted by the required wide range of oxygen fugacities of interest. Loss of volatile components from the sample also affects the validity of the experimental results. These losses, of iron and volatile components, can result in the time dependent character of the performed experiment, and produce non-equilibrium assemblages (Jaques and Green, 1979). The role of oxygen fugacity on partial melting can be obscured or distorted by the lack of bulk composition control.

OXYGEN FUGACITY BUFFERING AT HIGH PRESSURE: Melting of peridotitic

or analogous synthetic material requires high temperatures due to their refractory character. Such high temperatures will be well above the solidus of some standard solid oxygen buffers (eg. QMF, IWF). In addition, the rapid diffusion of hydrogen through noble metal capsules results in such a fast consumption of the buffer assemblages that a large quantity of buffering material is demanded for a reasonable long duration, and this may exceed the capacity of an ordinary high pressure solid medium piston cylinder apparatus. Furthermore, a detailed study of the effect of oxygen fugacity on partial melting may require detailed control of oxygen fugacity beyond the limits of the available calibrated solid buffers. All these deficiencies in experimental technique have hampered oxygen buffering at high pressure.

CHEMICAL ANALYSIS OF SMALL DEGREE OF PARTIAL MELTING: Since in the natural system the component number is always greater than that of coexisting phases (solid solution effect), even the initial melting is not virtually eutectic,(ie. the composition of the melt varies with the degree of partial melting even with small amounts of melting); indeed the dependence of melt composition on degree of melting is animportant matter for study. Unfortunately, the initial melt of small quantity is often subject to modification during quenching of experiments, because it occurs as films along grain boundaries and as pockets at grain junctions and frequently form thin quench overgrowths around solid phases. Glasses with these inhomogeneous textures will render imprecise any chemical analysis aimed at determining liquid composition; therefore, higher degrees of partial melting are almost a prerequisite for obtaining analytical data of reasonable quality in any study involving melt compositions.

PRECISE ESTIMATES OF THE AMOUNT OF MELT: Due to the poor control of bulk composition during experiments, the bulk composition of the products should be regarded as unknown. Although the detailed composition data of each phase can be easily acquired with precision by electron micro-probe analysis (provided the degree of partial melting is large enough), the direct determination of the relative quantities of each phase remains difficult. These data are critical for detailed evaluation of the

melting mechanism. Modal counting of experimental charges is regarded as inadequate for these detailed characterizations.

1.4. Aims of this study

Aims of this study are fourfold

- Conduct melting experiments with controlled oxygen fugacity to determine the general phase relationships in part of the system Fe-Mg-Si-Ti-O-Ca with special emphasis on assemblages containing ilmenite, ulvospinel, olivine or pyroxene and liquid (melt).

- Chose particular assemblages, analogous to natural ones, for detailed compositional characterization under various oxygen conditions.

- Analyse the acquired experimental compositional data for formulating the melting processes and involved chemical reactions, with emphasis on mechanisms which control the degree of partial melting and residue depletion.

- Apply the understanding from analogous experimental systems to natural systems of special interest from the viewpoints of redox reaction and magmatism.

1.5. Approach adopted

With special consideration to the effect of oxygen fugacity on partial melting and bearing in mind the problems mentioned in 1.3, a particular experimental approach was adopted in this study.

1. Operating at 1 atmospheric pressure. With the requirement of a large range of reliable oxygen fugacity control and relatively high running temperatures, it was decided to carry out the experiments at 1 atm with mixed gas as oxygen buffer. The gas mixing buffering technique enables a reliable oxygen partial pressure control across all values from above NNO, representative of that of arc volcanism, to near IW, the lowest limit of the Earth's mantle.

2. Using synthetic system. Although rock samples yield a closer approximation of natural systems, experiments on the synthetic systems can give a clearer image of the operating principles behind the apparent overall complexity. With fewer components, the experimenter can produce lower variance assemblages which will allow greater control over the experiments. With carefully chosen systems, some unnecessary complexity can be avoided (eg. volatile loss).

3. Using invariant assemblages (at fixed P, T, fO2). The invariant character of these assemblages means that the composition of coexisting phases are independent of both the amount of melt present and the small variation in bulk compositions (buffering effect). Because of the fewer number of coexisting phases than that of components (solid solution effect), which is characteristic of natural rock system, the decision to use invariant assemblages to investigate the effect of oxygen fugacity on partial melting confines the melting experiments to be carried out in simplified synthetic systems. The relative independence from bulk composition in the phase composition allows greater freedom in the subsequent manipulation of the acquired data, and such manipulation is essential for generating geologically pertinent information.

CHAPTER 2

EXPERIMENTAL PROCEDURE AND GENERAL PHASE RELATIONSHIP

2.1. Experimental technique

To satisfy the requirement of reliable control and gradual variation of oxygen fugacity over a large range of fugacities, the experiments had to be carried out in conventional vertical gas flow quenching furnaces at a pressure of one atmosphere. Oxygen fugacity was buffered by gas mixtures of H_2 and CO_2 (Deines *et al.*, 1974) and their ratio was monitored by a Katharometer which was calibrated against NNO and QFM to within ± 0.1 log fO_2 unit. Although there was not an attempt to calibrate the Katharometer at oxygen fugacities other than NNO and QFM or cross-check the oxygen fugacities by other means (such as an oxygen sensor), the extrapolation to the range outside calibration was thought to be valid (at least in the relative sense), and the extrapolation towards higher H_2 concentration (H_2/CO_2 ratio closer to 1) possibly resulted in smaller error.

The temperature profile was determined by step movements of a $Pt_{87}Rh_{13}$ thermocouple through the furnace tube at relevant temperature with appropriate gas flow rate. This located the hot spot range (about 3cm) which was found to have a thermal gradient less then 2.5°C. The thermocouple ($Pt_{87}Rh_{13}$) was calibrated against lithium metasilicate (Biggar, 1972) to within ± 2°C .

Mixtures of ferric iron oxide (analytical grade) and the compositions SiO_2, TiO_2, $CaSiO_3$ (prepared by gelling technique, Biggar, per. comm.) were used as starting materials. They were weighed in different proportions, mixed together, and finely ground by hand.

Due to the high operating temperature, charges were suspended on platinum wire hooks and hung in a platinum basket which was placed at the hot spot of the furnace for various durations. The charges were eventually drop-quenched in water. The iron

loss problem is believed to have been minimized by this technique. In some cases, the platinum hook was deliberately pressed to thin foil in order to facilitate the rate of iron absorption and achieve equilibrium with the charge. The concentration of the absorbed iron in the alloy was potentially an indicator of iron activity in the charge.

2.2. Attainment of equilibrium

It was expected that, in most of the experiments performed, there was no serious kinetic problem for reaching equilibrium, due to the relatively high operating temperature and supersolidus reactions. The coexisting liquid phase in all the experiments may be regarded as a flux, and liquid-solid reactions were the most dominant. The existence of a flux in the charge is believed to have considerably enhanced the rate of reaction and facilitated the attainment of equilibrium.

Due to the multiphase assemblage character of this study, reversed experiments, though desirable, would need so much effort that it was deemed to be beyond the scope of this project. However, one known sluggish process, iron diffusion into platinum foil was tested with reversal experiments.

Generally, the attainment of equilibrium was tested in the following ways:

- PHASE RULE: Gibbs' phase rule places a limit on the number of phases which may be present in a system of given complexity.

- HOMOGENEITY OF EACH SOLID PHASE:was checked. Due to the quench modification of glass, such a criterion is not applicable to glass.

- PHASE COMPOSITION OF AN INVARIANT ASSEMBLAGE: These compositions should not be bulk composition dependent.

- TEXTURE FEATURES: Coarse and facetted crystals indicate the free growth of crystals in melt, and combined with the chemical analysis to check homogeneity, this method indicates the lack of disequilibrium characteristics.

It was proved that five day duration is sufficient for iron diffusion into platinum foil (20 micron) to attain equilibrium. And it is believed that 24hr duration is enough for silicate-oxides-melt to reach equilibrium. A comparison of experimental results of an invariant assemblage at 1300°C, 1atm, and log fO_2=-7.0, with different durations is given in ***Fig. 2.1***.

2.3. Analytical technique

All the quenched charges were polished, and firstly, examined with optical microscopy, and then analysed on a Cameca electron microprobe, with 30s integration time. Synthetic periclase (for Mg), metallic iron (for Fe), natural olivine (for Mg), rutile (for Ti), and wollastonite (for Si, Ca) were used as standards (natural material are from Royal Scottish Museum). The accelerating potential was 20KV, beam current 20nA. ZAF corrections were carried out by using the procedure of Colby (1971).

Ferric contents of the oxide phases were calculated with assumed stoichiometry. The calculation procedures for ilmenite, ulvospinel and pseudobrookite are listed in Appendix I.

2.4. General phase relationships

Phases concerned in this study and their abbreviations are listed below.

Ilmenite	IL	$FeTiO_3$-$MgTiO_3$-Fe_2O_3
Ulvospinel	USP	Fe_2TiO_4-Mg_2TiO_4-Fe_3O_4-$MgFe_2O_4$
Olivine	OL	Fe_2SiO_4-Mg_2SiO_4
Orthopyroxene	PX	$FeSiO_3$-$MgSiO_3$
Pseudobrookite	PSB	$FeTi_2O_5$-$MgTi_2O_5$-Fe_2TiO_5
Perovskite	PEROV	$CaTiO_3$
Tridymite	TRI	SiO_2
Liquid	LQ	

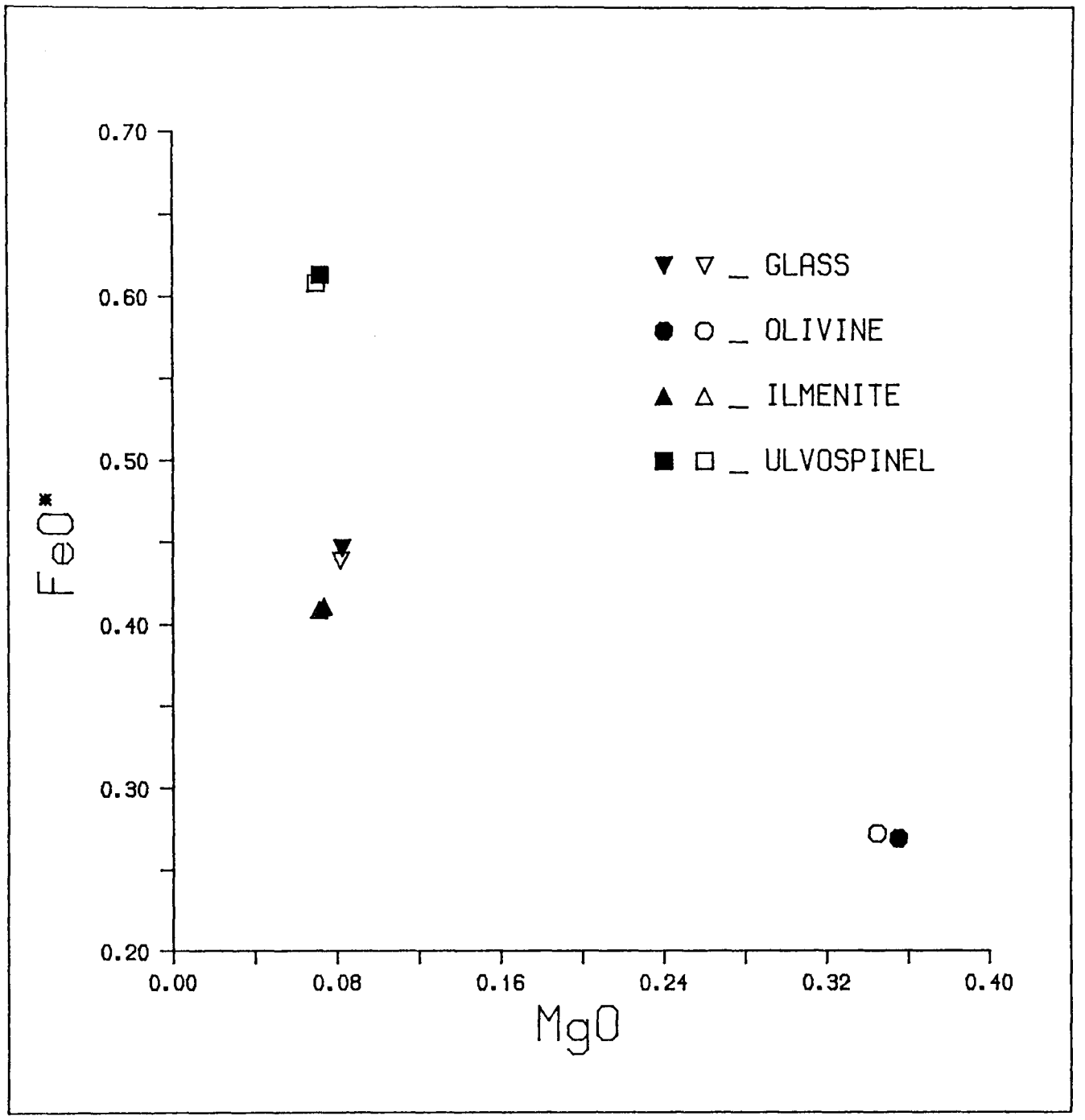

Fig. 2.1 *A comparison of experimental results for runs with different durations. Solid symbol, 5 days duration. Open symbol 24hr duration. The assemblage is Il+Usp+Ol+Lq in the system Mg-Fe-Ti-Si-O. The small difference between the two experiments suggests that 24hr is sufficient for the coexisting silicate-oxides-melt to reach equilibrium.*

2.4.1. System Fe-Mg-Si-Ti-O

Due to the extensive solid solution effect (Fe,Mg), the number of coexisting phases seldom reaches the number of components at 1300°C and 1 atm, with geologically relevant oxygen fugacity. It will be demonstrated later that the solid solution effect of Fe^{3+}-rich end members into the rhombohedral phase and cubic phase results in the similar ineffectiveness of change in fO_2 on the overall phase assemblages.

In order to quickly determine the overall features of the system, a number of experiments were carried out for synthesizing low variance assemblages.

Although in theory the Fe-Mg-Si-Ti-O five component system can produce a maximum of 7 phases in an assemblage, such an assemblage is unlikely to be stable at an arbitrarily chosen temperature pressure and oxygen fugacity (eg. 1300°C, 1atm, 10^{-9}). Actually, because of the extensive solid solution effect in the phases concerned, any assemblage with phase number greater than 4 is unlikely to be formed at a single arbitrary set of conditions. Therefore, determination of the composition relations of 4-phase assemblages was chosen as the first objective to be pursued in the system Fe-Mg-Si-Ti-O. At given but arbitrary values of T, P and fO_2, such 4-phase assemblages are invariant.

Four 4-phase assemblages were synthesized, (1) IL+USP+OL+LQ, (2) IL+PSB+OL+LQ, (3) PSB+OL+PX+LQ, (4) PSB+PX+TRI+LQ. Because these assemblages are invariant at fixed P, T, fO_2, the chemical compositions of each phase in the products are independent of the starting compositions. Probe analyses of the products are listed in **Tables 2.1, 2.2, 2.3** and **4.2**. Although the data listed here were derived from experiments at log fO_2 of -9.0, the above four invariant assemblages are stable over a wide range of oxygen fugacities. With the compositional control given by these 4-phase assemblages, the general phase relationship in the system Fe-Mg-Si-Ti-O can be reasonably envisaged (***Fig. 2.2***)

TABLE 2.1 ELECTRON MICROPROBE ANALYSES OF PHASES IN INVARIANT ASSEMBLAGE OL+IL+PSB+LQ

	OL	IL	PSB	LQ
MgO	35.2(0.4)	9.4(0.1)	8.3(0.1)	9.3(0.5)
SiO_2	37.6(0.1)	0.0(0.0)	0.1(0.0)	23.6(0.5)
TiO_2	0.7(0.2)	57.0(0.0)	72.7(0.2)	28.6(0.3)
FeO	25.8(0.1)	33.7(0.1)	18.9(0.1)	37.8(0.3)
SUM	99.3	100.1	100.0	99.3
CAT/OXY	3/4	2/3	3/5	--
Mg	1.4047	0.3286	0.4492	------
Si	0.9947	0.0000	0.0036	------
Ti	0.0141	1.0052	1.9849	------
Fe^{2+}	0.5777	0.6609	0.5739	------
SUM	2.9911	1.9946	3.0115	------
#	4	3	2	3

is the number of analyses. OL=Olivine. IL=Ilmenite. PSB=Pseudobrookite. LQ=Glass. Numbers in parentheses are 2 standard deviations.

TABLE 2.2 ELECTRON MICROPROBE ANALYSES OF PHASES IN INVARIANT ASSEMBLAGE OL+PX+PSB+LQ

	OL	PX	PSB	LQ
MgO	39.3(0.3)	29.6(0.2)	9.4(0.2)	11.6(0.6)
SiO_2	38.4(0.3)	54.9(0.2)	0.1(0.0)	31.5(0.6)
TiO_2	0.5(0.2)	1.3(0.1)	74.9(0.3)	25.9(1.0)
FeO	22.4(0.2)	14.4(0.3)	17.1(0.2)	31.0(0.8)
SUM	100.6	100.2	101.5	100.0
CAT/OXY	3/4	4/6	3/5	--
Mg	1.5222	1.5897	0.4935	------
Si	0.9864	1.9535	0.0047	------
Ti	0.0092	0.0351	1.9949	------
Fe^{2+}	0.4866	0.4332	0.5074	------
SUM	3.0044	4.0115	3.0005	------
#	5	6	5	4

is the number of analyses. OL=Olivine. PX=Protoenstitite. PSB=Pseudobrookite. LQ=Glass. Numbers in parentheses are 2 standard deviations.

TABLE 2.3 ELECTRON MICROPROBE ANALYSES OF PHASES IN INVARIANT ASSEMBLAGE TR+PX+PSB+LQ

	TR	PX	PSB	LQ
MgO	0.1(0.1)	29.8(0.2)	9.4(0.1)	11.9(0.2)
SiO_2	96.6(0.3)	54.7(0.1)	0.1(0.0)	35.4(0.5)
TiO_2	1.6(0.2)	1.4(0.1)	73.6(0.1)	23.0(0.4)
FeO	0.3(0.1)	14.0(0.1)	16.4(0.0)	27.3(0.9)
SUM	98.6	99.9	99.5	97.6
CAT/OXY	1/2	4/6	3/5	--
Mg	0.0015	1.6022	0.5054	-----
Si	0.9855	1.9498	0.0036	------
Ti	0.0124	0.0380	1.9964	------
Fe^{2+}	0.0026	0.4223	0.4947	------
SUM	1.0020	4.0123	3.0001	------
#	4	3	2	5

is the number of analyses. TR=Tridymite. PX=Protoenstitite PSB=Pseudobrookite. LQ=Glass. Numbers in the parentheses are 2 standard deviations.

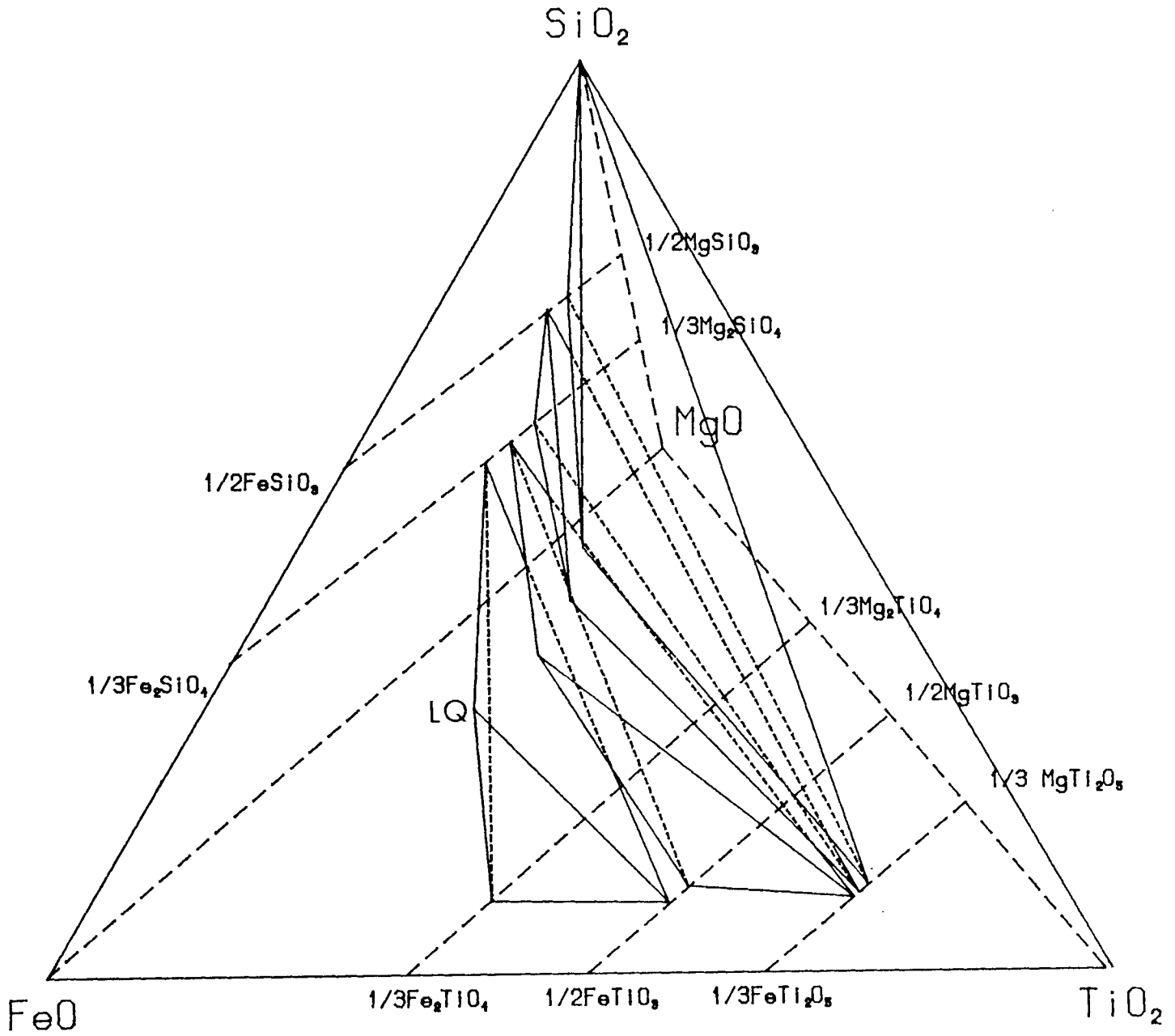

Fig. 2.2 *General phase relationships in the system Mg-Fe-Si-Ti-O at 1300°C, 1atm and log fO_2=-9.0. The assemblage IL+USP+OL+LQ (represented by the left most tetrahedron) is stable at relatively Fe-rich compositions. With increasing contents in silica and titanium, the invariant assemblages IL+PSB+OL+LQ, to PSB+OL+PX+LQ, and to PSB+PX+TRI+LQ are successively encountered. The spaces between the 4 tetrahedra represent higher variance assemblages. With compositions close to the FeO-SiO_2-TiO_2 plane a liquid phase is stable. With increasing MgO, assemblages become subsolidus. No attempt was made to synthesize more extreme assemblages, such as those with wustite or rutile.*

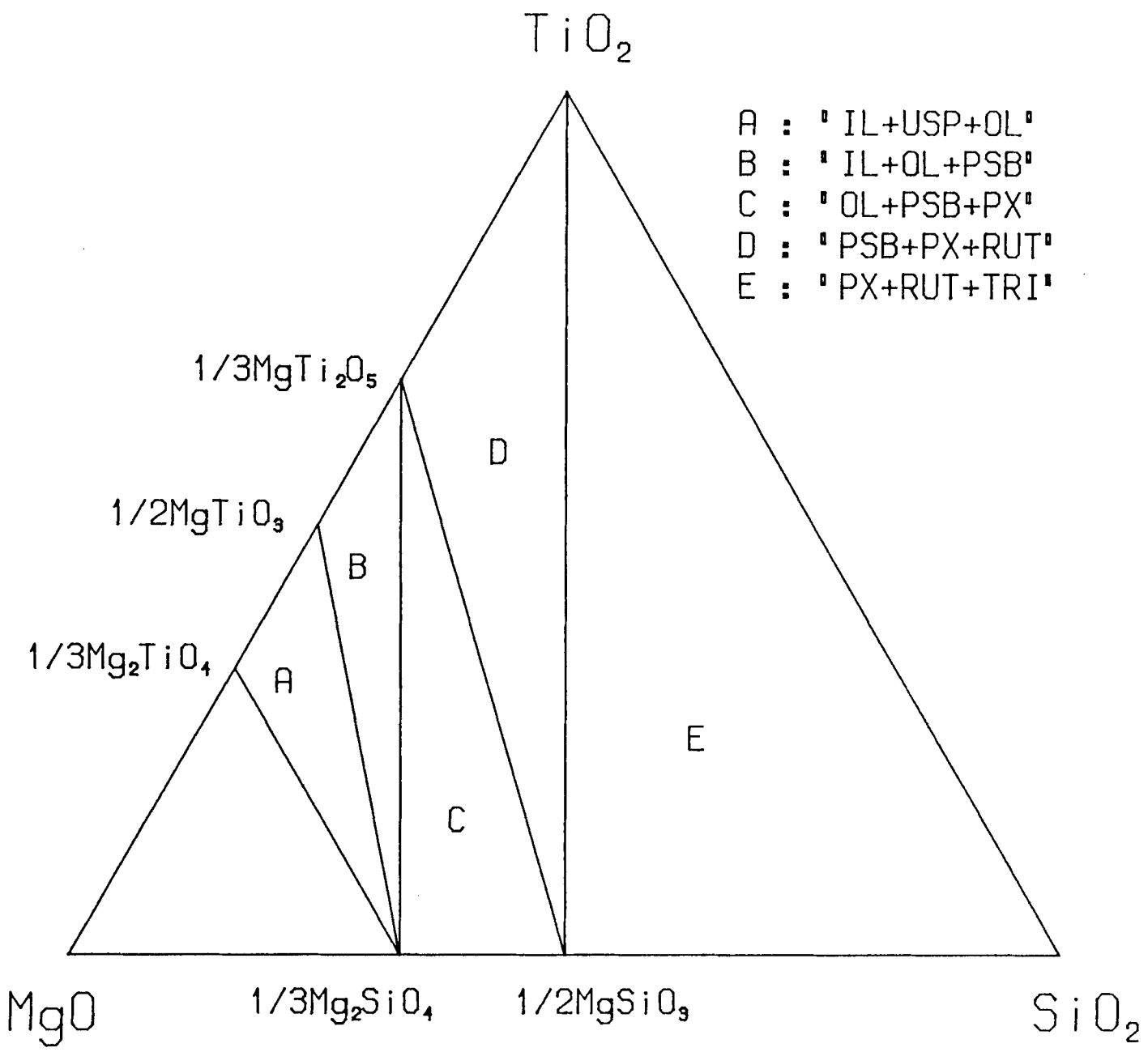

Fig. 2.3 *Solidus phase and subsolidus (above 1480°C and below solidus) phase relationships of the system MgO-SiO_2-TiO_2 (taken from MacGregor, 1969, 1965). The solidus or subsolidus phase relationships for the Si and Ti poor compositions (A, B, and C) are similar to* ***Fig. 2.2*** *OL+PX+IL is not a stable assemblage at temperature above (at least) 1480°C.*

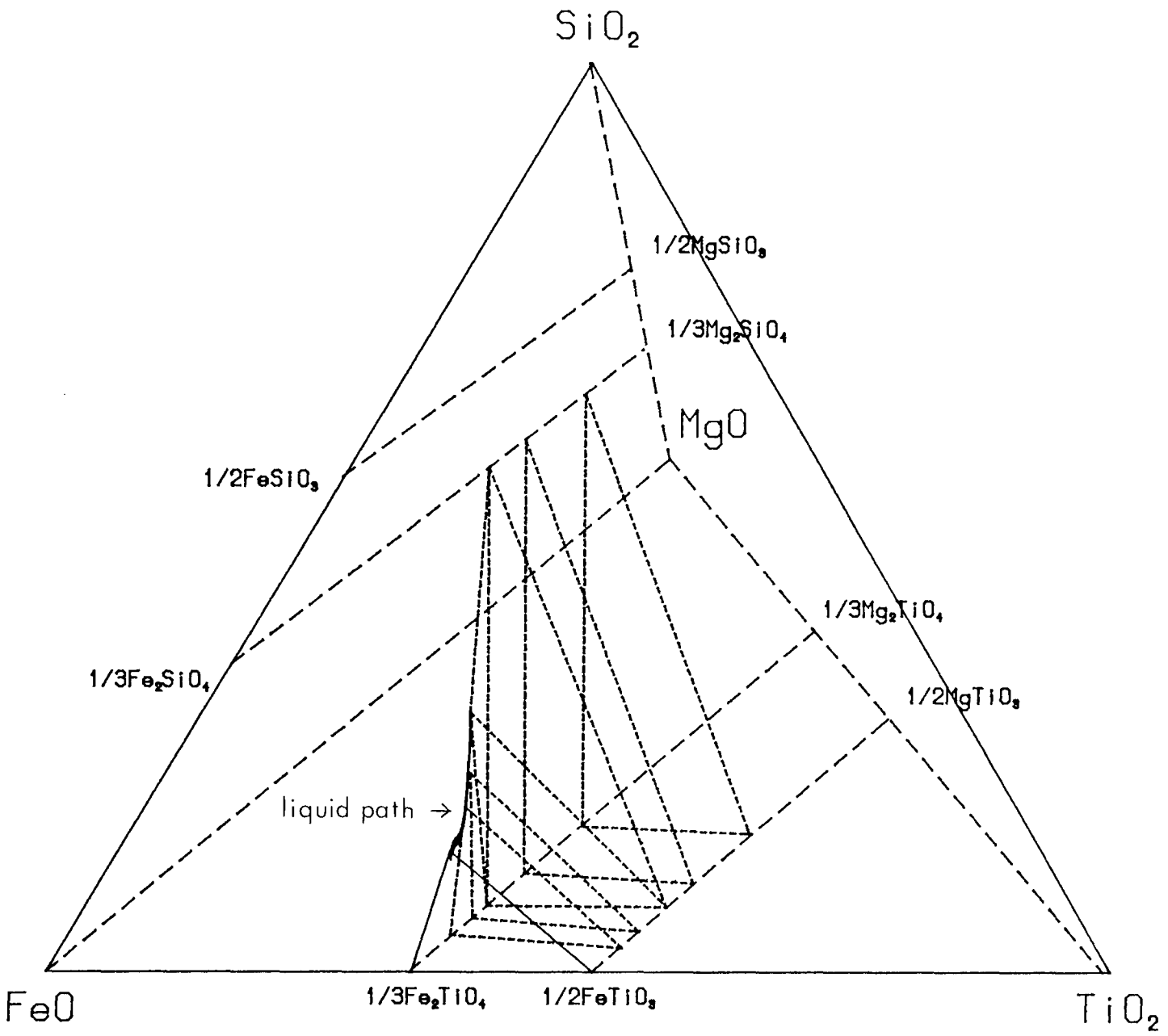

Fig. 2.4 *The assemblage IL+USP+OL+LQ and its closely related higher variance assemblages IL+USP+LQ and IL+USP+OL at 1300°C, 1atm and log fO_2=-9.0. The univariant character of both IL+USP+LQ and IL+USP+OL is represented by the triangular tie lines of the coexisting phases. The invariant feature of the IL+USP+OL+LQ is marked by the indifference to bulk compositions of the phase compositions of the small tetrahedron in between the IL+USP+LQ and IL+USP+OL assemblages. The IL+USP+OL assemblage was actually coexisting with a Ca-bearing liquid (see text); the effect of Ca on the subsolidus relationship is believed to be small, since its content in all the coexisting phases is low. Ferric contents, if there are any, are low, and neglected in the diagram.*

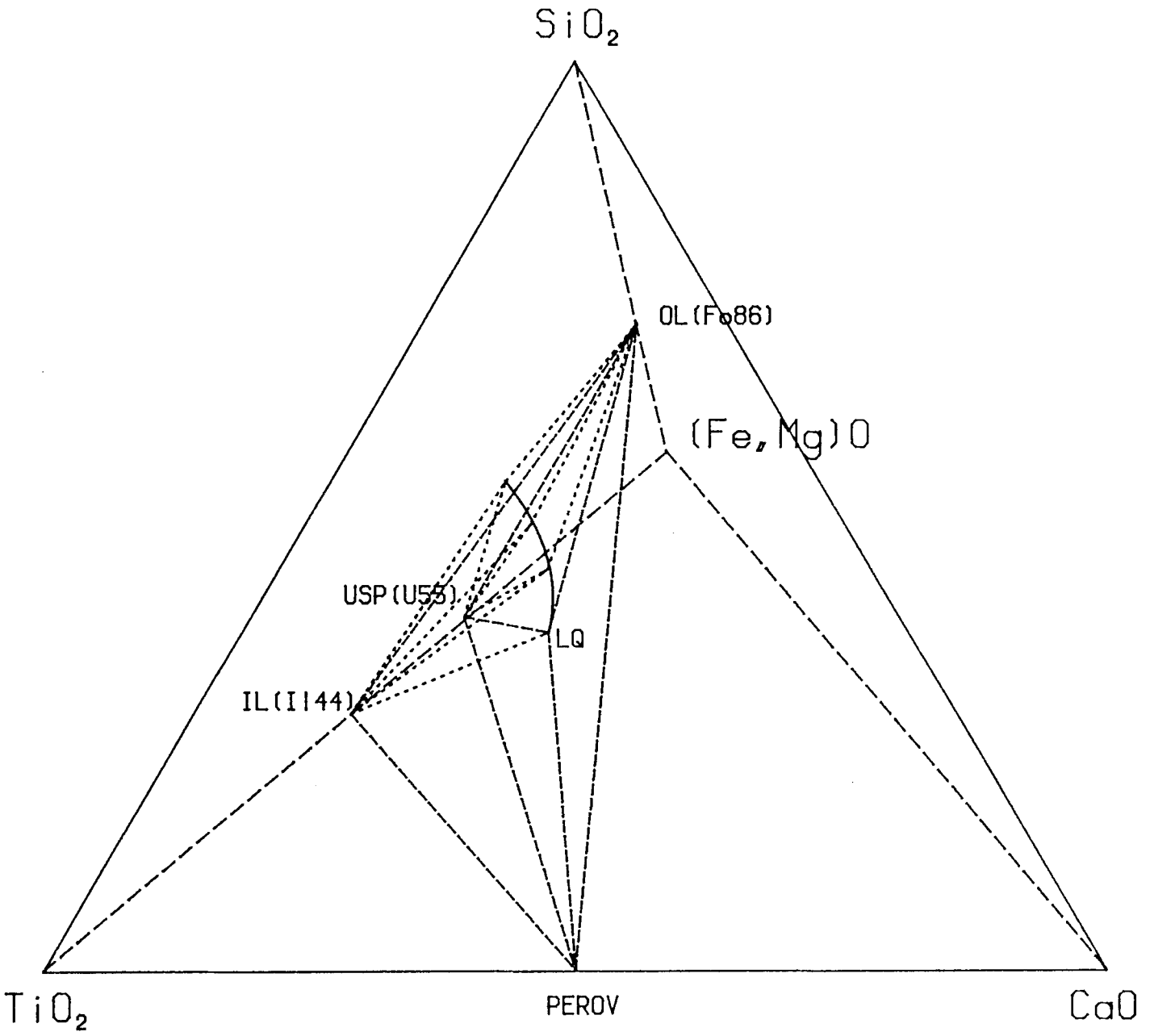

Fig. 2.5 *Transition from invariant assemblage IL+USP+OL+LQ (Ca-free) to invariant assemblage IL+USP+OL+PEROV+LQ (Ca-bearing). The solid line representing the composition change in the coexisting liquid. The dotted lines outlining the ever swollen tetrahedra represent the assemblage IL+USP+OL+LQ, and the dashed lines, IL+USP+OL+PEROV+LQ. The flattened tetrahedron onto the (Fe,Mg)O-SiO_2-TiO_2 plane is equivalent to the tetrahedron in* ***Fig. 2.4****. The numbers in parentheses represent the contents of corresponding end members in their solid solutions of the assemblage IL+USP+OL+PEROVE+LQ.*

The most outstanding feature of this system is that the linkage between silicate and Ti-bearing oxides is Fe-Mg partitioning. The occurrence of coexisting olivine, orthopyroxene and ilmenite seen in some natural rocks is not observed in this study. The present observations agree with the results of MacGregor (1965, 1969) (***Fig. 2.3***) for the system MgO-SiO_2-TiO_2. Thus, at 1300°C, addition of FeO to the system MgO-SiO_2-TiO_2 will not change the phase relationship for the relatively SiO_2 and TiO_2 poor compositions, but will drastically decrease the liquidus temperature. Subsolidus experiment at 1130°C (Woermann and Lamprecht, 1970), however, suggested that the assemblage OL+OPX+IL was stable. Therefore, at least one reaction boundary, the coexistence of IL+OPX (PS + OL = IL + OPX + LQ) must exist between 1130-1300°C.

Although at 1300°C, atmospheric pressure, the phase relationship indicated that there was no perfect geologically equivalent assemblage for simulating the melting processes in the mantle, the assemblage of LQ+IL+USP+OL was chosen as the closest analogue for more detailed study. This assemblage does exist in basaltic magma (eg. Morse, 1980).

With increasing bulk Mg content in the system (at fixed P, T, fO_2), the 4-phase IL+USP+OL+LQ assemblage gives way to the subsolidus assemblages IL+USP+OL (***Fig. 2.4***). With decreasing Mg and Si content, the field of the univariant assemblage IL+USP+LQ is entered; with decreasing Mg and Ti the field of OL+USP+LQ, and with decreasing Mg and Fe the field of OL+IL+LQ. These 3-phase assemblages are the bounding faces of the IL+USP+OL+LQ 4-phase volume (***Fig. 2.4***).

2.4.2. System Fe-Mg-Ca-Ti-Si-O

At the initial stage of this project, effort was oriented to the study of thermodynamic properties of ilmenite solid solutions, and thus a set of data concerning the Mg-Fe^{2+} partitioning between olivine and ilmenite was required. Due to the small

grain size in experiments involving Mg-rich liquid free assemblages, in the system Mg-Fe-Ti-Si-O, one more component (CaO) was added to the system in order to sustain the existence of a liquid phase as flux. Therefore, the assemblage of solid phases ilmenite, ulvospinel, and olivine in the Mg and Si rich portion of ***Fig. 2.4*** were equilibrated with a coexisting melt, and the experiments were actually carried out in the system of Fe-Mg-Ca-Si-Ti-O. However, since the concentrations of CaO in all the solid phases were low, the existence of the Ca-bearing flux was believed not to affect significantly the subsolidus phase relationships.

In the system Mg-Fe-Ca-Ti-Si-O, experiments were carried out only in the stability field of the Il+USP+OL+lQ univariant assemblage. With continuous increase in Ca and Mg contents, this univariant assemblage eventually moved into the composition field of the invariant assemblage (at fixed P, T, fO_2) having the five phases IL+OL+USP+PEROV+LQ (***Fig. 2.5***). Composition variation of coexisting phases will be discussed in Chapter 3.

CHAPTER 3

EFFECT OF CHANGE IN FO_2: ILLUSTRATED BY NEW EXPERIMENTAL DATA

The effects of changes in oxygen fugacity on the crystallization of basaltic magmas have been extensively studied (eg. review in Basaltic Volcanism Study Project, 1981). The major effects of increasing oxygen fugacity are the increase in the stability field of oxide minerals such as magnetite, and changes in compositions of both oxides and silicates. The effects of change of oxygen fugacity on the stability field of oxides and silicates have been demonstrated, for example, by Biggar (1974), Hill and Roeder (1974). The effect of oxygen fugacity on the compositions of oxides has been studied, for instance, by Buddington and Lindsley (1964), Speidel (1970), and Woermann *et al.*,(1969a, 1969b). An example of the effect of change in oxygen fugacity on compositions of silicates (Roeder and Emslie, 1970), is that increase in oxygen fugacity reduces the fayalite content in olivines.

In this chapter, the above generalization will be restated, but, the more specific phase relations in the system Mg-Fe-Ti-Si-O, or Mg-Fe-Ca-Ti-Si-O will be given.

For convenience, a subsystem, Mg-Fe-Ti-O, can be divided from the above two complicated systems, since the solubility of Si and Ca in the oxide phases (ulvospinel and ilmenite) is low and the presence of SiO_2 and CaO is not expected to significantly influence the oxide phase relationships.

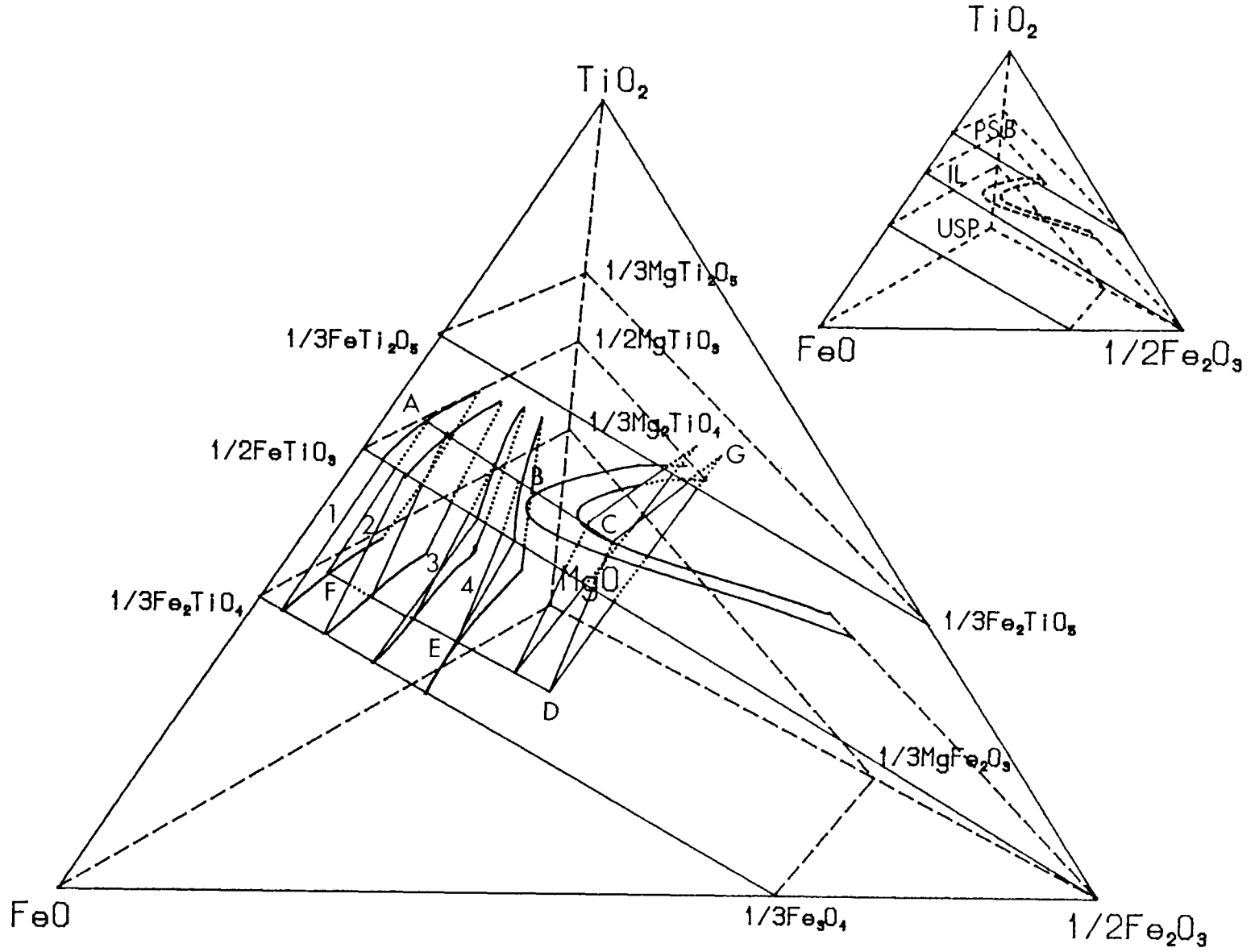

Fig. 3.1 *Effects of change in oxygen fugacity on the sub-system Mg-Fe-Ti-O at 1300°C and 1atm. Phases concerned are shown in the small diagram at top-right. Surfaces 1,2,3, and 4 represent experimentally determined coexisting pairs of IL+USP at oxygen fugacities log fO_2 = -9.0, -8.0, -7.0, and -6.6 respectively. The solvus of the ternary solid solution of `ilmenite` is adopted from Woermann et al., (1969b) (see also discussion in Chapter 5). Triangle CDG exemplifies the assemblage IL+USP+PSB. Surface ABCDEF represents IL+USP pairs coexisting with OL and LQ in the system Mg-Fe-Ti-Si-O (see text and* ***Fig. 3.2, 3.3****). The intersection of surface ABCDEF with the solvus of `ilmenite` defines the assemblage IL+USP+OL+PSB+LQ.*

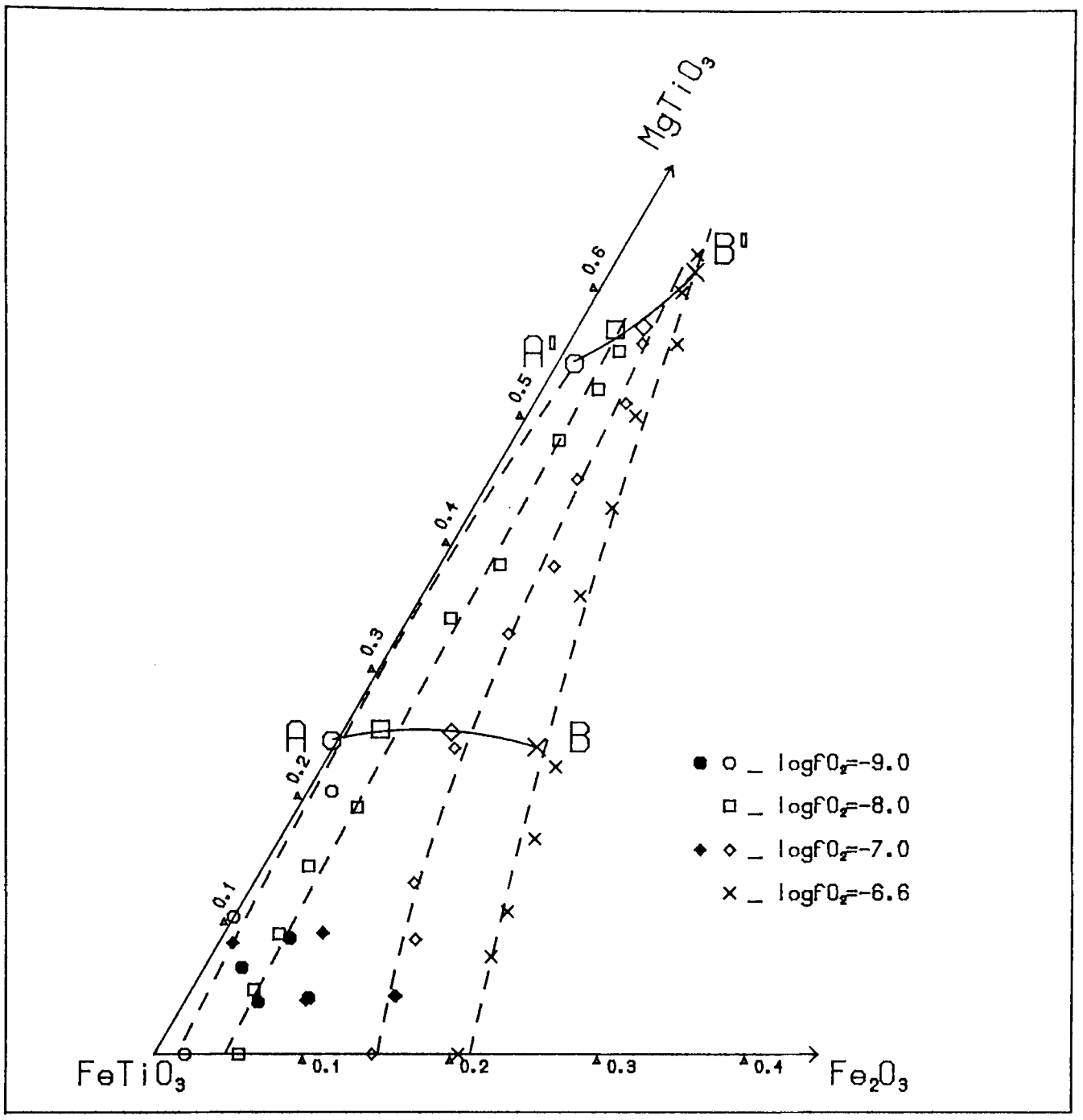

Fig. 3.2 *Details of the effects of change in oxygen fugacity on the composition of ilmenite at 1300°C and 1atm. Ilmenites below (i.e. less Mg-rich than) curve AB are from assemblage IL+USP+LQ in the system Mg-Fe-Ti-Si-O. Ilmenites in between curve AB and A'B' are from assemblage IL+USP+OL+LQ in the system Mg-Fe-Ca-Ti-Si-O. Large symbols along AB and A'B' are from assemblage IL+USP+OL+LQ, and IL+USP+OL+PEROV+LQ in systems Mg-Fe-Ti-Si-O and Mg-Fe-Ca-Ti-Si-O respectively. Open symbols are from this study. Solid symbols are from recalculations of Speidel's (1970). The large scattering of his data may suggest poor attainment of equilibrium in his experiments.*

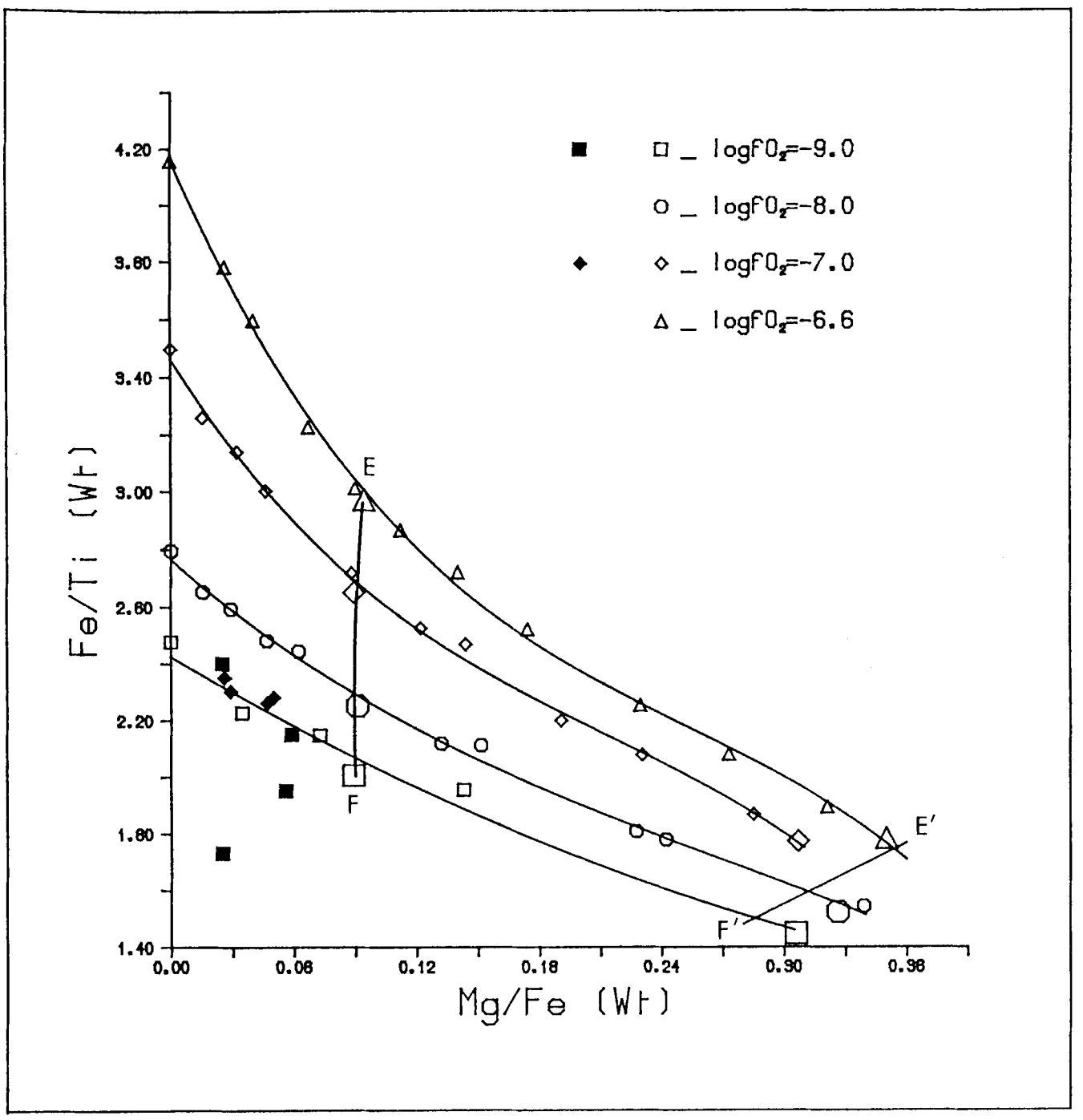

Fig. 3.3 *Details of the effects of change in oxygen fugacity on the composition of Ulvospinel at 1300°C and 1atm. Ulvospinels at the* left *side of (i.e. less Mg-rich than) curve EF are from assemblage IL+USP+LQ in the system Mg-Fe-Ti-Si-O. Ulvospinels in between curve EF and E'F' are from assemblage IL+USP+OL+LQ in the system Mg-Fe-Ca-Ti-Si-O. Large symbols along EF and E'F' are from assemblage IL+USP+OL+LQ, and IL+USP+OL+PEROV+LQ in systems Mg-Fe-Ti-Si-O and Mg-Fe-Ca-Ti-Si-O respectively. Open symbols are from this study. Solid symbols are from recalculations of Speidel's (1970). The large scattering of his data may suggest poor attainment of equilibrium in his experiments.*

The phase relationships of the system Mg-Fe-Ti-O have been partially studied by Speidel (1970) and Woermann *et al.*,(1969a, 1969b) at different oxygen fugacities, and 1atm total pressure. In this study, more data are collected at 1300°C and a wider range of oxygen fugacities in the presence of SiO_2, or SiO_2+CaO. Combining the data of Woermann *et al.*, (1969b) on the solvus of ilmenite solid-solution, a schematic phase diagram in part of the system Mg-Fe-Ti-O has been constructed (***Fig. 3.1***). Experimental data for constructing this diagram are listed in **Appendix II**.

The general phase relationship (in the subsystem Mg-Fe-Ti-O) determined in this study agrees with the result of Speidel (1970), but large discrepancies exist in the detailed compositions of the coexisting IL+ USP pairs. The effects of change in oxygen fugacity on the compositions of coexisting ilmenites and ulvospinels as determined in this study, are shown in ***Fig. 3.2*** and ***3.3*** (**Appendix II**). At 1300°C, Speidel's data (1970) show more reduced character for ulvospinels, and ilmenites at log fO_2=-7.0, but more oxidized for ilmenites at log fO_2=-9.0. In general, his data show large scattering, which is in conflict with the univariant character of the IL+USP assemblage (at fixed P,T, and fO_2), and may indicate lack of equilibrium of his experiments. The effects of change in oxygen fugacity on the compositions of ilmenites in this study, however, agree reasonably well with those of Woermann *et al.*, (1969b), except that a significantly more reduced signature appears at the Fe-rich compositions of this study. The appearance of the pseudobrookite+ulvospinel assemblage (***Fig. 3.1***) in this study also approximately coincides with the solvus position characterized by Woermann *et al.*, (1969b) (**Chapter 5**).

Note that for bulk compositions between the ilmenite and spinel planes, a change of oxygen fugacity has a relatively small effect on the overall phase assemblage until such bulk compositions are sufficiently oxidized that they intersect the ilmenite plane or move into the ilmenite solvus volume, at which point, pseudobrookite appears.

When the component SiO_2 is added (the system Mg-Fe-Ti-Si-O), then the field of

coexisting oxides can be divided into two by the plane ABCDEF (***Fig. 3.1***), which represents the ilmenite and ulvospinel pairs coexisting with both olivine and liquid. Towards the more Mg-rich direction, the coexisting pairs coexist with olivine only (subsolidus), and towards Mg-poor direction, the pairs coexist with liquid only. Such phase assemblage transition relationships have been discussed in **Chapter 2** (***Fig. 2.4***) at log fO_2=-9.0.

As mentioned in chapter 2 (***Fig. 2.4***), the actual phase relationships in the system Mg-Fe-Ti-Si-O at the relatively Mg-rich compositions, ie. the assemblage IL+USP+OL were determined in the present studies in the presence of CaO. Addition of CaO sustains the existence of a liquid phase which can drastically enhance the rate of reaction and increase the crystal size of the charge. Study of the phase relationships of IL+USP+OL in this way is not believed to seriously modify the relationships, since the solubility of CaO in both olivine and oxides is low. Therefore, the IL+USP pairs behind plane ABCDEF in ***Fig. 3.1***, as determined experimentally, were in equilibrium with olivine and a Ca-bearing liquid phase. However, with continuing increase in CaO concentration in the liquid phase, perovskite eventually precipitates, and the precipitation of perovskite marks the maximum MgO concentration studied experimentally.

The effects of change in oxygen fugacity on the MgO contents in coexisting olivine and oxides will be discussed in chapter 4. The results of this study show that, with increase in oxygen fugacity, olivine becomes more Mg-rich. In general, the maximum of the olivine stability field (which corresponds to the minimum Mg Number of olivine for a given bulk composition similar to basalt) occurs at an oxygen fugacity near metallic iron precipitation (Biggar 1974). Departure from the above oxygen fugacity value towards either oxidation or reduction reduces the stability field of olivine.

In this study, all experiments were carried out at oxygen fugacities above metallic iron precipitation. The iron activity of the system at different oxygen fugacities may be

monitored by measuring the quantity of iron absorbed into a platinum foil which is in equilibrium with the charge (***Fig. 3.4***). Such data are potentially important for calculating iron oxide activities in the multicomponent systems (eg. Petric *et al.*, 1981; Petric and Jacob, 1982), provided that the thermodynamic data for this calculation are sufficiently reliable.

The effect of change in oxygen fugacity on the partition of Mg-Fe^{2+} between olivine and coexisting ilmenite is shown in ***Fig. 3.5***. Such information is important in characterizing the thermodynamic properties of the coexisting pairs (eg. Andersen and Lindsley, 1981).

With the calculated iron oxide activities and the partition data amongst coexisting OL+IL+USP, internally consistent thermodynamic models may be developed for describing all the coexisting solid solutions. Conversely, with partitioning data of OL-IL-USP from natural rock, intensive variables (eg. oxygen fugacity, iron oxide activity) may be calculated from the investigated data set, provided that temperature can be estimated independently. Conceivably, the assemblage OL+OPX+IL+USP is a potentially very powerful intensive variable indicator (T, fO_2, a_{Fe}...) (eg. Frost, *et al.*, 1988; O'Neill and Wall, 1987).

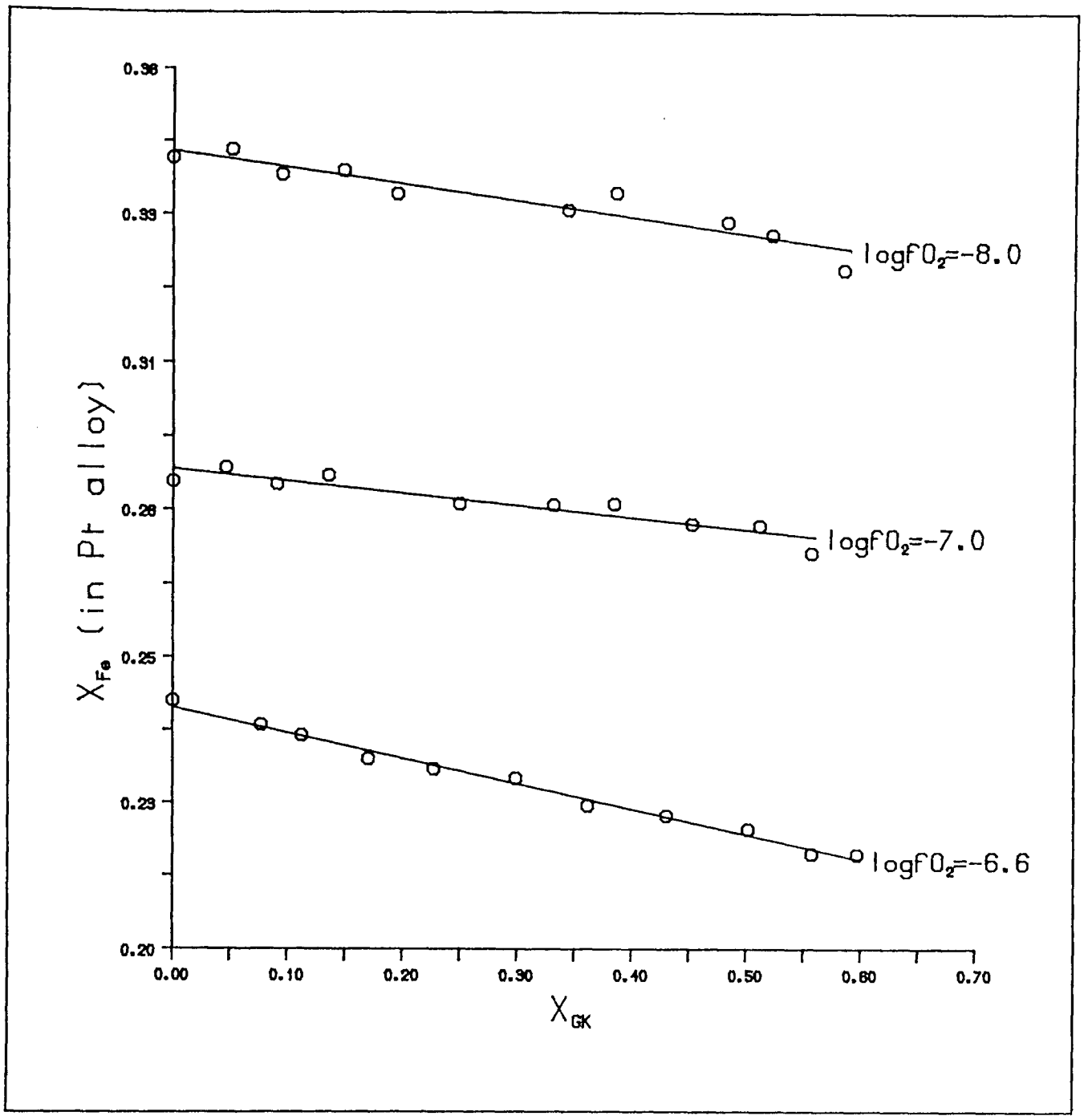

Fig. 3.4 *The effects of oxygen fugacity and Mg contents on the concentration of metallic iron in platinum foil.* X_{GK} *is the mole fraction of geikielite in ilmenite solid solution The Pt-foil is about 20 micron in thickness, and heated together with the charge for 5 days at 1300°C and various oxygen fugacities. The Pt-Fe alloy is binary, and the Fe content of this alloy can be used as a measure of Fe activity of the multicomponent system. The high correlation of the acquired data demonstrates the univariant character of the assemblage (at fixed* $P, T,$ *and* fO_2*) and supports the attainment of equilibrium.*

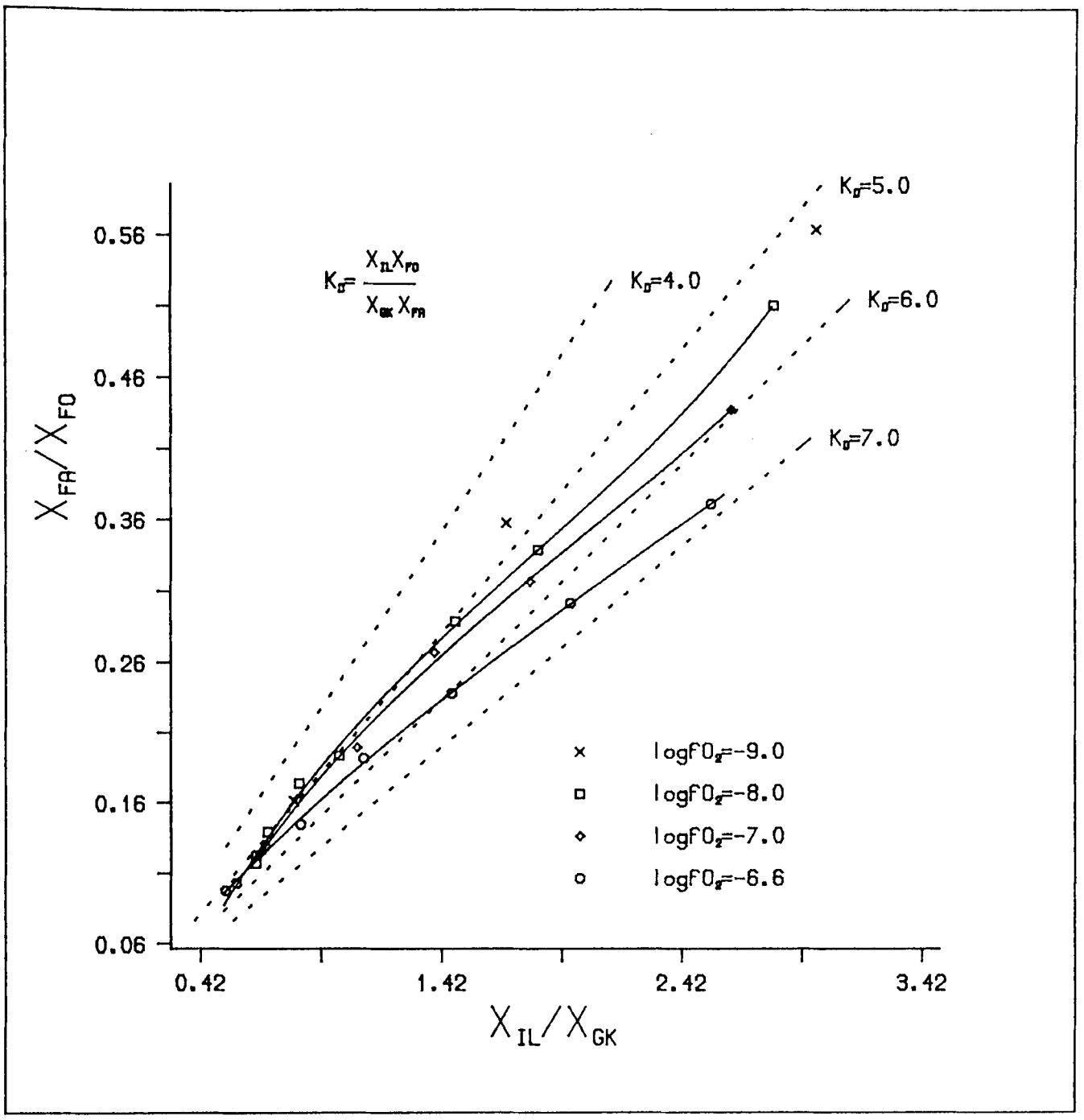

Fig. 3.5 *The effects of oxygen fugacity on Mg-Fe^{2+} partition between ilmenite and olivine. X axis: ratio of mole fractions of ilmenite to geikielite in IL_{SS}. Y axis: ratio of mole fraction of fayalite to forsterite in OL_{SS}.*

CHAPTER 4

OXIDATION MELTING

Although the absolute value of oxygen partial pressure in most terrestrial magmas is low in comparison with the values of other volatile species, its influence on petrogenesis is not as trivial as its absolute magnitude. Obviously, it is not the free oxygen molecules, rather it is the more abundant other gas species and variable-valency cations, dominantly Fe, that are involved in the complicated petrogenetic processes. General roles of volatile species and the mechanism of changing Fe^{3+}/Fe^{2+} ratio on partial melting has been reviewed in Chapter 1. In this Chapter, the effect of changing Fe^{3+}/Fe^{2+} ratio as function of oxygen fugacity on the partial melting of samples of particular chosen bulk compositions is given detailed description.

The data presented in this chapter are from the experiments carried out in the systems Mg-Fe-Si-Ti-O and Mg-Fe-Ca-Si-Ti-O. The results from these two systems are similar and show the importance of redox control on the melting mechanism envisaged from the analysis of the simple system Fe-Si-O (Osborn and Muan 1960) discussed in Chapter 1.

Due to the high sensitivity of partial melting to change of temperature, all the experiments on melting were carried out with relatively short durations, 24hr, so that the whole set of experiments were finished within a shorter time span. This was hoped to have reduced the possibility of instrument failure and temperature drifting. Homogeneity of each phase was achieved on both the individual grain scale and the whole charge scale. Equilibrium was believed to have been attained (see discussion in Chapter 2). The temperature deviation between different runs was believed to be within $\pm 2^{o}$C.

4.1. General consideration

The problem of bulk composition control in experiments has been discussed in Chapter 1. Even setting apart from the problem of iron loss into platinum during experiments, the actual Fe^{3+}/Fe^{2+} ratio in the charge, especially in the glass can not be satisfactorily determined by electron microprobe analysis. Therefore, the redox melting which is believed to be redox-transition-metal controlled partial melting, can not be clearly related to the Fe^{3+}/Fe^{2+} ratio in the charge.

Nevertheless, the controlled oxygen fugacity and its influence on the Fe^{3+}/Fe^{2+} ratio in the solid phases calculated from assumed stoichiometry does imply an intrinsic correlation between oxygen fugacity and the Fe^{3+}/Fe^{2+} in the charge. Therefore, the relationship between partial melting and oxygen fugacity reflects the relationship of partial melting and Fe^{3+}/Fe^{2+} ratio in the charge. Consequently, in this study, the melting characteristics are described as a function of oxygen fugacity without specifying the actual Fe^{3+}/Fe^{2+} ratio in the charge.

When the experimental charge is buffered by an external source, with changing oxygen fugacity, the actual mass change is the introduction or extraction of oxygen. Although in most cases, it is difficult to quantify this change, the importance of studying the redox melting still exists, since it yields information about the redistribution of other components between coexisting phases, and this can be determined with reasonably high precision. The precise determination of introduced or extracted oxygen is important for characterizing the redox capacity of the charge (ie. the quantity of oxygen needed to generate a specific redox perturbation); it is not, however, crucial to the study of degree of partial melting under controlled oxygen fugacity, because the study of partial melting is basically concerned with the mass redistribution of non-volatile components. The contribution of the introduced or extracted oxygen can be neglected for simplicity.

Therefore, in the attempt to clarify the effect of oxygen fugacity on the melting processes, experiments were designed to obtain data in a chemical system with fixed compositions in non-volatile components at assigned P and T (see Chapter 1).

However, it is not desirable to base the experiments and their interpretation on specific bulk compositions as loaded into the experimental charges. This is both because of the difficulty of estimating the amount of iron loss in platinum during the experiment and the possibility of small amount of partial melting, which causes problems of experimental determination (see Chapter 1), in the most geologically relevant bulk compositions of interest.

However, by using invariant assemblages at given P, T and fO_2, close dependence on the bulk composition of the loaded charge can be avoided, and calculation of features of specific bulk compositions carried out by a reversed procedure. This is to determine the compositions of coexisting phases in the invariant assemblage first, then, calculate the possible starting bulk compositions by changing the proportions of the coexisting phases. So long as the experimental charge lies within the bulk compositional field of a particular invariant assemblage (eg. IL+USP+OL+LQ, ***Fig. 2.2***) and thereby yields coexisting phases which may be carefully analysed, it is possible to use the phase analyses to calculate phase proportions for all bulk compositions, which yield the invariant assemblage, or to put the phases together in all possible proportions in order to obtain the whole range of bulk compositions yielding the given assemblage. This means that while experiments may be performed on charges yielding large amount of melt, the composition relations for material yielding small amount of melt may be calculated from the experimental data.

Using hypothetical system X-Y-Z, a simple illustration for the study procedure is given in ***Fig. 4.1***.

Figure 4.2, illustrates the compositional characteristics of the invariant assemblage of IL+USP+OL+LQ in the real system of Mg-Fe-Si-Ti-O at two different oxygen

fugacities (see also Table 4.2 and 4.6). The small tetrahedron A represents the assemblage at oxygen fugacity of $10^{-6.6}$ bar, whilst B shows the position of the assemblage at $10^{-9.0}$ bar (total iron was plotted as FeO in the diagram). Due to the invariant character of this assemblage at fixed P, T and oxygen fugacity, the relatively small compositional change caused by iron loss into platinum will not affect the composition of each phase, and a large degree of partial melting can be achieved in the experimental charges by carefully selecting bulk compositions. The intersection of the two tetrahedra A and B represents the possible compositions which yield the same assemblage at different oxygen fugacities. With chosen bulk composition and known compositions of each phases, it is possible to perform mass balance calculations to quantify the relative quantity of each phase as a function of oxygen fugacity.

Therefore, calculating relations for the desired bulk compositions from analysed coexisting phases is the characteristic of the experimental design, and such a design, will allow much greater flexibility in bulk composition option with a limited number of runs. Furthermore, a closer simulation to geological composition can be reasonably achieved while maintaining experimental accuracy by choosing the most suitable compositions for experimentation.

In the system of Mg-Fe-Ca-Si-Ti-O, the assemblage of IL+USP+OL+PEROV+LQ was used in the similar manner.

4.2. Phase compositions and oxygen fugacity

General effects of change in oxygen fugacity on the compositions of coexisting phases in part of the system Mg-Fe-Ca-Ti-Si-O have been discussed in Chapter 3. This section is specially devoted to the assemblage IL+USP+OL+LQ in the system Mg-Fe-Ti-Si-O and IL+USP+OL+PEROV+LQ in the system Mg-Fe-Ca-Ti-Si-O.

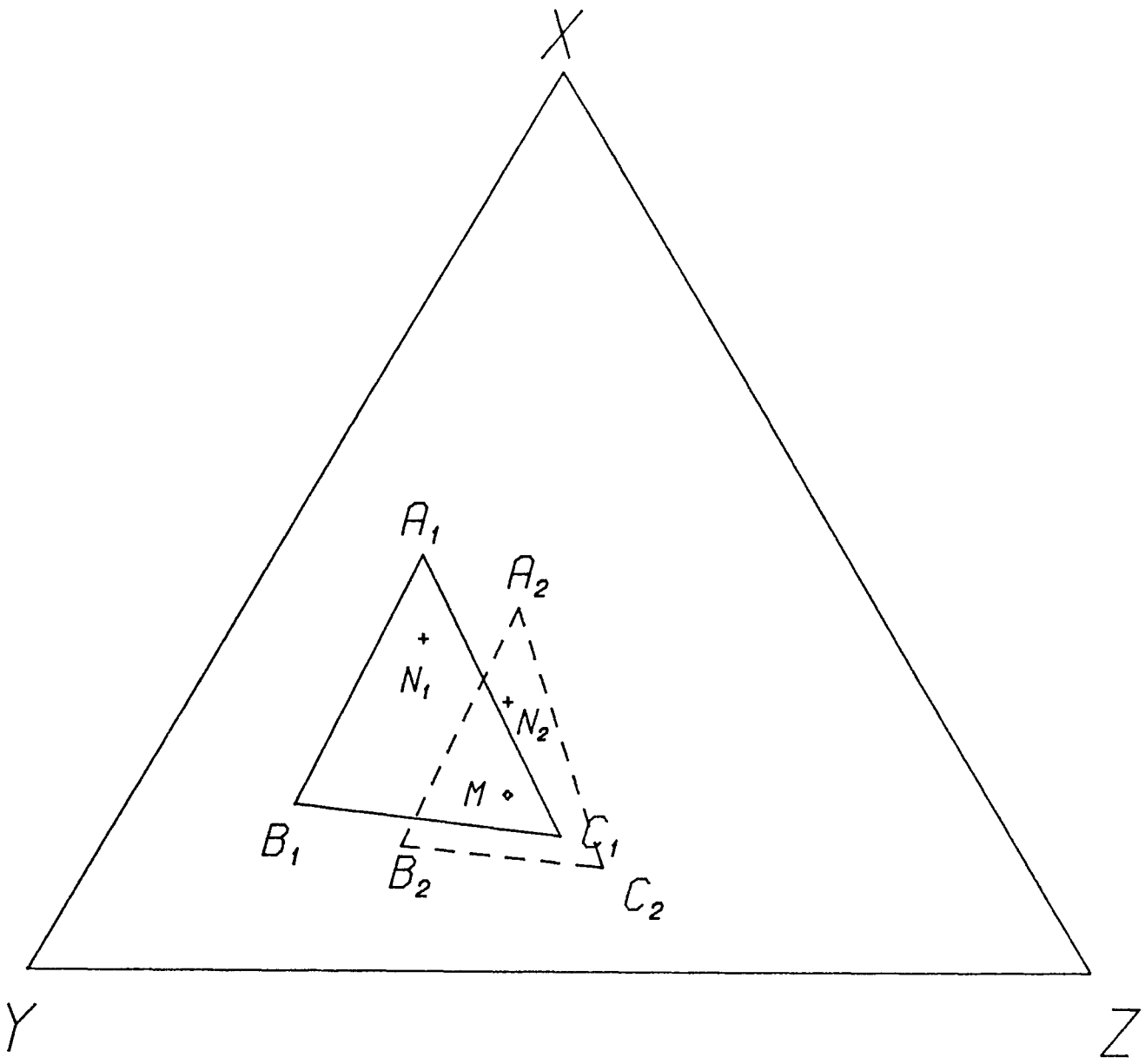

Fig. 4.1 *Illustration of study procedure by using hypothetical simple system. X,Y,Z are components (oxygen is omitted because it is not involved in mass balance calculations) A-B-C is an invariant assemblage at fixed P,T and fO_2, and is shown for two sets of conditions ($A_1+B_1+C_1$ and $A_2+B_2+C_2$). $A_{1,2}$ is the liquid phase.*

Study procedure:

1. Choose approximate bulk composition N_1 and N_2 for experimentation, thereby ensuring charges which will produce invariant assemblages with large degrees of partial melting.

2. Examine the effects of changing experimental conditions on a bulk composition of more geological relevance. For example:

(a). Choose Bulk composition M to ensure that M is within the stability field of the assemblage at different conditions, and is analogous to natural peridotite.

(b). Perform mass balance calculation by using the chosen bulk composition M and experimentally determined phase compositions of A,B,C at different experimental conditions (1,2). Thus, quantity of each phase can be determined in bulk composition M at different oxygen fugacities (at fixed P and T).

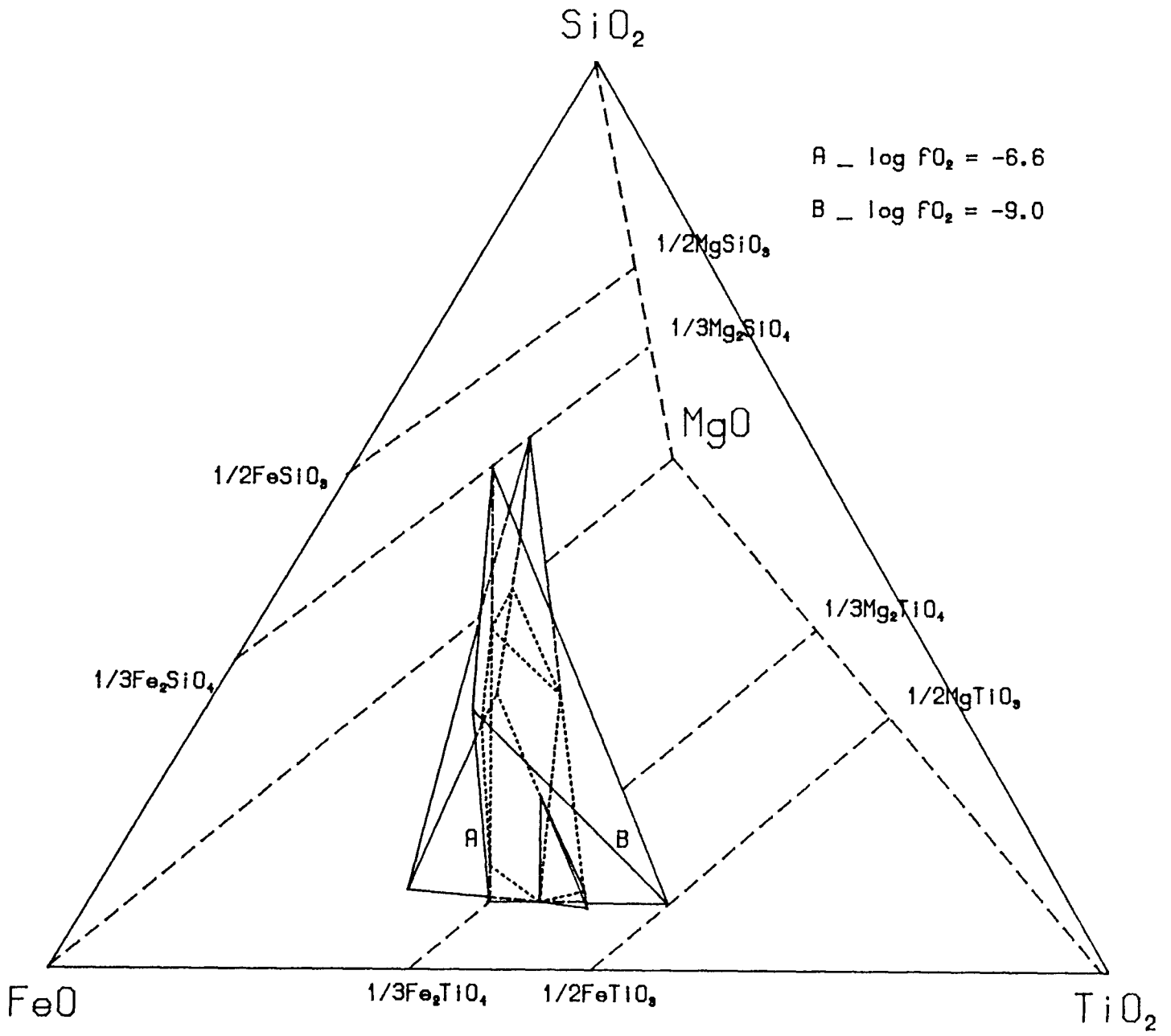

Fig. 4.2 *Composition overlap of the assemblage of IL+USP+OL+LQ at different oxygen fugacities. Oxides in mole percent. Total iron calculated as FeO. Tetrahedra A and B represent the assemblage IL+USP+OL+LQ at two different fO_2 conditions at 1300°C, 1atm. The intersection (dot-lined irregular polyhedron) of the two small tetrahedra A and B represents the bulk compositions satisfying oxygen fugacities for both A and B. The displacement of A and B is continuous as fO_2 changes. The enrichment of Fe in oxides, and Mg in olivine with increasing fO_2 is obvious.*

Extensive solid solution of the coexisting solid phases is the major character of the system. The high tolerance of these phases to the impact of changing oxygen fugacity results in the stable appearance of the assemblages over a large range of oxygen fugacity at 1300°C and atmospheric pressure.

For simplicity, despite the wide changes in phase compositions, these solid phases are referred as olivine (OL)for the silicate phase, ilmenite (IL) and ulvospinel (USP) for the rhombohedral and cubic oxide phases respectively.

OLIVINE: This solid solution is dominated by the two end members fayalite and forsterite. Monticellite mole fraction is low (<3.2 mole%), and so is the titanium concentration (<0.73 wt%). The effect of oxygen fugacity on compositions of olivine is rather simple. Similar to that observed by Roeder and Emslie (1970), with increasing oxygen fugacity, the olivines become more Fo rich (***Fig. 4.3***, Table 4.1-4.10).

ILMENITE: This solid solution can be sufficiently described with three end members, ilmenite ($FeTiO_3$), haematite (Fe_2O_3), and geikielite ($MgTiO_3$). Calcium content in this solid solution is low (<0.5 wt%), and silica is almost negligible (<0.03 wt%). In the assemblage IL+USP+OL+LQ where the iron content is relatively high, with increasing oxygen fugacity, this solid solution becomes more haematite rich, poor in ilmenite, but remains almost constant in geikielite content. In the assemblage IL+USP+OL+PEROV+LQ where the Mg content is high, with increasing oxygen fugacity, there is a significant increase in geikielite concentration (***Fig. 4.4***, Table 4.1-4.10). At very reducing conditions, this solid-solution becomes more obviously cation deficient (Simons and Woermann, 1978; O'Neill *et al.*, 1988).

ULVOSPINEL: This solid solution can be satisfactorily described with four end members, ulvospinel (Fe_2TiO_4), magnesian ulvospinel (Mg_2TiO_4), magnetite (Fe_3O_4), and magnesian ferrite ($MgFe_2O_4$). The contents of CaO and SiO_2 are less than 0.1 wight percent. With increase in oxygen fugacity, this phase becomes significantly enriched in magnetite, slightly increases in magnesian ferrite, constantly decreases in

ulvospinel, but keeps almost constant the magnesian ulvospinel content (***Fig. 4.5***, Table 4.3). At very reducing conditions, ulvospinel also becomes more cation-deficit$^{en}_{\wedge}$ (Simons and Woermann, 1978; O'Neill *et al.*, 1988).

PEROVSKITE: This phase only exists in the Ca-bearing system. It is noticeable that these perovskites are relatively rich in iron (upto 1.3 wt% FeO) (Table 4.6-4.10).

GLASS: Despite aiming for experimental run composition yielding a large proportion of glass, the problem of quenching modification of the glass remains, and the glass analyses show larger variations than those of the coexisting solids. These variations have been given serious consideration in all the subsequent manipulations. Changes in liquid composition of the assemblage IL+USP+Ol+PEROV+LQ in response to that of oxygen fugacity are not obvious (Table 4.6-4.10, ***Fig. 4.7***). However, in the assemblage IL+USP+OL+LQ, a general trend of compositional variation is shown: with increasing in oxygen fugacity, the liquid phase becomes progressively enriched in MgO, SiO_2, but reduced in TiO_2,and total iron (***Fig 4.6***, Table 4.1-4.5)

Because of the extensive solution character of the major phases in the assemblages concerned, the impact of the change in oxygen fugacity (within certain range) results in the modifications in compositions of the coexisting phases rather than an abrupt transition in the assemblage. The high sensitivity of the solid phases to changes in oxygen fugacity suggests that the change of oxygen fugacity (or oxygen content) in a charge dominated by solids results in a large extent of mass redistribution, and the consequence of this is possibly a larger (or smaller) degree of partial melting. More precisely, the amount of partial melting is likely to be sensitive to the redox state of the charge.

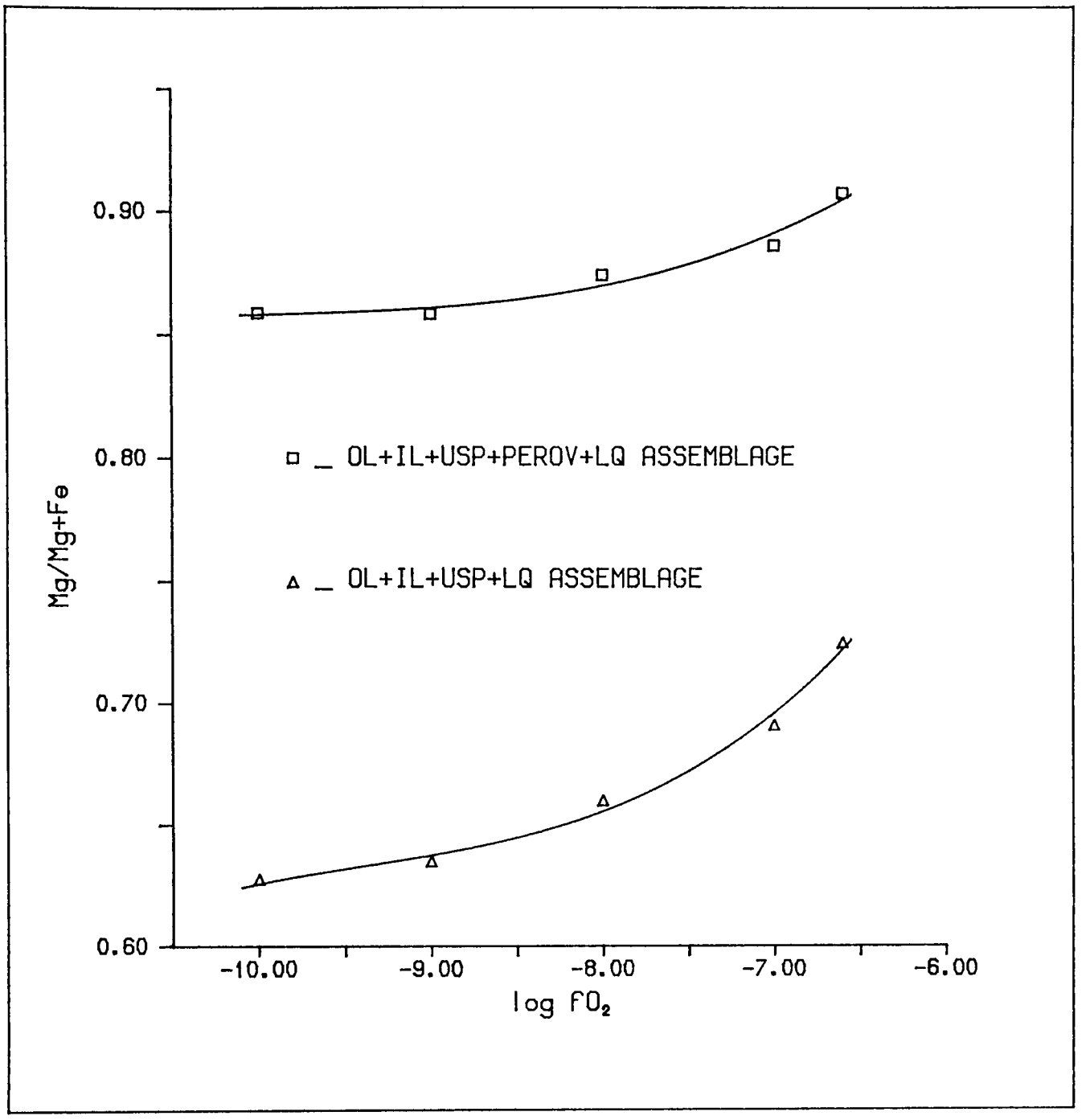

Fig. 4.3 *Effect of oxygen fugacity on compositions of olivines. Simple trend has been illustrated: with increase in fO_2, olivine becomes more Mg-rich. The composition range of olivine in the assemblage IL+USP+OL+PEROV+LQ is close to peridotitic olivine; and the olivine in assemblage IL+USP+OL+LQ more similar to that from basalts. Error in analyses is smaller than the symbols. If olivine is a major constituent of certain rock type, the effect of fO_2 on its composition will result in extensive mass redistribution amongst coexisting phases.*

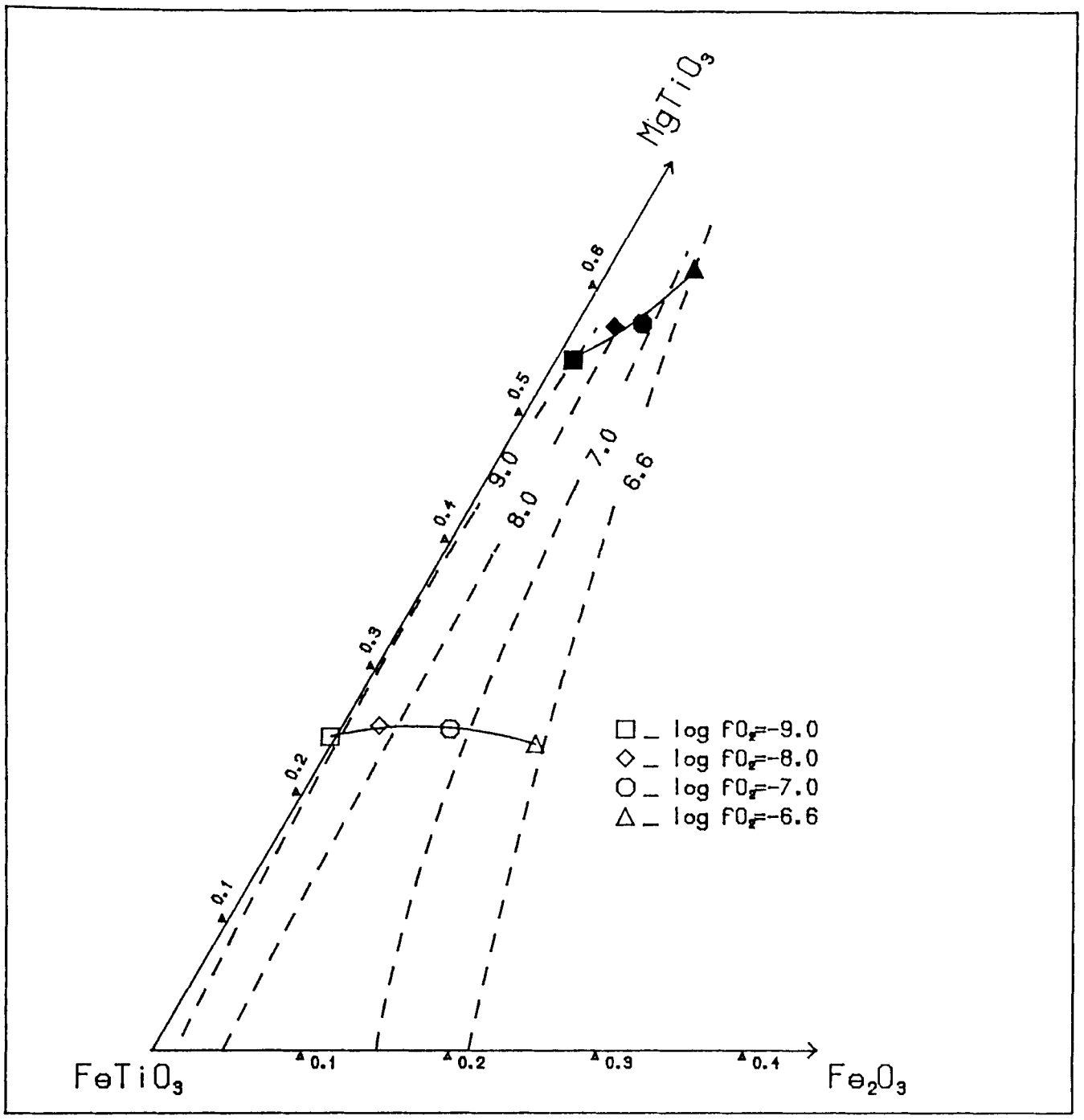

Fig. 4.4 *Effect of oxygen fugacity on the composition of ilmenite. Ilmenites produced at* $logfO_2$*=-10.0 are slightly cation deficient and not shown in this diagram. With increasing* fO_2 *the ilmenite in the assemblage IL+USP+OL+LQ becomes haematite rich without significant Mg variations. In the assemblage IL+USP+OL+PEROV+LQ, the ilmenite shows a general trend of Mg enrichment, similar to that of coexisting olivine. Open symbols, IL+USP+OL+LQ. Solid symbols, IL+USP+OL+PEROV+LQ. Dashed lines are oxygen isobars derived from an independent set of experiments discussed in Chapter 3. Error in analyses is smaller than the symbols.*

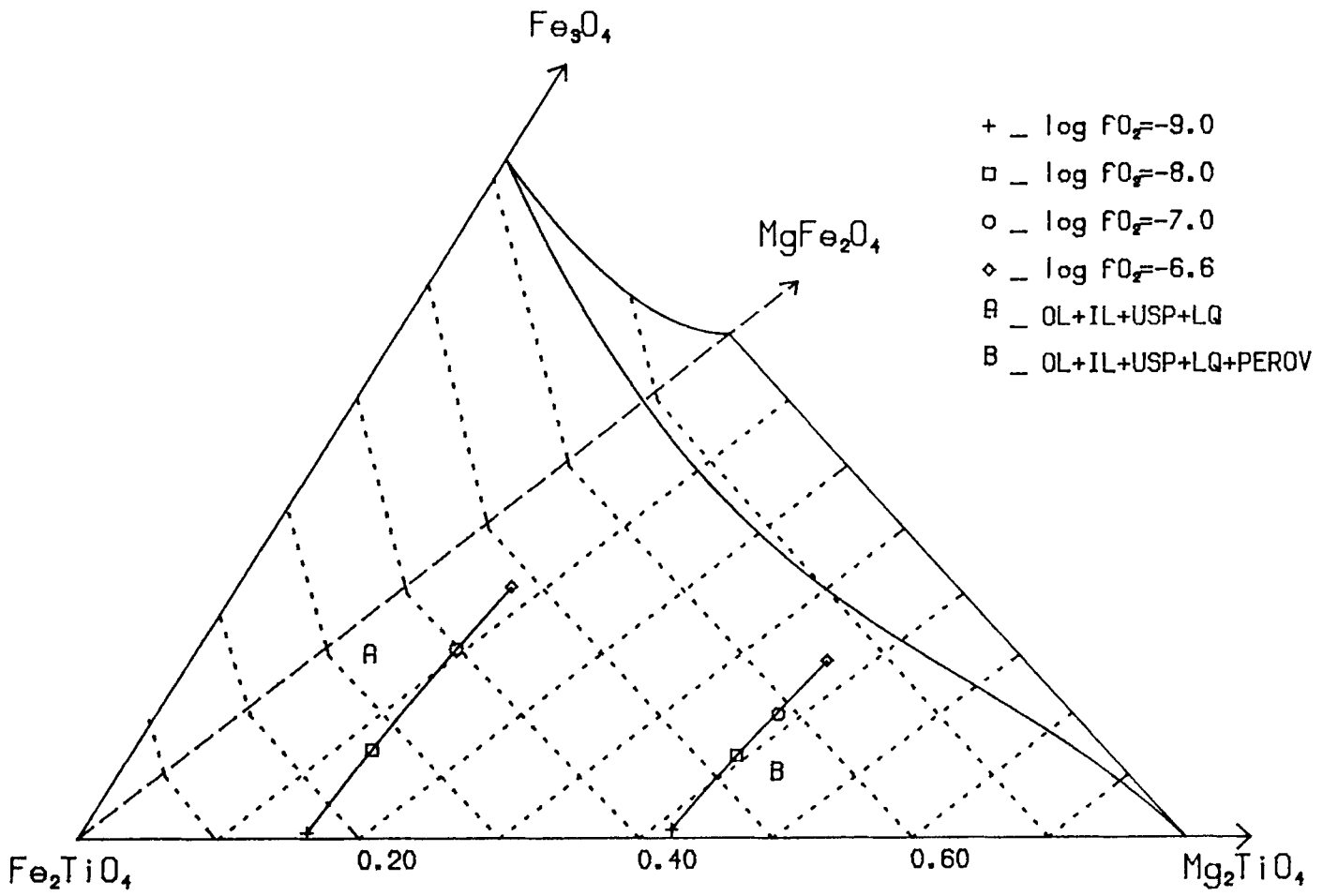

Fig. 4.5 *Effect of oxygen fugacity on the composition of ulvospinel. Ulvospinels produced at log fO_2=-10.0 are not illustrated here due to its cation deficiency. Ferric contents are calculated assuming the stoichiometry of the four end members.*

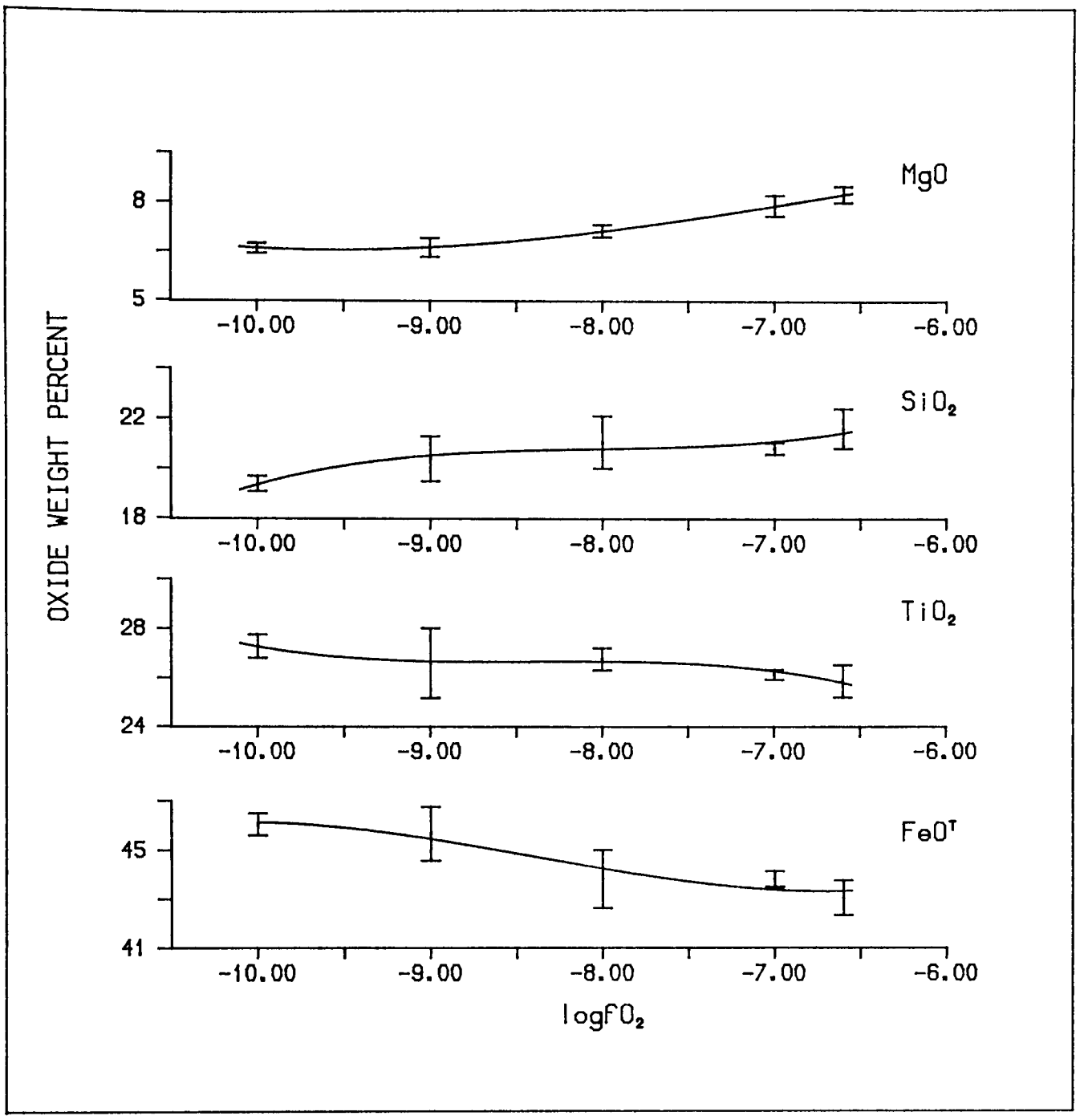

Fig. 4.6 *Effect of oxygen fugacity on composition of glass in assemblage IL+USP+OL+LQ. Variation in composition in response to the change in fO_2 is much smaller than that in the coexisting solids for the fO_2 range concerned. However, trends of variation still shown. Total iron calculated as FeO. Error bars represent 1 standard deviation.*

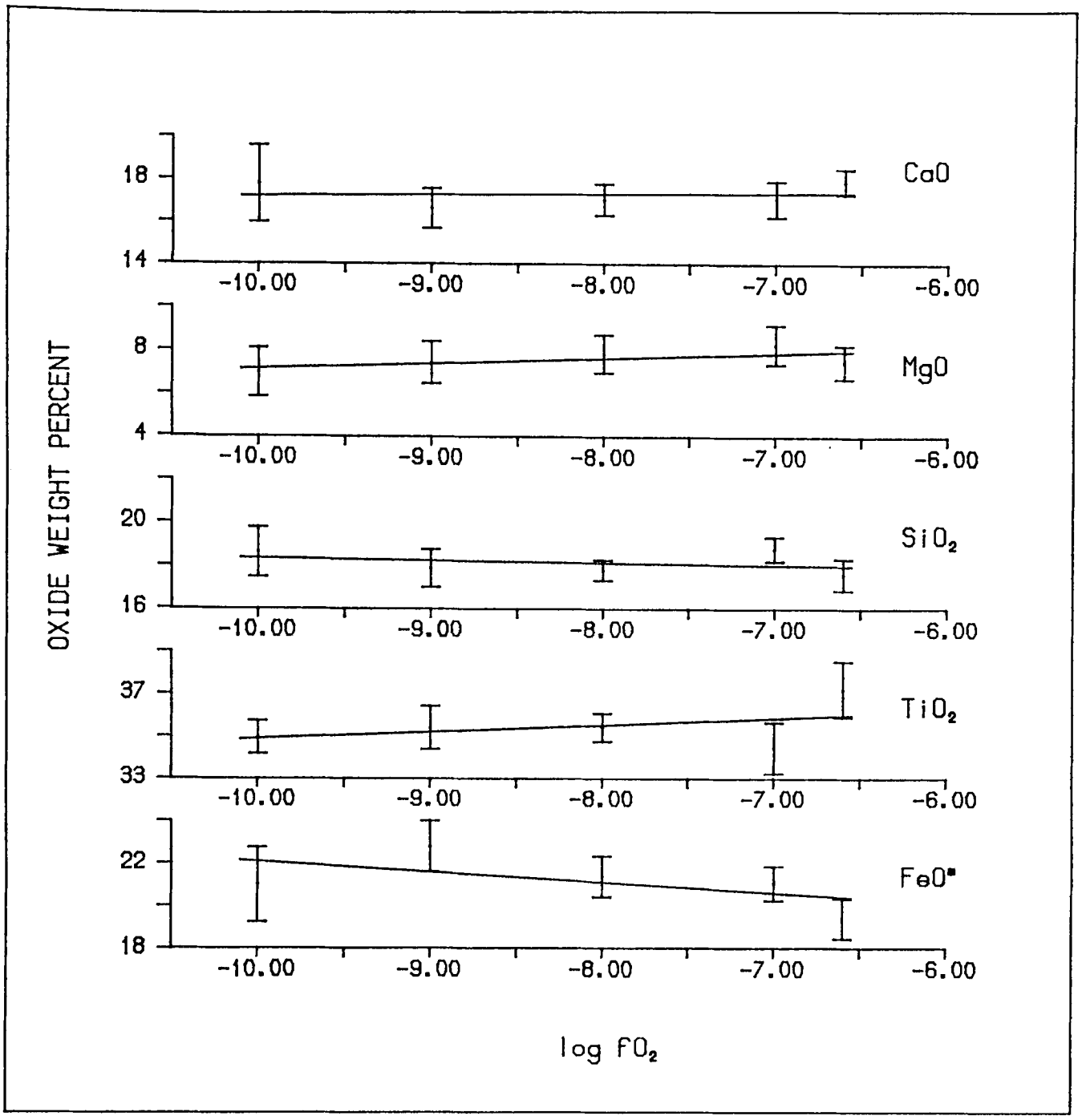

fig. 4.7 *Effect of oxygen fugacity on composition of glass in assemblage IL+USP+OL+PEROV+LQ. Poor analyses have made the subtle composition variation trend undistinguishable. Error bars are standard deviations.*

TABLE 4.1 ELECTRON MICROPROBE ANALYSES OF PHASES IN ASSEMBLAGE IL+USP+OL+LQ AT $\log fO_2$=-10.0

	IL	USP	OL	LQ
MgO	6.94(0.07)	6.41(0.10)	30.26(0.09)	6.75(0.17)
SiO_2	0.01(0.01)	0.11(0.01)	36.46(0.15)	19.37(0.31)
TiO_2	56.90(0.12)	38.48(0.09)	0.72(0.16)	27.27(0.48)
FeO	36.62(0.18)	54.57(0.18)	32.33(0.12)	46.05(0.45)
SUM	100.47	99.57	99.77	99.44
CAT/OXY	2/3	3/4	3/4	--
Mg	0.2452	0.3374	1.2418	------
Si	0.0002	0.0038	0.9920	------
Ti	1.0142	1.0218	0.0149	------
Fe^{2+}	0.7259	1.6114	0.7444	------
SUM	1.9855	2.9744	2.9931	------
#	6	5	5	5

is the number of analyses. IL=Ilmenite. OL=Olivine. USP=Ulvospinel. LQ=Glass. Standard deviation in parentheses.

TABLE 4.2 ELECTRON MICROPROBE ANALYSES OF PHASES IN ASSEMBLAGE IL+USP+OL+LQ AT $\log fO_2$=-9.0

	IL	USP	OL	LQ
MgO	7.03(0.13)	6.46(0.08)	31.03(0.39)	6.77(0.32)
SiO_2	0.02(0.01)	0.11(0.02)	36.44(0.19)	20.38(0.91)
TiO_2	55.97(0.12)	36.36(0.07)	0.74(0.09)	26.59(1.43)
FeO	37.36(0.13)	54.84(0.19)	31.48(0.27)	45.66(1.10)
Fe_2O_3	------	1.53(0.24)	------	------
SUM	100.38	99.32	99.69	99.40
CAT/OXY	2/3	3/4	3/4	--
Mg	0.2496	0.3436	1.2697	------
Si	0.0004	0.0040	0.9886	------
Ti	1.0026	0.9755	0.0153	------
Fe^{2+}	0.7443	1.6359	0.7227	------
Fe^{3+}	------	0.0410	------	------
SUM	1.9969	3.0000	2.9963	------
#	5	4	5	10

is the number of analyses. IL=Ilmenite. OL=Olivine. USP=Ulvospinel. LQ=Glass. Standard deviation in parentheses. Ferric iron calculated from assumed stoichiometry.

TABLE 4.3 ELECTRON MICROPROBE ANALYSES OF PHASES IN ASSEMBLAGE IL+USP+OL+LQ AT $\log fO_2=-8.0$

	IL	USP	OL	LQ
MgO	7.18(0.05)	6.79(0.11)	32.37(0.31)	7.33(0.21)
SiO_2	0.02(0.01)	0.14(0.02)	36.83(0.28)	21.05(1.06)
TiO_2	54.13(0.23)	33.28(0.11)	0.73(0.19)	26.77(0.45)
FeO	35.90(0.16)	51.34(0.11)	29.77(0.34)	43.82(1.20)
Fe_2O_3	2.61(0.30)	7.21(0.13)	------	------
SUM	99.84	98.76	99.70	98.97
CAT/OXY	2/3	3/4	3/4	--
Mg	0.2566	0.3627	1.3126	------
Si	0.0005	0.0049	0.9900	------
Ti	0.9760	0.8977	0.0150	------
Fe^{2+}	0.7199	1.5400	0.6773	------
Fe^{3+}	0.0471	0.1946	------	------
SUM	2.0001	2.9999	2.9949	------
#	5	6	5	12

is the number of analyses. IL=Ilmenite. OL=Olivine. USP=Ulvospinel. LQ=Glass. Standard deviation in parentheses. Ferric iron calculated from assumed stoichiometry.

TABLE 4.4 ELECTRON MICROPROBE ANALYSES OF PHASES IN ASSEMBLAGE IL+USP+OL+LQ AT $\log fO_2=-7.0$

	IL	USP	OL	LQ
MgO	7.13(0.10)	7.00(0.12)	34.45(0.29)	8.18(0.35)
SiO_2	0.02(0.02)	0.15(0.04)	37.31(0.24)	20.81(0.24)
TiO_2	51.25(0.04)	29.73(0.03)	0.83(0.12)	26.13(0.20)
FeO	33.40(0.23)	47.85(0.20)	27.18(0.23)	43.83(0.32)
Fe_2O_3	8.30(0.11)	14.44(0.10)	------	------
SUM	100.10	99.17	99.77	98.95
CAT/OXY	2/3	3/4	3/4	--
Mg	0.2550	0.3735	1.3779	------
Si	0.0005	0.0055	0.9893	------
Ti	0.9246	0.8001	0.0168	------
Fe^{2+}	0.6701	1.4321	0.6100	------
Fe^{3+}	0.1498	0.3889	------	------
SUM	2.0000	3.0001	2.9940	------
#	5	4	5	8

is the number of analyses. IL=Ilmenite. OL=Olivine. USP=Ulvospinel. LQ=Glass. Standard deviation in parentheses. Ferric iron calculated from assumed stoichiometry.

TABLE 4.5 ELECTRON MICROPROBE ANALYSES OF PHASES IN ASSEMBLAGE IL+USP+OL+LQ AT $\log fO_2$=-6.6

	IL	USP	OL	LQ
MgO	6.76(0.03)	7.58(0.07)	36.59(0.10)	8.57(0.27)
SiO_2	0.02(0.02)	0.16(0.01)	37.52(0.10)	21.61(0.80)
TiO_2	47.46(0.07)	27.14(0.03)	0.38(0.13)	25.86(0.67)
FeO	30.67(0.05)	44.53(0.11)	24.53(0.14)	43.05(0.72)
Fe_2O_3	15.25(0.23)	19.69(0.11)	------	------
SUM	100.16	99.10	99.02	99.11
CAT/OXY	2/3	3/4	3/4	--
Mg	0.2431	0.4037	1.4564	------
Si	0.0005	0.0055	0.9903	------
Ti	0.8610	0.7296	0.0076	------
Fe^{2+}	0.6188	1.3314	0.5478	------
Fe^{3+}	0.2768	0.5298	------	------
SUM	2.0002	3.0000	3.0021	------
#	4	5	3	6

is the number of analyses. IL=Ilmenite. OL=Olivine. USP=Ulvospinel. LQ=Glass. Standard deviation in parentheses. Ferric iron calculated from assumed stoichiometry.

TABLE 4.6 ELECTRON MICROPROBE ANALYSES OF PHASES IN ASSEMBLAGE IL+USP+OL+PEROV+LQ AT $\log fO_2 = -10.0$

	IL	USP	OL	PEROV	LQ
MgO	16.66(0.13)	17.60(0.07)	44.92(0.26)	0.18(0.02)	6.96(1.14)
SiO_2	0.02(0.01)	0.07(0.01)	39.48(0.02)	0.07(0.01)	18.59(1.15)
TiO_2	60.35(0.15)	40.98(0.15)	0.58(0.10)	59.15(0.18)	34.94(0.87)
FeO	23.27(0.10)	40.90(0.04)	13.08(0.13)	0.12(0.06)	20.99(1.76)
CaO	0.44(0.12)	0.43(0.18)	1.16(0.08)	41.17(0.23)	17.74(1.82)
SUM	100.74	99.98	99.22	101.65	99.22
CAT/OX	2/3	3/4	3/4	2/3	--
Mg	0.5497	0.8554	1.6947	0.0057	------
Si	0.0004	0.0022	0.9875	0.0015	------
Ti	1.0042	1.0049	0.0110	0.9930	------
Fe^{2+}	0.4307	1.1154	0.2769	0.0202	------
Ca	0.0104	0.0151	0.0315	0.9848	------
SUM	1.9955	2.9930	3.0016	2.0052	------
#	4	3	4	3	7

is the number of analyses. IL=Ilmenite. OL=Olivine. USP=Ulvospinel. LQ=Glass. PEROV=Perovskite. Standard deviation in parentheses.

TABLE 4.7 ELECTRON MICROPROBE ANALYSES OF PHASES IN ASSEMBLAGE IL+USP+OL+PEROV+LQ AT $logfO_2$=-9.0

	IL	USP	OL	PROVE	LQ
MgO	16.52(0.08)	17.16(0.06)	44.99(0.09)	0.13(0.02)	7.43(0.98)
SiO_2	0.01(0.00)	0.07(0.01)	39.37(0.17)	0.06(0.04)	17.86(0.88)
TiO_2	59.76(0.16)	38.96(0.35)	0.62(0.03)	59.08(0.28)	35.40(1.02)
FeO	23.90(0.16)	40.70(0.54)	13.17(0.09)	1.09(0.14)	22.81(1.20)
Fe_2O_3	0.55(0.26)	3.12(0.45)	------	------	------
CaO	0.30(0.03)	0.27(0.03)	1.15(0.06)	41.34(0.25)	16.57(0.94)
SUM	101.04	100.28	99.30	101.70	100.07
CAT/OX	2/3	3/4	3/4	2/3	--
Mg	0.5454	0.8374	1.6973	0.0043	------
Si	0.0002	0.0022	0.9846	0.0013	------
Ti	0.9953	0.9593	0.0118	0.9919	------
Fe^{2+}	0.4427	1.1147	0.2788	0.0203	------
Fe^{3+}	0.0092	0.0769	------	------	------
Ca	0.0071	0.0095	0.0311	0.9890	------
SUM	1.9999	3.0000	3.0036	2.0068	------
#	4	5	4	6	11

is the number of analyses. IL=Ilmenite. OL=Olivine. USP=Ulvospinel. LQ=Glass. PEROV=Perovskite. Standard deviation in parentheses. Ferric iron calculated from assumed stoichiometry.

TABLE 4.8 ELECTRON MICROPROBE ANALYSES OF PHASES IN ASSEMBLAGE IL+USP+OL+PEROV+LQ AT $logfo_2$=-8.0

	IL	USP	OL	PROVE	LQ
MgO	17.37(0.28)	18.28(0.14)	46.04(0.07)	0.15(0.02)	7.84(0.89)
SiO_2	0.02(0.01)	0.06(0.01)	39.64(0.11)	0.04(0.01)	17.78(0.48)
TiO_2	59.05(0.31)	36.99(0.06)	0.52(0.10)	59.35(0.17)	35.42(0.67)
FeO	21.75(0.28)	36.99(0.34)	11.73(0.17)	1.29(0.18)	21.37(0.97)
Fe_2O_3	2.21(0.30)	7.19(0.06)	------	------	------
CaO	0.32(0.01)	0.27(0.02)	1.07(0.02)	41.54(0.20)	16.99(0.74)
SUM	100.72	99.78	99.00	102.37	99.40
CAT/OX	2/3	3/4	3/4	2/3	--
Mg	0.5721	0.8908	1.7297	0.0051	------
Si	0.0004	0.0020	0.9873	0.0008	------
Ti	0.9812	0.9096	0.0099	0.9907	------
Fe^{2+}	0.4019	1.0114	0.2473	0.0240	------
Fe^{3+}	0.0368	0.1769	------	------	------
Ca	0.0076	0.0094	0.0288	0.9879	------
SUM	2.0000	3.0001	3.0030	2.0085	------
#	4	4	3	5	9

is the number of analyses. IL=Ilmenite. OL=Olivine. USP=Ulvospinel. LQ=Glass. PEROV=Perovskite. Standard deviation in parentheses. Ferric iron calculated from assumed stoichiometry.

TABLE 4.9 ELECTRON MICROPROBE ANALYSES OF PHASES IN ASSEMBLAGE IL+USP+OL+PEROV+LQ AT $\log fO_2$=−7.0

	IL	USP	OL	PROVE	LQ
MgO	17.30(0.18)	18.25(0.26)	47.15(0.04)	0.17(0.02)	8.28(0.91)
SiO_2	0.02(0.01)	0.07(0.02)	39.77(0.16)	0.09(0.03)	18.77(0.56)
TiO_2	57.74(0.33)	33.73(0.08)	0.54(0.16)	59.15(0.07)	34.45(1.21)
FeO	20.71(0.54)	34.01(0.29)	10.72(0.04)	1.23(0.06)	21.06(0.80)
Fe_2O_3	4.39(0.45)	13.46(0.19)	------	------	------
CaO	0.31(0.04)	0.26(0.05)	0.98(0.03)	40.72(0.13)	17.02(0.85)
SUM	100.47	99.78	99.16	101.36	99.58
CAT/OX	2/3	3/4	3/4	2/3	--
Mg	0.5719	0.8918	1.7603	0.0058	------
Si	0.0004	0.0021	0.9844	0.0020	------
Ti	0.9630	0.8318	0.0101	0.9955	------
Fe^{2+}	0.3841	0.9329	0.2245	0.0231	------
Fe^{3+}	0.0733	0.3321	------	------	------
Ca	0.0074	0.0092	0.0263	0.9764	------
SUM	2.0001	2.9999	3.0056	2.0028	------
#	5	5	3	4	14

is the number of analyses. IL=Ilmenite. OL=Olivine. USP=Ulvospinel. LQ=Glass. PEROV=Perovskite. Standard deviation in parentheses. Ferric iron calculated from assumed stoichiometry.

TABLE 4.10 ELECTRON MICROPROBE ANALYSES OF PHASES IN ASSEMBLAGE IL+USP+OL+PEROV+LQ AT $\log fO_2$=-6.6

	IL	USP	OL	PROVE	LQ
MgO	18.85(0.11)	20.17(0.12)	48.72(0.11)	0.16(0.01)	7.48(0.78)
SiO_2	0.02(0.00)	0.09(0.00)	40.25(0.14)	0.05(0.01)	17.58(0.73)
TiO_2	57.46(0.17)	32.51(0.18)	0.73(0.16)	59.04(0.09)	37.22(1.31)
FeO	17.71(0.15)	29.81(0.12)	8.77(0.05)	1.29(0.09)	19.39(0.94)
Fe_2O_3	6.18(0.33)	16.53(0.20)	------	------	------
CaO	0.30(0.03)	0.28(0.03)	0.97(0.07)	41.09(0.10)	17.85(0.59)
SUM	100.42	99.39	99.44	101.63	99.54
CAT/OX	2/3	3/4	3/4	2/3	--
Mg	0.6168	0.9775	1.7973	0.0053	------
Si	0.0004	0.0030	0.9842	0.0011	------
Ti	0.9485	0.7948	0.0136	0.9924	------
Fe^{2+}	0.3251	0.8106	0.1815	0.0241	------
Fe^{3+}	0.1021	0.4045	------	------	------
Ca	0.0071	0.0097	0.0257	0.9836	------
SUM	2.0000	3.0001	3.0023	2.0065	------
#	4	3	4	5	8

is the number of analyses. IL=Ilmenite. OL=Olivine. USP=Ulvospinel. LQ=Glass. PEROV=Perovskite. Standard deviation in parentheses. Ferric iron calculated from assumed stoichiometry.

4.3. Bulk composition selection

In section 4.1, it has been discussed that the bulk compositions required to generate the invariant assemblages can be calculated from the compositions of the coexisting phases. The compositional overlapping feature of the invariant assemblages (***Figs. 4.1*** and ***4.2***) offers a possibility that the selected bulk compositions satisfy the assemblages at different oxygen fugacities. However, not all the overlapping compositions are of equal geological interest, and bulk compositions have been selected for recalculations that will give the best approximation of the natural rock compositions.

Due to the simplicity of the synthetic system in comparison to their natural counterparts, the approach to natural compositions is relatively crude. The absence of some important natural phases from the simple system, and the bulk composition constraints imposed by the requirement of being within the stability field of the invariant assemblages (as in ***Figs. 4.1*** and ***4.2***) cause some modal disproportion of the coexisting phases in the synthetic system compared to natural rock. This is particularly so, if the bulk composition selected is intended to satisfy the assemblages over a large range of oxygen fugacity.

The procedure followed involved, firstly, calculating a bulk composition from phase compositions of an assemblage at an arbitrarily chosen oxygen fugacity. Then, the calculated bulk composition was used in the mass balance equations (Section 4.4) to calculate the phase proportions of the same assemblage at different oxygen fugacities. If the calculated results showed that the selected bulk composition was within the stability field of the same invariant assemblage at various oxygen fugacities, then the selected bulk composition was successful. It is a trial and error process, and in practice, effort was to chose compositions with minimum TiO_2 and FeO (total iron as FeO) in order to closely simulate the geological situations (eg. mantle peridotite or oceanic crust).

4.4. Mass balance calculation

Obviously, mass balance can only be performed for the non-volatile components. Oxygen (treated as volatile) content of the charge is not constant as the result of changing oxygen fugacity. For convenience, the concerned components were calculated as MgO, CaO, FeO, SiO_2, and TiO_2.

Definition: r_i is the mole fraction of the component i in the bulk composition,

α_{ij} is mole fraction of the component i in the phase, j,

x_j is mole fraction of the phase j in the assemblage of a particular bulk composition.

Then, for n phase assemblage

$$\sum_{j=1}^{n} \alpha_{ij} x_j = r_i \qquad (4.1)$$

(i=1,K; K is the number of components involved)

In the case of Mg-Fe-Si-Ti-O system, without considering the oxygen, the mass balance involves four components in four coexisting phases, thus, equation 4.1 produces a set of four simultaneous linear algebraic equations. Similarly, in the system Mg-Ca-Fe-Si-Ti-O mass balance involves five components in five coexisting phases.

The mole fraction of component i in phase j, α_{ij}, is known from probe analyses of the charge. If the bulk composition, r_i, can be successfully selected (Section 4.3), the mole fraction of each phase in the charge can be calculated by solving the set of simultaneous equations.

Obviously, it is a straight forward calculation if only the averages of the probe analyses for the coexisting phases are used; however, such a calculation does not evaluate any error caused by the scatter in the probe analyses. In order to estimate

the precision and assure the confidence in calculated results, a linear least square regression scheme was used in the mass balance calculations. However, only the effect of the scatter in probe analyses of any one individual phase was evaluated by this procedure. The overall error is estimated from the summation of the errors caused by the different individual phases.

A linear regression program P1R in the statistic package BMDP available in the ERCC regional computing system was used in the calculation. Instead of using solely averages of the probe analyses, individual analyses of a phase concerned and averages of other phases were used as input. For example, in the system Mg-Fe-Si-Ti-O where four components are involved in the mass balance amongst four coexisting phases, if there are 10 probe analyses for the glass of a particular charge and the effect of their scatter are to be examined, individual analyses of the glass and averages of other phases are used in equation 4.1; therefore, instead of four, forty equations are generated. Then, the linear regression program P1R calculates the unknown x_j for the best fit of the forty equations, and the associated errors. Obviously, these errors are inherited from the probe analyses of the glass.

It was found that the calculated error was related not only to the error in probe analysis but also to the concentration of the phase concerned; phases with higher concentration contribute more to the induced error. Consequently, glass and olivine were particularly examined for their contribution to the error (tabulated in Tables 4.11 and 4.12), since the probe analyses of the glass showed relatively large scattering, and olivine was the major constituent of the charge. The small error caused by ilmenite and ulvospinel was not presented due to their small scatter in probe analyses and their accessory character in the charge. Data concerning the effect of oxygen fugacity on the relative quantity of each phase calculated from several selected bulk compositions have been listed in Table **4.11** (for system Mg-Fe-Si-Ti-O) and **4.12** (for system Mg-Fe-Ca-Si-Ti-O).

4.5. Oxidation melting

The calculated results from section 4.4 indicate that the oxidation state can strongly influence the degree of partial melting. If an extremely reduced starting composition is subject to oxidation, more melt is generated. The dissolution of olivine and ilmenite (and perovskite in Ca-bearing system) is the major response of these bulk compositions to oxidation. However, ulvospinels precipitate as the result of increase in oxygen fugacity in both systems. The mass redistribution of these bulk compositions into different phase proportions is remarkably more sensitive to the change of oxygen fugacity at relative oxidizing conditions (near NNO) than it is at reducing conditions.

The effect of change in oxygen fugacity on partial melting, solid dissolution and precipitation for the assemblage IL+USP+OL+LQ is shown in ***Fig. 4.8***, and that for the assemblage IL+USP+PEROV+OL+LQ in ***Fig. 4.9***. The influence of selecting different bulk compositions on the recalculations for the assemblage IL+USP+OL+LQ is illustrated in ***Fig. 4.10***. It may be seen that a similar pattern of change in melt proportion with oxygen fugacity is determined by the mass redistribution calculations for a range of bulk compositions.

TABLE 4.11 EFFECT OF OXYGEN FUGACITY AND BULK COMPOSITION ON RELATIVE QUANTITY OF EACH PHASE AND ERROR CAUSED BY PROBE ANALYSES

(In system Mg-Fe-Si-Ti-O)

BULK COMPOSITION: A

MgO 36.15 FeO 27.42 TiO_2 8.39 SiO_2 28.03

(ERROR DUE TO PROBE ANALYSES OF GLASS)

$logfO_2$	LQ	OL	IL	USP
-10.0	3.00(0.11)	81.99(0.05)	12.51(0.07)	2.49(0.10)
-9.0	6.19(0.13)	79.95(0.06)	11.75(0.09)	2.09(0.12)
-8.0	11.33(0.18)	75.99(0.08)	8.71(0.11)	3.95(0.14)
-7.0	19.82(0.19)	70.25(0.08)	5.04(0.12)	4.89(0.13)
-6.6	27.05(0.50)	64.63(0.22)	1.85(0.38)	6.46(0.37)

(ERROR DUE TO PROBE ANALYSES OF OLIVINE)

$logfO_2$	LQ	OL	IL	USP
-10.0	3.01(0.33)	82.00(0.14)	12.50(0.21)	2.50(0.30)
-9.0	6.32(0.63)	79.90(0.29)	11.75(0.40)	2.02(0.55)
-8.0	11.49(0.56)	75.93(0.26)	8.69(0.36)	3.88(0.44)
-7.0	19.88(0.39)	70.22(0.17)	5.02(0.25)	4.87(0.28)
-6.6	27.24(0.28)	64.57(0.13)	1.79(0.21)	6.41(0.21)

Bulk composition in mole percent. Numbers in parentheses are standard deviations associated with the range of probe analyses of glass and olivine from the pertinent experimental charges. These errors calculated only for glass and olivine (see text) and give two tabulations for each bulk composition.

TABLE 4.11 (Cont.)

BULK COMPOSITION: B

MgO 37.11 FeO 26.82 TiO_2 7.77 SiO_2 28.30

(ERROR DUE TO PROBE ANALYSES OF GLASS)

$logfO_2$	LQ	OL	IL	USP
-9.0	2.95(0.06)	83.02(0.03)	12.00(0.04)	2.03(0.06)
-8.0	8.24(0.13)	79.01(0.06)	8.98(0.08)	3.77(0.10)
-7.0	16.74(0.16)	73.21(0.07)	5.11(0.10)	4.94(0.11)
-6.6	24.33(0.45)	67.41(0.20)	1.75(0.34)	6.50(0.33)

(ERROR DUE TO PROBE ANALYSES OF OLIVINE)

$logfO_2$	LQ	OL	IL	USP
-9.0	3.03(0.66)	82.98(0.30)	12.00(0.42)	1.99(0.58)
-8.0	8.36(0.59)	78.96(0.27)	8.96(0.38)	3.71(0.46)
-7.0	16.79(0.42)	73.18(0.18)	5.10(0.26)	4.92(0.30)
-6.6	24.49(0.30)	67.35(0.13)	1.70(0.22)	6.45(0.21)

BULK COMPOSITION: C

MgO 38.70 FeO 25.53 TiO_2 7.07 SiO_2 28.71

(ERROR DUE TO PROBE ANALYSES OF GLASS)

$logfO_2$	LQ	OL	IL	USP
-8.0	2.97(0.04)	84.01(0.02)	11.00(0.03)	2.01(0.03)
-7.0	11.46(0.12)	78.13(0.06)	6.82(0.08)	3.59(0.09)
-6.6	19.53(0.36)	72.12(0.16)	3.35(0.27)	5.00(0.26)

TABLE 4.11 (Cont.)

(ERROR DUE TO PROBE ANALYSES OF OLIVINE)

$\log fO_2$	LQ	OL	IL	USP
−8.0	3.02(0.62)	83.99(0.29)	11.00(0.40)	1.99(0.49)
−7.0	11.50(0.44)	78.12(0.20)	6.81(0.28)	3.58(0.31)
−6.6	19.66(0.31)	72.08(0.14)	3.30(0.23)	4.96(0.22)

BULK COMPOSITION: D

MgO 41.56 FeO 23.38 TiO_2 5.38 SiO_2 29.68

(ERROR DUE TO PROBE ANALYSES OF GLASS)

$\log fO_2$	LQ	OL	IL	USP
−7.0	2.99(0.07)	87.00(0.04)	8.00(0.05)	2.00(0.03)
−6.6	12.02(0.23)	80.52(0.10)	4.04(0.17)	3.41(0.17)

(ERROR DUE TO PROBE ANALYSES OF OLIVINE)

$\log fO_2$	LQ	OL	IL	USP
−7.0	3.01(0.49)	86.99(0.22)	8.00(0.31)	2.00(0.34)
−6.6	12.10(0.35)	80.49(0.16)	4.02(0.27)	3.39(0.26)

TABLE 4.12 EFFECT OF OXYGEN FUGACITY AND BULK COMPOSITION ON RELATIVE QUANTITY OF EACH PHASE AND ERROR CAUSED BY PROBE ANALYSES

(in system Mg-Fe-Ca-Ti-Si-O)

BULK COMPOSITION:

MgO 47.59 FeO 11.21 TiO_2 10.06 SiO_2 26.42 CaO 4.72

(ERROR DUE TO PROBE ANALYSES OF GLASS)

$logfO_2$	LQ	OL	IL	USP	PROVE
-10.0	3.25(0.39)	77.65(0.14)	8.41(0.35)	4.23(0.38)	6.46(0.22)
-9.0	3.56(0.19)	77.86(0.07)	9.32(0.15)	2.79(0.17)	6.48(0.10)
-8.0	7.98(0.33)	75.02(0.12)	7.67(0.26)	4.48(0.28)	4.86(0.18)
-7.0	11.35(0.27)	73.06(0.10)	7.39(0.20)	4.49(0.21)	3.72(0.15)
-6.6	17.18(0.24)	70.00(0.08)	4.22(0.18)	7.55(0.18)	1.06(0.14)

(ERROR DUE TO PROBE ANALYSES OF OLIVINE)

$logfO_2$	LQ	OL	IL	USP	PROVE
-10.0	3.11(0.13)	77.69(0.05)	8.37(0.12)	4.30(0.13)	6.53(0.07)
-9.0	3.47(0.09)	77.88(0.08)	9.30(0.07)	2.83(0.08)	6.52(0.05)
-8.0	7.84(0.19)	75.05(0.07)	7.64(0.15)	4.55(0.16)	4.93(0.10)
-7.0	11.11(0.21)	73.12(0.08)	7.34(0.16)	4.59(0.16)	3.83(0.12)
-6.6	16.85(0.40)	70.07(0.14)	4.18(0.30)	7.67(0.30)	1.21(0.23)

Bulk composition in mole percent. Numbers in parentheses are standard deviations associated with the range of probe analyses of glass and olivine from the pertinent experimental charges. These errors calculated only for glass and olivine (see text) and give two tabulations for the selected bulk composition.

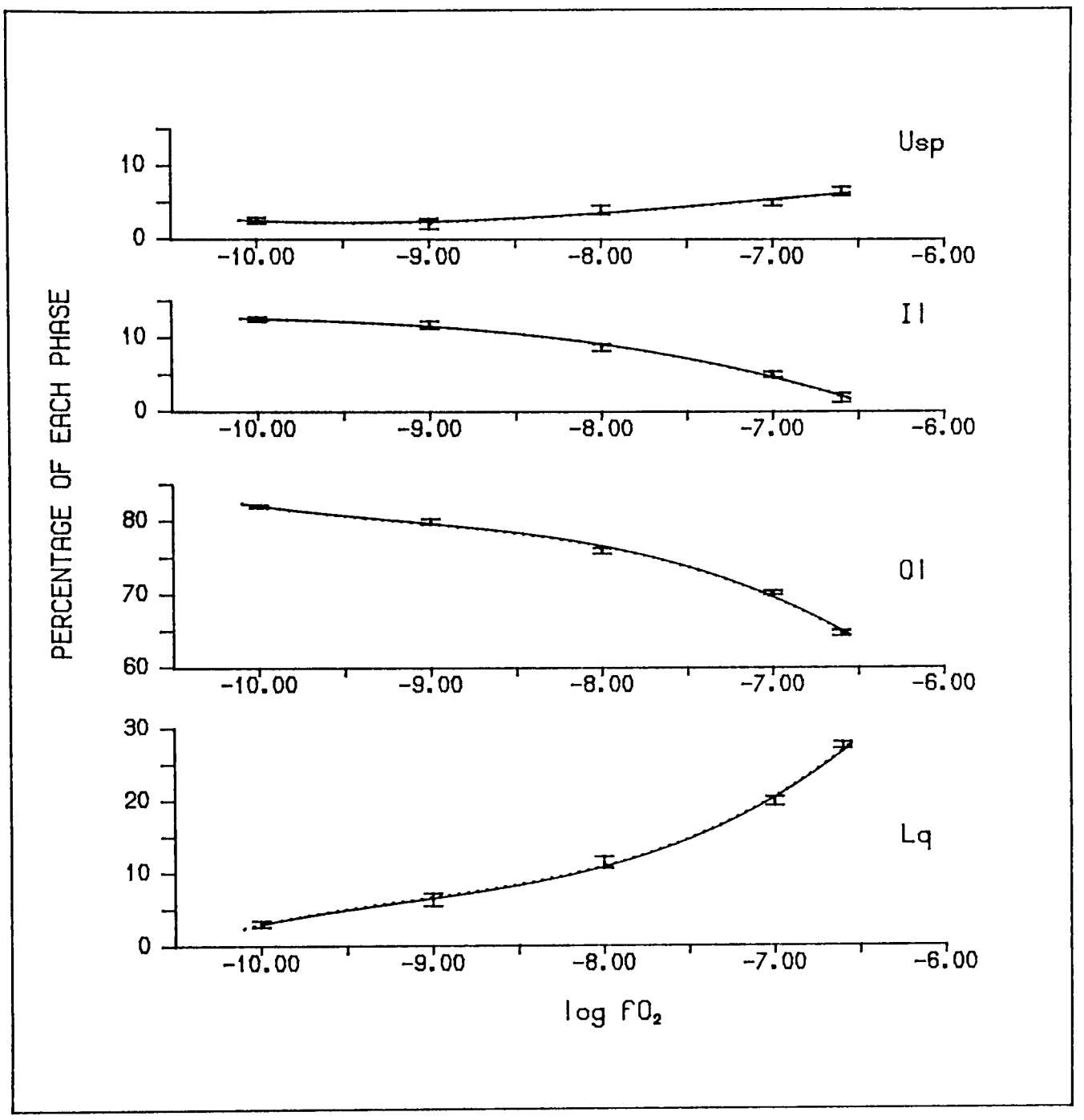

Fig. 4.8 *'Mole' fraction of each phase as function of oxygen fugacity in the system Mg-Fe-Si-Ti-O. Bulk composition: A (*Table 4.11*). Curves are plotted from a 3-degree polynomial regression. Solid line represents data calculated with individual glass analyses as input, dotted line with individual olivine analyses as input. The plots from the two calculation schemes are almost undistinguishable. Error bars are plotted from the means of the two calculation schemes (eg.* 0.5•(3.00+3.01) *in* **Table 4.11**, *bulk composition A, column LQ, log* fO_2 *= -10) to the sum of one half of the difference between the results of the two calculation schemes (i.e.* 0.5•(3.01−3.00)*) and both of the standard errors inherited from the probe analyses of glass (*0.11*) and olivine (0.33).*

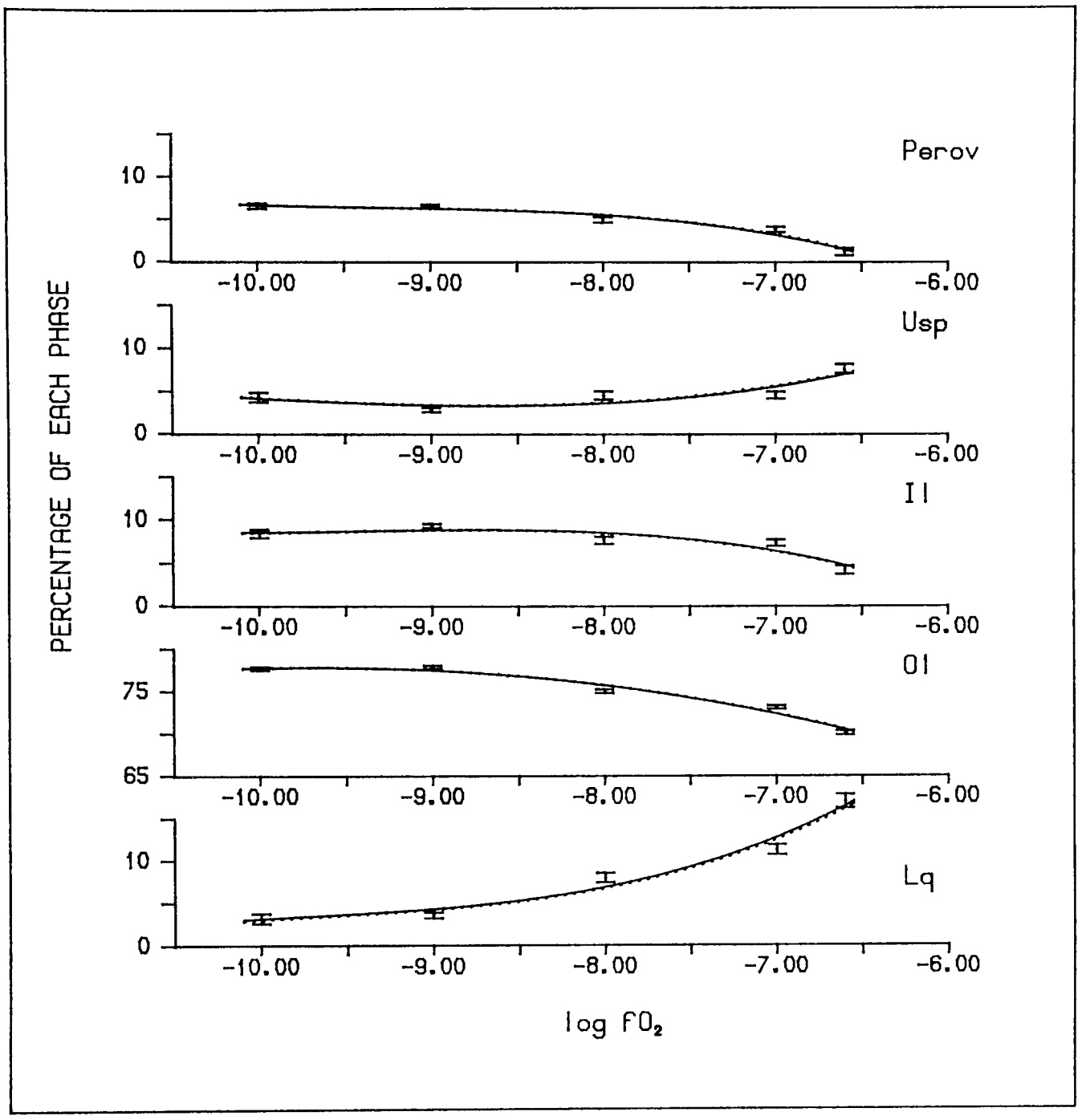

Fig. 4.9 *'Mole' fraction of each phase as function of oxygen fugacity in the system Mg-Fe-Ca-Si-Ti-O. Bulk composition as in* Table 4.12. *Curves are plotted from a 3-degree polynomial regression. Solid line represents data calculated with individual glass analyses as input, dotted line with individual olivine analyses as input. The plots from the two calculation schemes are almost undistinguishable. Error bars are plotted from the means of the two calculation schemes to the sum of one half of the difference between the results of the two calculation scheme and both of the standard errors inherited from the probe analyses of glass and olivine.*

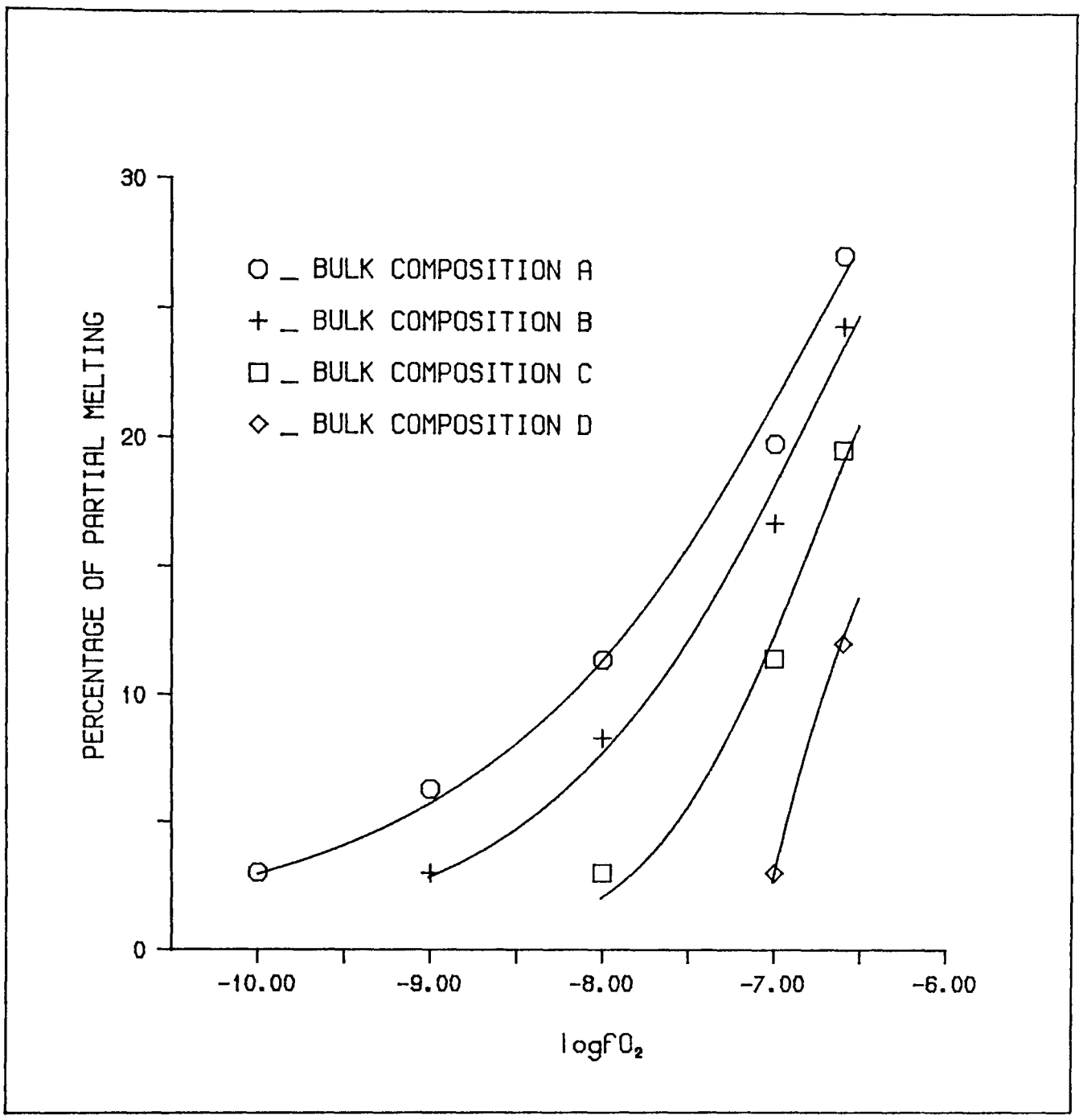

Fig. 4.10 *Effect of bulk composition on partial melting illustrated by comparing a few bulk compositions. A,B,C and D are corresponding bulk compositions in* Table 4.11. *Another data point at more oxidizing condition is included in the regression of data from C and D (see Chapter 5).*

CHAPTER 5

REDUCTION MELTING

It has been shown in Chapter 4 that changes in oxygen fugacity can cause significant changes in mass distribution, and that oxidation of a relatively reduced chemical system with bulk compositions analogous to rock samples can result in partial melting. The oxygen fugacity range covered in the discussion of Chapter 4 is from low, near WM to moderate, NNO.

Although oxygen fugacities near NNO seem appropriate for many basic magmas, some evidence suggests that conditions 2-3 log fO_2 units higher than NNO exists in arc volcanism (eg. Arculus and Wills, 1980; Conrad and Kay, 1984). However, the oxidation state of arc volcanism remains uncertain, with debate on the extent to which the observed highly oxidizing conditions should be attributed to high level or surfacial oxidation during magma ascent or eruption. It is possible that the relatively oxidized character of the calc-alkaline series rocks are inherited from the highly oxidized subducted oceanic crust, and that arc volcanism probably involves partial fusion which is accompanied by the reduction of the subducted crust. There may be situations in which part of the subducted oceanic crust undergoes little reduction in the trench-arc region, and therefore, the oxidation state associated with it remains highly oxidizing. Thus answering the question on the effect of change in oxygen fugacity on partial melting at oxidizing conditions above NNO is geologically meaningful.

Reduction melting (i.e. the generation of melt by reduction in oxygen fugacity or oxygen content) has been exemplified in the simplified system Fe-Si-O (at relatively oxidizing conditions) in Chapter 1. In the more complicated system Mg-Fe-Si-Ti-O with compositions analogous to rock compositions, common existing solid solutions IL_{ss}, USP_{ss}, and OL_{ss} replace simple end member mineral compositions, and the response to change in oxygen fugacity involves changes in the composition of these phases.

From the physico-chemical viewpoint, there is no arbitrary boundary between oxidizing and reducing. Although, literally, oxidation melting and reduction melting are two oppositely contrasting concepts or results, the basic thermodynamic principles concerning the effect of change in oxygen fugacity on the compositions of individual phases are common to both. This chapter is virtually an extension of Chapter 4, and the division between them is basically for the convenience of discussion, emphasizing the different consequences of change in oxygen fugacity. Some data presented in chapter 4 are also plotted in Figures in this chapter to show the overall continuity of the data.

5.1. Phase relationships

General phase relationships in system Mg-Fe-Si-Ti-O have been discussed in Chapters 2 and 3 where most of the discussion was restricted to relatively reducing conditions (<NNO). At higher oxygen fugacities, a ternary solvus is encountered in the rhombohedral solid solutions at Mg-rich compositions (***Fig. 3.1***, ***Fig. 5.1***). This solvus has been determined by Woermann *et al.* (1969b), and a zone or a `band` of IL+USP+PSB assemblage was shown to represent its possible position (***Fig. 5.1***). Because the experimental technique of Woermann *et al.* (1969b) was not given a detailed discussion (Chapter 6), it is not known whether `band` P (***Fig. 5.1***) represents the compositions of ilmenite or the starting bulk compositions of the experiments. If `band` P represents the compositions of ilmenite, then, curve Q may represent the true position of the solvus. If `band` P represents the bulk compositions of experiments, then curve P represents the solvus, and curve Q represents the intersection of line `DG` (cf Woermann *et al.*, 1969b) with the IL-GK-HM plane (***Fig. 3.1***). Thus, the `band` determined by Woermann *et al.* (1969b) represents either the likelihold of a metastable IL+USP+PSB assemblage at near solvus conditions, or the bulk compositions for generating the IL+USP+PSB assemblage in their experiments.

Ideally, the univariant assemblage IL+USP+PSB in the system Mg-Fe-Ti-O (at fixed P and T) represents a curve (if ilmenite compositions are plotted on to the

IL-GK-HM plane). In the system Mg-Fe-Si-Ti-O, the univariant assemblage IL+USP+OL+LQ (at fixed P and T) also represents a curve (if ilmenite compositions are plotted) (***Fig. 3.1***, curve ABC on the surface ABCDEF; ***Fig. 3.2***, curve AB; ***Fig. 5.1*** curve ABC). Due to the low solubility of silica in all the coexisting oxides, the oxides, in this situation, can be conveniently regarded as in a subsystem independent of silicate and melt, thus, the position of the univariant solvus curve is not expected to be significantly displaced in the Si-bearing system. The intersection of these two univariant curves (IL+USP+OL+LQ represented by curve ABC in ***Fig. 5.1*** and ***3.1***; and the solvus represented by region P in ***Fig. 5.1***), possibly generates two invariant assemblages, IL+USP+OL+LQ+PSB and HM+USP+OL+LQ+PSB at two specific corresponding oxygen fugacities (***Fig 3.1***) at 1300°C and 1atm.

In this study, three experiments were carried out in the system Mg-Fe-Ti-Si-O, to continue the investigation of the melting processes at relatively oxidizing conditions. Amongst them, two produced the invariant (at fixed P and T) assemblage IL+USP+OL+LQ+PSB (***Fig. 3.1, 5.1***, and Table 5.2, 5.3). Obviously, the ilmenites produced in these two experiments are within the reported `band` of Woermann *et al.* (1969b). No attempt was made to clarify whether the assemblages represent a metastable state or a true intersection with the solvus. It is taken as granted that the composition relationship amongst coexisting phases is valid.

5.2. Phase composition and oxygen fugacity

The detailed relationships between oxygen fugacity and phase compositions at more oxidizing conditions are similar to those described in chapter 4 for lower oxidizing conditions. Olivine shows a continuous increase in forsterite content(***Fig 5.2***), ilmenite in haematite (***Fig. 5.1***), and ulvospinel in magnetite and magnesian ferrite contents, with increase in oxygen fugacity. Where present,the pseudobrookite also becomes ferric rich with increase in oxygen fugacity. In comparison to experiments at relatively reducing conditions, the glass composition shows a much stronger dependence on

oxygen fugacity conditions. There is a significant increase in Mg and Si, and decrease in Fe and Ti in the melt with increase in oxygen fugacity (***Fig 5.3***). Data concerning the phase composition relationship with oxygen fugacity is listed in Table 5.1-5.3.

5.3. Mass balance calculation and results

Without specifying oxygen content in the assemblage IL+USP+PSB+OL+LQ, it is impossible to calculate the proportions of the coexisting phases with the calculation procedure stated in Chapter 4, since the stated procedure calculates the mass distribution of four component amongst four phases. Furthermore, although the oxygen fugacity of this assemblage is fixed at fixed P and T, the actual oxygen content in this assemblage can vary within a certain limit, and thus affect the proportions of the coexisting phases (oxygen buffering effect). Therefore, mass balance calculations in the 5-phase assemblage, if possible, is to examine the possible range of the proportions of the coexisting phases.

For mass balance calculation, the 5-phase assemblage, IL+USP+PSB+OL+LQ, may be divided into 5 four phase assemblages, ie, IL+USP+OL+LQ, USP+PSB+OL+LQ, IL+PSB+OL+LQ , IL+USP+PSB+LQ, and IL+USP+PSB+OL which define the compositional boundary conditions. The last two assemblages of the above are obviously not closely relevant to the melting study (OL-out and LQ-out). Similarly, the assemblage IL+PSB+OL+LQ is more Ti-rich than the range of bulk compositions experimentally investigated before (**Chapter 4**). Therefore, the two assemblages IL+USP+OL+LQ and USP+PSB+OL+LQ were used in calculations to examine the effects of change in oxygen fugacity on partial melting.

TABLE 5.1 ELECTRON MICROPROBE ANALYSES OF PHASES IN ASSEMBLAGE IL+USP+OL+LQ AT log fO_2 = −6.1

	IL	USP	OL	LQ
MgO	6.32(0.14)	7.82(0.08)	30.26(0.09)	9.47(0.09)
SiO_2	0.02(0.01)	0.16(0.01)	36.46(0.15)	22.87(0.69)
TiO_2	42.96(0.26)	24.02(0.18)	0.72(0.16)	23.36(0.47)
FeO	27.40(0.28)	41.33(0.20)	32.33(0.12)	42.47(0.36)
Fe_2O_3	22.32(0.10)	25.95(0.26)	------	------
SUM	99.02	99.28	99.77	98.17
CAT/OXY	2/3	3/4	3/4	--
Mg	0.2313	0.4164	1.5122	------
Si	0.0005	0.0058	0.9803	------
Ti	0.7932	0.6454	0.0103	------
Fe^{2+}	0.5626	1.2349	0.5067	------
Fe^{3+}	0.4124	0.6976	------	------
SUM	2.0000	3.0001	3.0095	------
#	4	4	4	6

is the number of analyses. IL=Ilmenite. OL=Olivine. USP=Ulvospinel. LQ=Glass. Standard deviation in parentheses. Ferric iron calculated from assumed stoichiometry. Ferric content in glass not determined, total iron calculated as FeO.

TABLE 5.2 ELECTRON MICROPROBE ANALYSES OF PHASES IN ASSEMBLAGE IL+USP+OL+PSB+LQ AT log fO_2 = −5.9

	IL	USP	OL	PSB	LQ
MgO	6.21(0.17)	7.80(0.10)	39.09(0.19)	6.65(0.08)	9.67(0.30)
SiO_2	0.02(0.01)	0.18(0.01)	37.97(0.32)	0.10(0.01)	24.43(1.27)
TiO_2	41.14(0.20)	22.03(0.14)	0.53(0.13)	60.30(0.10)	21.83(1.02)
FeO	25.94(0.20)	39.42(0.31)	22.28(0.31)	10.56(0.12)	42.02(0.80)
Fe_2O_3	25.59(0.27)	29.47(0.21)	------	21.18(0.11)	------
SUM	98.90	98.90	99.87	98.79	97.95
CAT/OX	2/3	3/4	3/4	3/5	--
Mg	0.2281	0.4176	1.5260	0.3711	------
Si	0.0005	0.0064	0.9827	0.0036	------
Ti	0.7623	0.5953	0.0104	1.6980	------
Fe^{2+}	0.5346	1.1842	0.4879	0.3306	------
Fe^{3+}	0.4745	0.7966	------	0.5967	------
SUM	2.0000	3.0001	3.0070	3.0000	------
#	6	3	5	4	14

is the number of analyses. IL=Ilmenite. OL=Olivine. USP=Ulvospinel. LQ=Glass. PSB=Pseudobrookite. Standard deviation in paretheses. Ferric iron calculated from assumed stoichiometry. Ferric content in glass not calculated, total iron expressed as FeO.

TABLE 5.3 ELECTRON MICROPROBE ANALYSES OF PHASES IN ASSEMBLAGE IL+USP+OL+PSB+LQ AT $\log fO_2$=−5.3

	IL	USP	OL	PSB	LQ
MgO	6.06(0.07)	7.84(0.12)	39.62(0.09)	6.30(0.10)	10.95(0.24)
SiO_2	0.02(0.01)	0.17(0.03)	38.52(0.08)	0.09(0.01)	28.59(1.95)
TiO_2	39.16(0.46)	19.53(0.03)	0.50(0.13)	59.28(0.45)	19.10(1.25)
FeO	24.43(0.45)	36.94(0.10)	21.06(0.24)	10.18(0.11)	39.82(0.81)
Fe_2O_3	29.36(0.64)	34.24(0.47)	------	23.52(0.37)	------
SUM	99.03	98.72	99.70	99.37	98.46
CAT/OX	2/3	3/4	3/4	3/5	--
Mg	0.2229	0.4216	1.5491	0.3510	------
Si	0.0005	0.0059	0.9842	0.0031	------
Ti	0.7269	0.5295	0.0104	1.6666	------
Fe^{2+}	0.5043	1.1139	0.4618	0.3182	------
Fe^{3+}	0.5453	0.9292	------	0.6616	------
SUM	1.9999	3.0001	3.0055	2.9999	------
#	5	3	4	2	5

is the number of analyses. IL=Ilmenite. OL=Olivine. USP=Ulvospinel. LQ=Glass. PSB=Pseudobrookite. Standard deviation in parentheses. Ferric iron calculated from assumed stoichiometry. Ferric content in glass not calculated, total iron expressed as FeO.

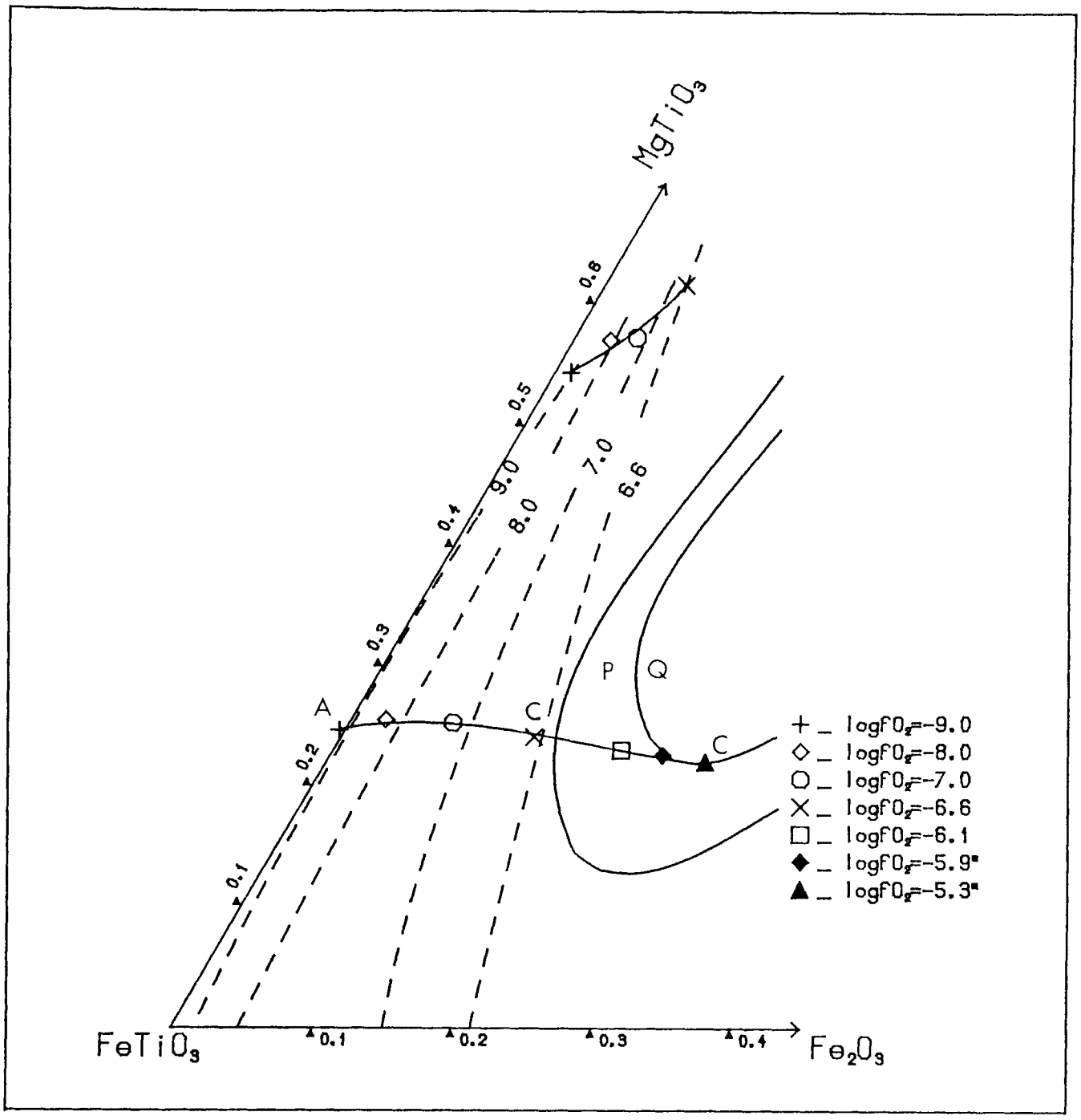

Fig. 5.1 *Composition of ilmenite at different oxygen fugacities (1300°C and 1atm). Solid line (lower, ABC; see also* ***Fig. 3.1****) for univariant assemblage IL+USP+OL+LQ in system Mg-Fe-Si-Ti-O; solid line (upper) for univariant assemblage IL+USP+OL+PEROV+LQ in system Mg-Fe-Ca-Si-Ti-O (same as* ***Fig. 4.3****) Dashed lines for oxygen partial pressure contours determined from an independent set of experiments (see Chapter 3). The two solid curves P and Q are adopted from Woermann et al. (1969b) represent the ternary solvus: P the IL+USP+PSB coexisting region, Q the USP+PSB region. Solid symbols represent compositions of ilmenite in the invariant assemblage IL+USP+PSB+OL+LQ at two specific oxygen fugacities, thus represent the intersection of the univariant curve ABC with the solvus. Analytical error is smaller than the symbols. The ilmenite composition of log* fO_2 *- -6.1 is in discrepancy with the result of Woermann et al. (1969).*

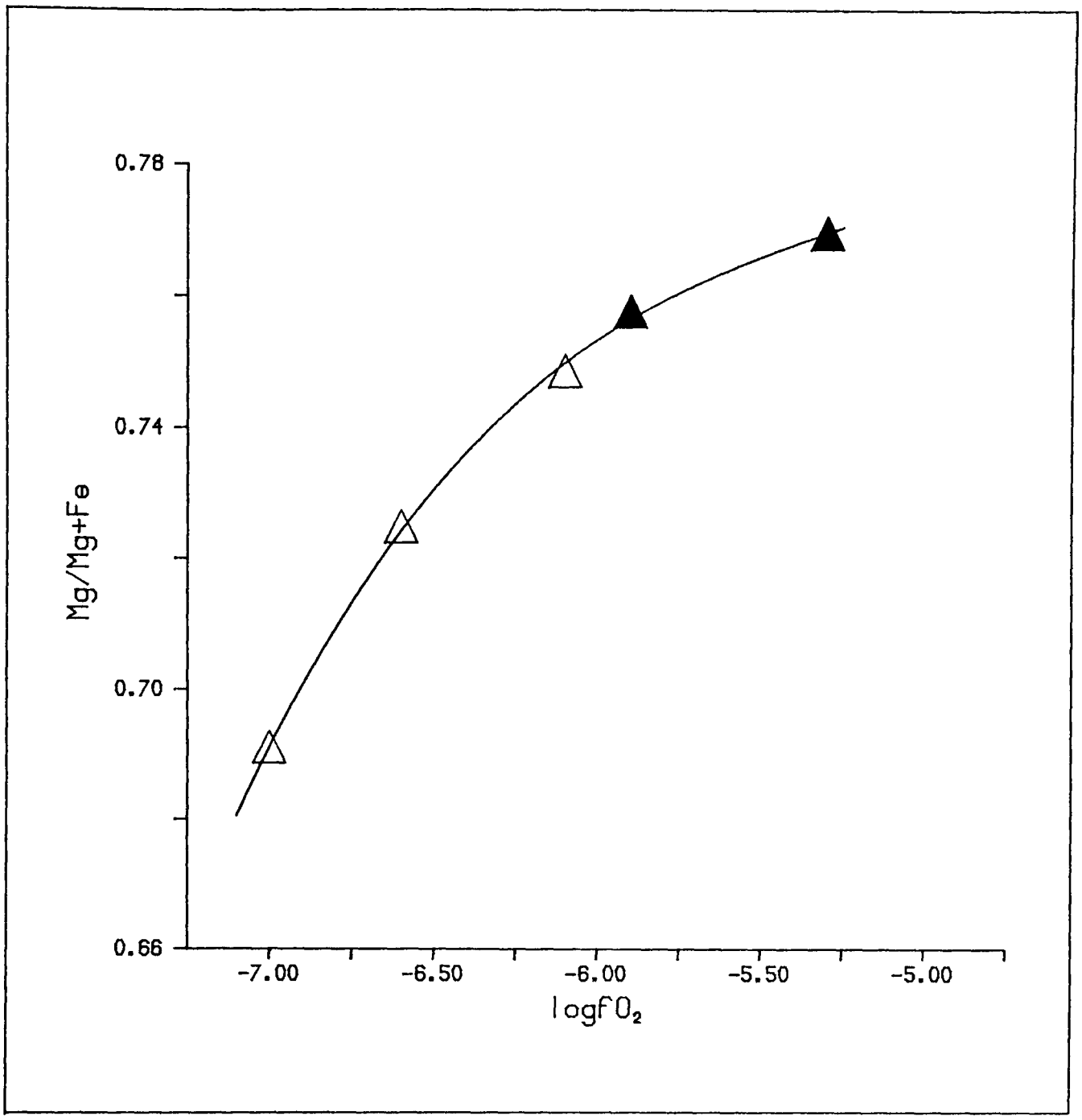

Fig. 5.2 *Effect of oxygen fugacity on olivine compositions. Solid symbols for olivines in the assemblage IL+USP+OL+PSB+LQ, blank for IL+USP+OL+LQ. Curve is drawn from a 3-degree polynomial regression. Error smaller than symbols.*

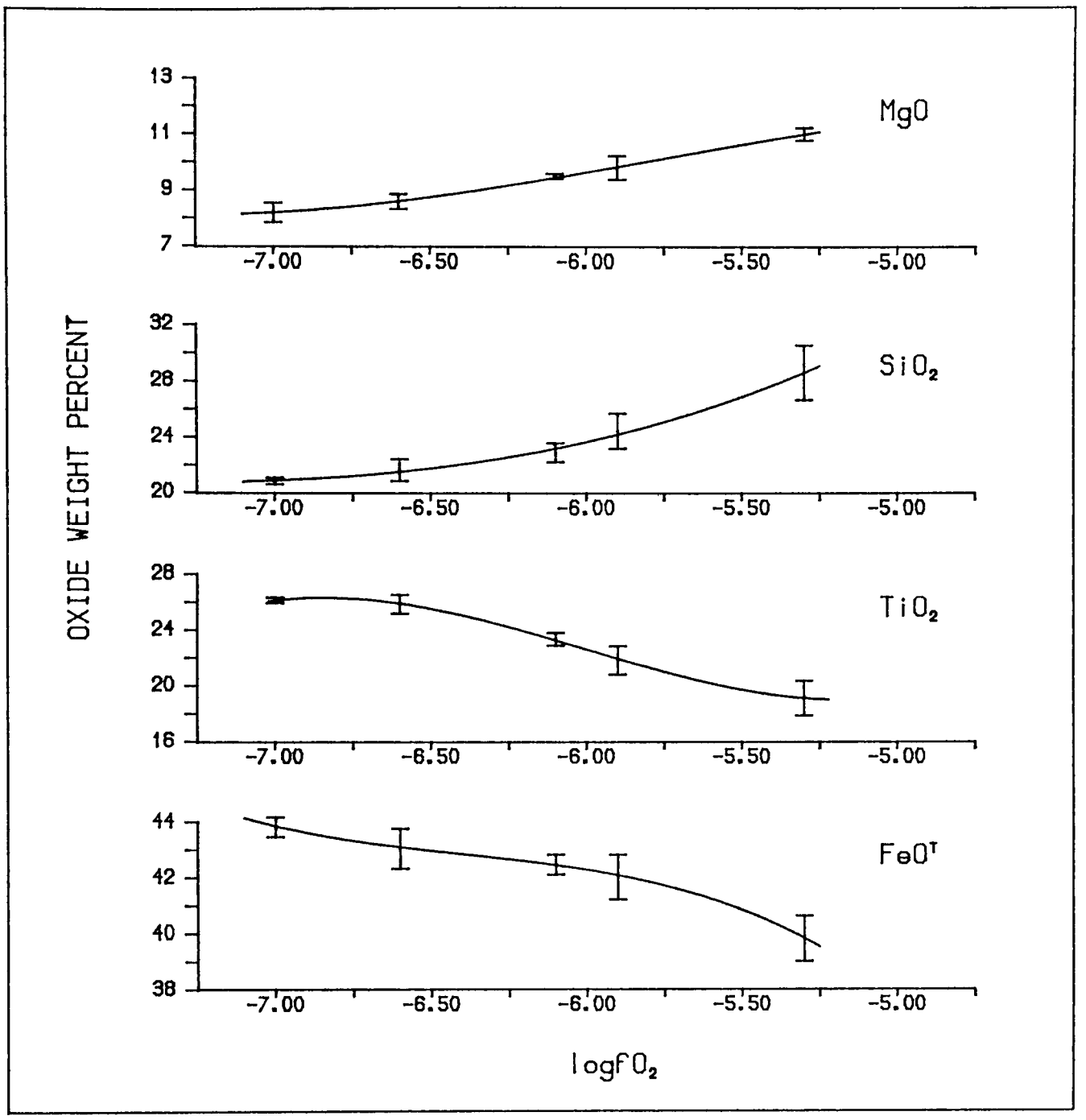

Fig. 5.3 *Effect of oxygen fugacity on the composition of glass. At relatively oxidizing condition, the compositional trend is much more obvious than at reducing conditions (**Fig. 4.6**). Error bars are standard deviations.*

Such calculations give the result of two extreme situations, ie. either ilmenite or pseudobrookite is absent. and the results will define the limit of melt production of the IL+USP+PSB+OL+LQ assemblage.

The calculation procedure is the same as in Chapter 4. In order to keep the continuity in observation, bulk compositions selected in Chapter 4 are used here again, and therefore, data derived from the calculations in Chapter 4 are easily compared with the data analyses in this chapter. The calculated results for assemblage IL+USP+OL+LQ are listed in Table 5.4 and plotted in ***Fig. 5.4-5.6***, and for assemblage USP+PSB+OL+LQ, are listed in Table 5.5. It is shown by the Tables that change of oxide assemblage in the system does not significantly influence the quantities of melt and olivine but only the proportions of oxides.

5.4. Reduction melting

Combining the above data with the calculated results from Chapter 4, it is apparent that, as oxygen fugacity increases, a maximum in the degree of partial melting is encountered. For a given bulk composition, increase in oxygen fugacity beyond about log fO_2 = -6 results in the quantity of melt decreasing as the result of precipitation of oxides. Therefore, if highly oxidized (log fO_2 > -6) material of appropriate bulk composition is reduced (at constant P and T), partial melting will result.

TABLE 5.4 EFFECT OF OXYGEN FUGACITY AND BULK COMPOSITION ON RELATIVE QUANTITY OF EACH PHASE AND ERROR CAUSED BY PROBE ANALYSES (IL+USP+OL+LQ)

BULK COMPOSITION: A
MgO 36.15 FeO 27.42 TiO_2 8.39 SiO_2 28.03

(ERROR DUE TO PROBE ANALYSES OF GLASS)

$logfO_2$	LQ	OL	IL	USP
-6.1	32.51(0.41)	60.08(0.19)	1.63(0.34)	5.78(0.31)
-5.9	31.21(0.45)	59.31(0.22)	3.48(0.40)	5.97(0.35)
-5.3	28.32(0.88)	57.61(0.50)	7.08(0.85)	6.95(0.74)

(ERROR DUE TO PROBE ANALYSES OF OLIVINE)

$logfo_2$	LQ	OL	IL	USP
-6.1	32.74(0.30)	60.03(0.14)	1.33(0.25)	5.90(0.23)
-5.9	31.55(0.29)	59.18(0.14)	3.36(0.26)	5.91(0.23)
-5.3	28.76(0.19)	57.41(0.11)	6.92(0.18)	6.90(0.16)

BULK COMPOSITION: B
MgO 37.11 FeO 26.82 TiO_2 7.77 SiO_2 28.30

(ERROR DUE TO PROBE ANALYSES OF GLASS)

$logfO_2$	LQ	OL	IL	USP
-6.1	30.07(0.31)	62.80(0.15)	1.07(0.26)	6.05(0.24)
-5.9	28.94(0.42)	61.99(0.21)	2.75(0.37)	6.30(0.33)
-5.3	26.30(0.82)	60.29(0.46)	6.03(0.79)	7.35(0.68)

(ERROR DUE TO PROBE ANALYSES OF OLIVINE)

$logfO_2$	LQ	OL	IL	USP
-6.1	30.25(0.30)	62.76(0.14)	0.84(0.25)	6.15(0.22)
-5.9	29.26(0.30)	61.87(0.15)	2.63(0.27)	6.24(0.24)
-5.3	26.71(0.18)	60.11(0.10)	5.88(0.17)	7.30(0.15)

Bulk composition in mole percent. Numbers in parentheses are standard deviations associated with the range of probe analyses of glass and olivine from pertinent experimental charges. These errors calculated only for glass and olivine (see chapter 4) and give two tabulations for each bulk composition.

TABLE 5.4 (Cont.)

BULK COMPOSITION: C

MgO 38.70 FeO 25.53 TiO_2 7.07 SiO_2 28.71

(ERROR DUE TO PROBE ANALYSES OF GLASS)

$logfO_2$	LQ	OL	IL	USP
-6.1	25.69(0.27)	67.45(0.13)	2.13(0.22)	4.72(0.20)
-5.9	24.89(0.36)	66.58(0.18)	3.44(0.32)	5.08(0.28)
-5.3	22.70(0.71)	64.90(0.40)	6.12(0.68)	6.24(0.59)

(ERROR DUE TO PROBE ANALYSES OF OLIVINE)

$logfO_2$	LQ	OL	IL	USP
-6.1	25.82(0.34)	67.45(0.16)	1.95(0.28)	4.80(0.25)
-5.9	25.16(0.32)	66.48(0.16)	3.34(0.29)	5.03(0.25)
-5.3	23.02(0.22)	64.77(0.12)	6.02(0.20)	6.20(0.18)

BULK COMPOSITION:D

MgO 41.56 FeO 23.38 TiO_2 5.38 SiO_2 29.68

(ERROR DUE TO PROBE ANALYSES OF GLASS)

$logfO_2$	LQ	OL	IL	USP
-6.1	18.90(0.20)	75.69(0.09)	1.63(0.17)	3.78(0.15)
-5.9	18.71(0.27)	74.63(0.13)	2.22(0.24)	4.43(0.21)
-5.3	17.16(0.53)	72.98(0.30)	3.95(0.51)	5.89(0.44)

(ERROR DUE TO PROBE ANALYSES OF OLIVINE)

$logfO_2$	LQ	OL	IL	USP
-6.1	19.08(0.36)	75.66(0.17)	1.48(0.36)	3.84(0.27)
-5.9	18.92(0.36)	74.55(0.18)	2.14(0.32)	4.39(0.28)
-5.3	17.43(0.22)	72.86(0.12)	3.86(0.21)	5.86(0.18)

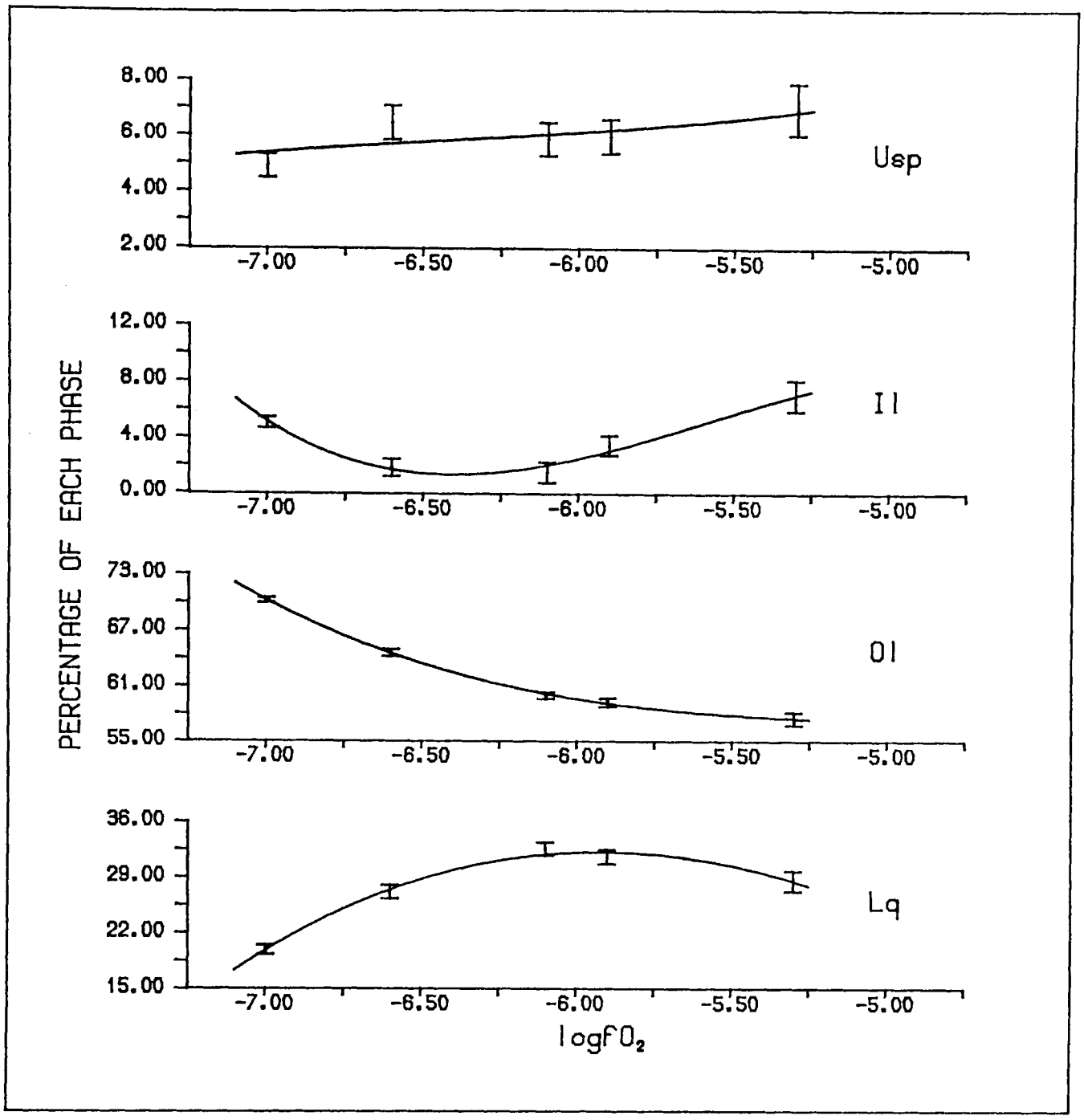

Fig. 5.4 *"Mole" percentage of each phase as function of oxygen fugacity in the system Mg-Fe-Si-Ti-O for bulk composition A* (Table 5.4). *Curves are plotted from polynomial regressions. Error bars are plotted from the means of the two calculation schemes (with individual glass analyses as input and olivine analyses as input) to the sum of one half of the difference between the results of the two calculations and both of the standard errors inherited from the probe analyses of glass and olivine (see section 4.4).*

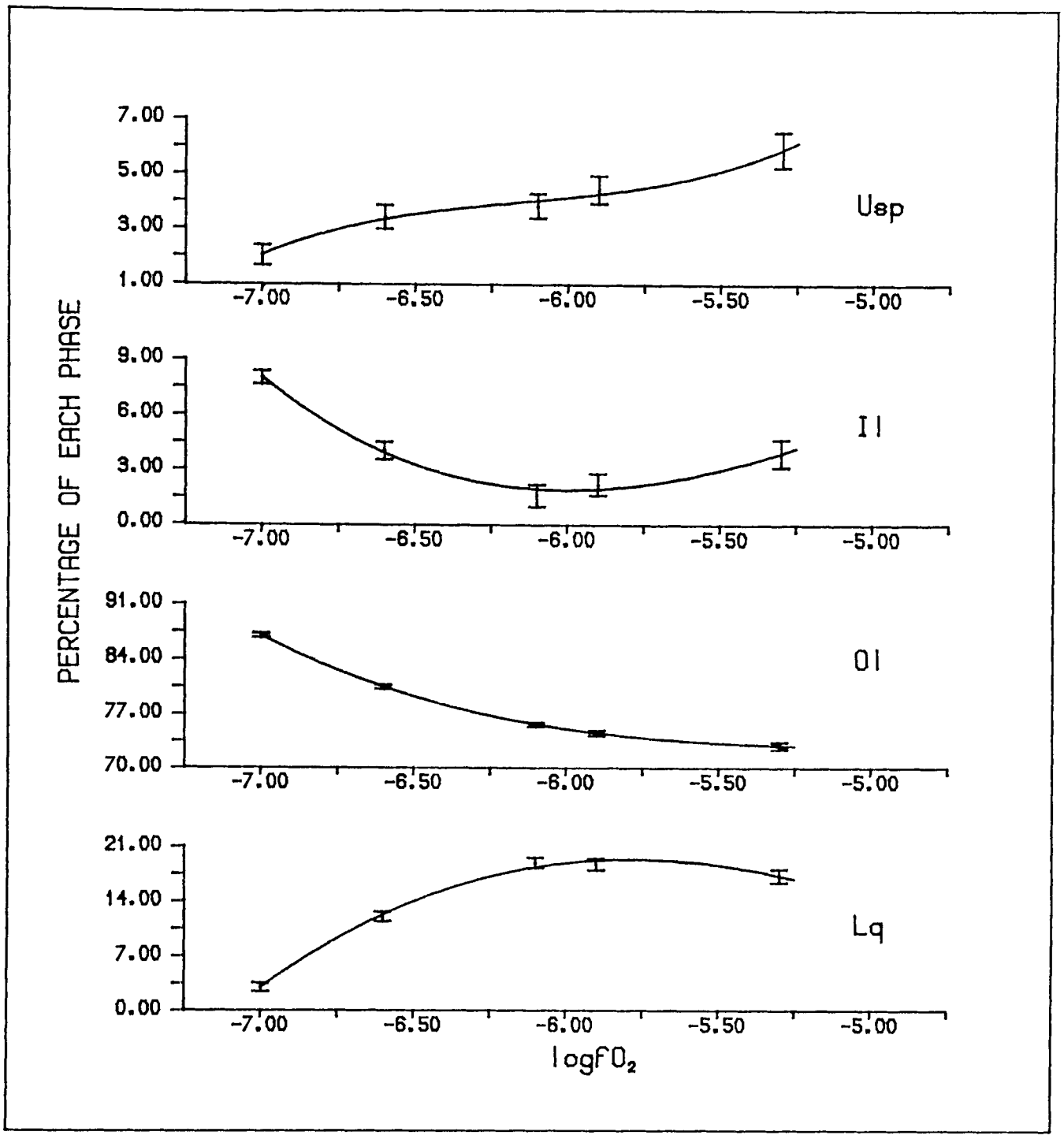

Fig. 5.5 *"Mole" percentage of each phase as function of oxygen fugacity in the system Mg-Fe-Si-Ti-O. Bulk composition is D in* (Table 5.4). *The legends for this diagram are the same as those in* ***Fig.5.4***.

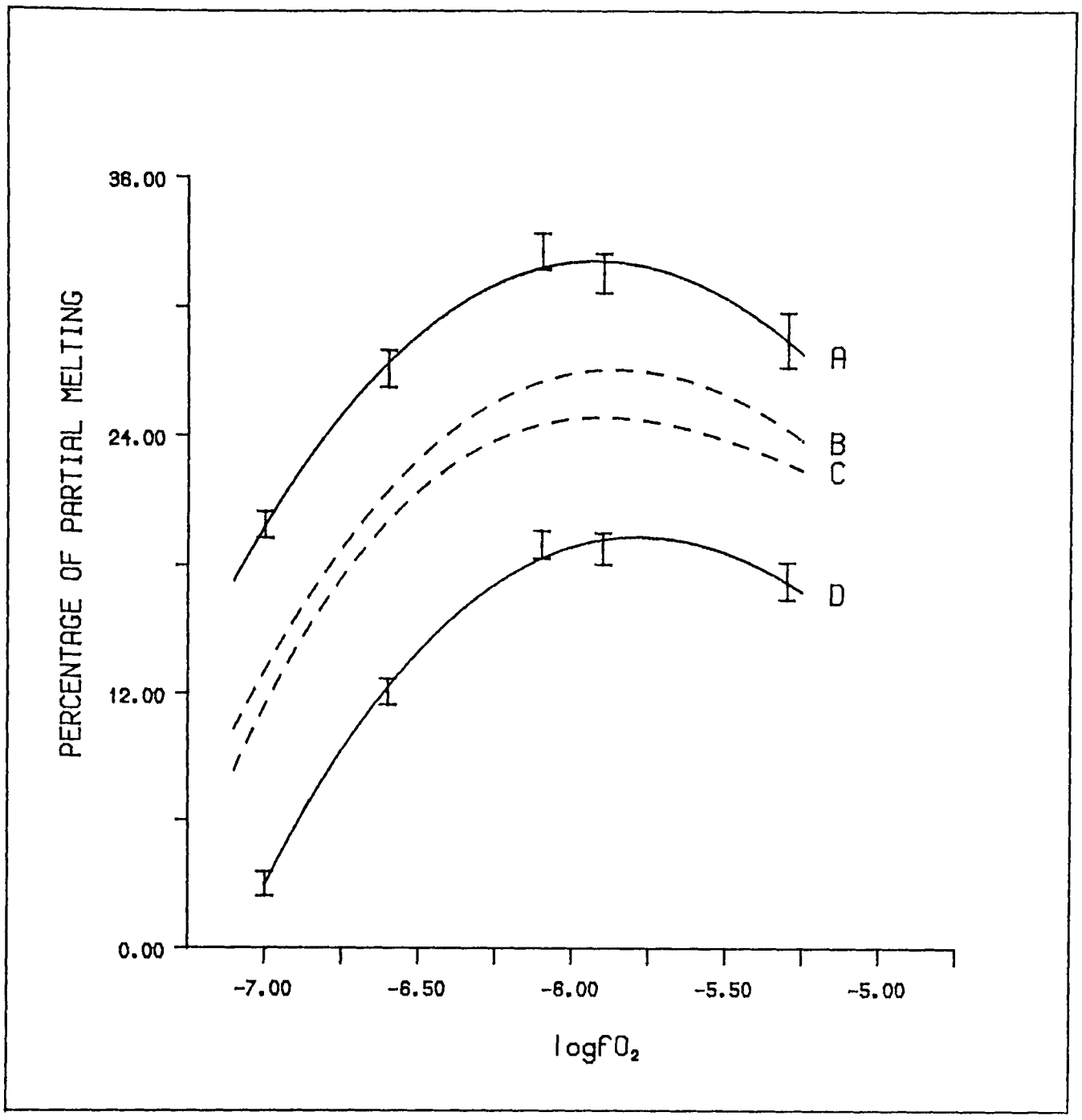

Fig. 5.6 *Effect of bulk composition on partial melting. The legends for this diagram is similar to those in* ***Fig. 5.4****. A,B,C and D represent the bulk compositions in* Table 5.4. *The dashed lines are for bulk compositions B and C, and are inserted to show their similarity to A and D. Curves are from 3-degree polynomial regressions.*

TABLE 5.5 EFFECT OF OXYGEN FUGACITY AND BULK COMPOSITION ON RELATIVE QUANTITY OF EACH PHASE AND ERROR CAUSED BY PROBE ANALYSES (USP+PSB+OL+LQ)

BULK COMPOSITION: A

MgO 36.15 FeO 27.42 TiO_2 8.39 SiO_2 28.03

(ERROR DUE TO PROBE ANALYSES OF GLASS)

$logfO_2$	LQ	OL	PSB	USP
-5.9	31.43(0.41)	59.12(0.20)	1.64(0.18)	7.78(0.20)
-5.3	28.70(0.88)	57.23(0.49)	3.34(0.41)	10.69(0.47)

(ERROR DUE TO PROBE ANALYSES OF OLIVINE)

$logfO_2$	LQ	OL	PSB	USP
-5.9	31.74(0.28)	59.00(0.14)	1.59(0.12)	7.66(0.16)
-5.3	28.43(0.16)	57.10(0.09)	4.04(0.08)	10.41(0.09)

BULK COMPOSITION: B

MgO 37.11 FeO 26.82 TiO_2 7.77 SiO_2 28.30

(ERROR DUE TO PROBE ANALYSES OF GLASS)

$logfO_2$	LQ	OL	PSB	USP
-5.9	29.13(0.38)	61.84(0.19)	1.23(0.16)	7.73(0.21)
-5.3	26.63(0.82)	59.97(0.45)	2.84(0.38)	10.53(0.43)

(ERROR DUE TO PROBE ANALYSES OF OLIVINE)

$logfO_2$	LQ	OL	PSB	USP
-5.9	29.42(0.30)	61.73(0.14)	1.24(0.13)	7.61(0.17)
-5.3	26.38(0.17)	59.86(0.10)	3.49(0.08)	10.27(0.09)

Bulk composition in mole percent. Numbers in parentheses are standard deviations associated with the range of probe analyses of glass and olivine from the pertinent charges. These errors calculated only for glass and olivine (see section 4.4) and give two tabulations for each bulk composition.

TABLE 5.5 (Cont.)

BULK COMPOSITION: C

MgO 38.70 FeO 25.53 TiO_2 7.07 SiO_2 28.71

(ERROR DUE TO PROBE ANALYSES OF GLASS)

$logfO_2$	LQ	OL	PSB	USP
-5.9	25.11(0.33)	66.40(0.16)	1.61(0.14)	6.87(0.19)
-5.3	23.00(0.70)	64.60(0.39)	2.90(0.33)	9.49(0.37)

(ERROR DUE TO PROBE ANALYSES OF OLIVINE)

$logfO_2$	LQ	OL	PSB	USP
-5.9	25.36(0.32)	66.30(0.15)	1.58(0.14)	6.77(0.18)
-5.3	22.79(0.20)	64.50(0.12)	3.46(0.09)	9.27(0.11)

BULK COMPOSITION:D

MgO 41.56 FeO 23.38 TiO_2 5.38 SiO_2 29.68

(ERROR DUE TO PROBE ANALYSES OF GLASS)

$logfO_2$	LQ	OL	PSB	USP
-5.9	18.86(0.25)	74.51(0.12)	1.04(0.11)	5.58(0.14)
-5.3	17.38(0.53)	72.77(0.30)	1.86(0.25)	7.98(0.28)

(ERROR DUE TO PROBE ANALYSES OF OLIVINE)

$logfO_2$	LQ	OL	PSB	USP
-5.9	19.05(0.35)	74.44(0.17)	1.01(0.15)	5.51(0.20)
-5.3	17.22(0.21)	72.69(0.12)	2.29(0.10)	7.81(0.11)

CHAPTER 6

RESIDUE DEPLETION AND AN EXTENDED SUMMARY

6.1. Residue depletion

With known phase compositions and proportions of coexisting phases as determined in Chapters 4 and 5, bulk composition of the residue (unmolten part corresponding to total solid phase portion) can be estimated through simple calculations. The composition of the residue may then be set alongside the changing composition and amount of the liquid at different oxygen fugacities.

Definitions: r_i' is the mole fraction of component i in the residue,

α_{ij} is the mole fraction of component i in phase j,

x_j is the mole fraction of phase j in the charge.

Then,

$$r_i' = \frac{\sum_{j=1}^{n} \alpha_{ij} x_j}{\sum_{i=1}^{n+1} \sum_{j=1}^{n} \alpha_{ij} x_j} \qquad (6.1)$$

(n is the number of solid phases in the charge.)

The mole fraction of component i in phase j (α_{ij}) can be derived from probe analysis, and the mole fraction of phase j in a particular chosen bulk composition can be calculated from the procedures stated in Chapter 4 and 5. Therefore, the residue bulk composition can be calculated from equation 6.1 and its dependence on oxygen fugacity can be characterized. The residue bulk compositions as functions of oxygen fugacity for bulk composition A, B, C, and D (in system Mg-Fe-Ti-Si-O, see **Chapter 4** and **5**) have been listed in **Table 6.1** and illustrated in ***Figs. 6.1*** and ***6.2*** for bulk

composition A and D. Data for the Ca-bearing system are presented in Table 6.2 and ***Fig. 6.3***.

At relatively reducing conditions, with increase in oxygen fugacity, the MgO content in the residue increases until it reaches a maximum value; with further increase in oxygen fugacity, the MgO content in the residue drops. A similar but not so pronounced trend is shown in SiO_2 contents. The FeO and TiO_2 contents in the residue, however, shows a contrasting trend to MgO and SiO_2, and show minima near where MgO and SiO_2 have maxima. These maxima and minima compositions occur at about the same log fO_2 value (-6.0), and approximately coincide with the oxygen fugacities of maximum degree of partial melting (***Figs. 5.4 - 5.6***). Small changes in primary bulk composition do not affect the general variation pattern of the residue bulk compositions.

Conventionally, the degree of depletion in natural systems is often described in terms of Mg/(Mg+Fe) ratio, the Mg-number (Mg'). The Mg number of the residue is also calculated and listed in Table 6.1. As expected from the above, the Mg number reaches its maximum at an oxygen fugacity of 10^{-6} bar (about 0.5 log fO_2 unit above NNO) at 1300^0C; and the degree of depletion decreases with either increase or decrease in oxygen fugacity from this value (***Fig. 6.4-6.5***).

The difference between maximum depletion as given by bulk solid Mg-number and olivine Mg-number, further illustrated in ***Fig. 6.4*** and ***6.5*** suggests that the common practice of using Mg number of olivine as an index for degree of depletion may be hazardous, though it is usually done in the context of constant oxygen fugacity (i.e. melting by thermal rather than redox perturbation). Olivine has a single composition variation trend, the change of its Mg number coincides with that of bulk composition only at relatively reducing conditions. At highly oxidizing conditions, with olivine becoming more Mg rich, the residue is subject to smaller degree of depletion because the amount of melting decreases as the result of precipitation of oxides.

TABLE 6.1 EFFECT OF OXYGEN FUGACITY AND BULK COMPOSITION ON RESIDUE COMPOSITION (COMPOSITIONS IN MOLE FRACTION)

BULK COMPOSITION: A

MgO 0.3615 FeO 0.2742 TiO_2 0.0839 SiO_2 0.2803

$logfO_2$	MgO	SiO_2	TiO_2	FeO	Mg'	OS*
-10.0	0.3692	0.2822	0.0793	0.2692	0.5783	0.183(0.009)
-9.0	0.3781	0.2837	0.0744	0.2638	0.5890	0.173(0.015)
-8.0	0.3927	0.2862	0.0652	0.2560	0.6054	0.165(0.015)
-7.0	0.4173	0.2920	0.0502	0.2405	0.6344	0.141(0.012)
-6.6	0.4434	0.2950	0.0345	0.2271	0.6614	0.128(0.019)
-6.1	0.4608	0.2929	0.0304	0.2160	0.6808	0.122(0.020)
-5.9	0.4543	0.2847	0.0392	0.2219	0.6719	0.158(0.022)
-5.3	0.4360	0.2686	0.0554	0.2401	0.6449	0.242(0.036)

BULK COMPOSITION: B

MgO 0.3711 FeO 0.2682 TiO_2 0.0777 SiO_2 0.2830

$logfO_2$	MgO	SiO_2	TiO_2	FeO	Mg'	OS*
-9.0	0.3790	0.2846	0.0732	0.2632	0.5902	0.169(0.014)
-8.0	0.3940	0.2876	0.0636	0.2548	0.6073	0.159(0.013)
-7.0	0.4183	0.2930	0.0491	0.2396	0.6359	0.137(0.011)
-6.6	0.4451	0.2966	0.0329	0.2254	0.6639	0.122(0.017)
-6.1	0.4637	0.2954	0.0272	0.2137	0.6846	0.112(0.016)
-5.9	0.4583	0.2880	0.0350	0.2187	0.6769	0.145(0.020)
-5.3	0.4418	0.2734	0.0497	0.2352	0.6526	0.220(0.032)

Numbers in parentheses are standard deviations (see text).
Mg, is the Mg number = Mg/(Mg+Fe) of the "residue".
OS* is the sum of oxides to silicate ratio (IL+USP)/OL.

TABLE 6.1 (Cont.)

BULK COMPOSITION: C

MgO 0.3870 FeO 0.2553 TiO_2 0.0707 SiO_2 0.2871

$logfO_2$	MgO	SiO_2	TiO_2	FeO	Mg′	OS*
−8.0	0.3951	0.2886	0.0658	0.2505	0.6120	0.155(0.012)
−7.0	0.4194	0.2941	0.0513	0.2352	0.6407	0.133(0.009)
−6.6	0.4467	0.2983	0.0351	0.2199	0.6701	0.115(0.014)
−6.1	0.4663	0.2980	0.0283	0.2074	0.6922	0.102(0.015)
−5.9	0.4632	0.2925	0.0337	0.2107	0.6873	0.127(0.018)
−5.3	0.4497	0.2804	0.0456	0.2243	0.6672	0.190(0.027)

BULK COMPOSITION: D

MgO 0.4156 FeO 0.2338 TiO_2 0.0538 SiO_2 0.2968

$logfO_2$	MgO	SiO_2	TiO_2	FeO	Mg′	OS*
−7.0	0.4242	0.2988	0.0486	0.2283	0.6501	0.115(0.009)
−6.6	0.4532	0.3045	0.0315	0.2109	0.6825	0.092(0.011)
−6.1	0.4762	0.3067	0.0209	0.1963	0.7081	0.071(0.013)
−5.9	0.4751	0.3028	0.0242	0.1979	0.7060	0.088(0.014)
−5.3	0.4659	0.2941	0.0326	0.2075	0.6919	0.134(0.019)

Numbers in parentheses are standard deviations.

TABLE 6.2 EFFECT OF OXYGEN FUGACITY AND BULK COMPOSITION ON RESIDUE COMPOSITION (COMPOSITIONS IN MOLE FRACTION)

BULK COMPOSITION: (as in **Table 4.12**)

MgO 0.4759 FeO 0.1121 TiO_2 0.1006 SiO_2 0.2642 CaO 0.0472

$logfO_2$	MgO	SiO_2	CaO	TiO_2	FeO	Mg′
−10.0	0.3844	0.3182	0.0377	0.1152	0.1445	0.7268
−9.0	0.3855	0.3189	0.0376	0.1142	0.1438	0.7283
−8.0	0.4014	0.3253	0.0314	0.1037	0.1383	0.7437
−7.0	0.4149	0.3299	0.0260	0.0954	0.1338	0.7562
−6.6	0.4422	0.3421	0.0143	0.0736	0.1278	0.7758

Mg′ is the Mg number = Mg/(Mg+Fe) of the "residue".

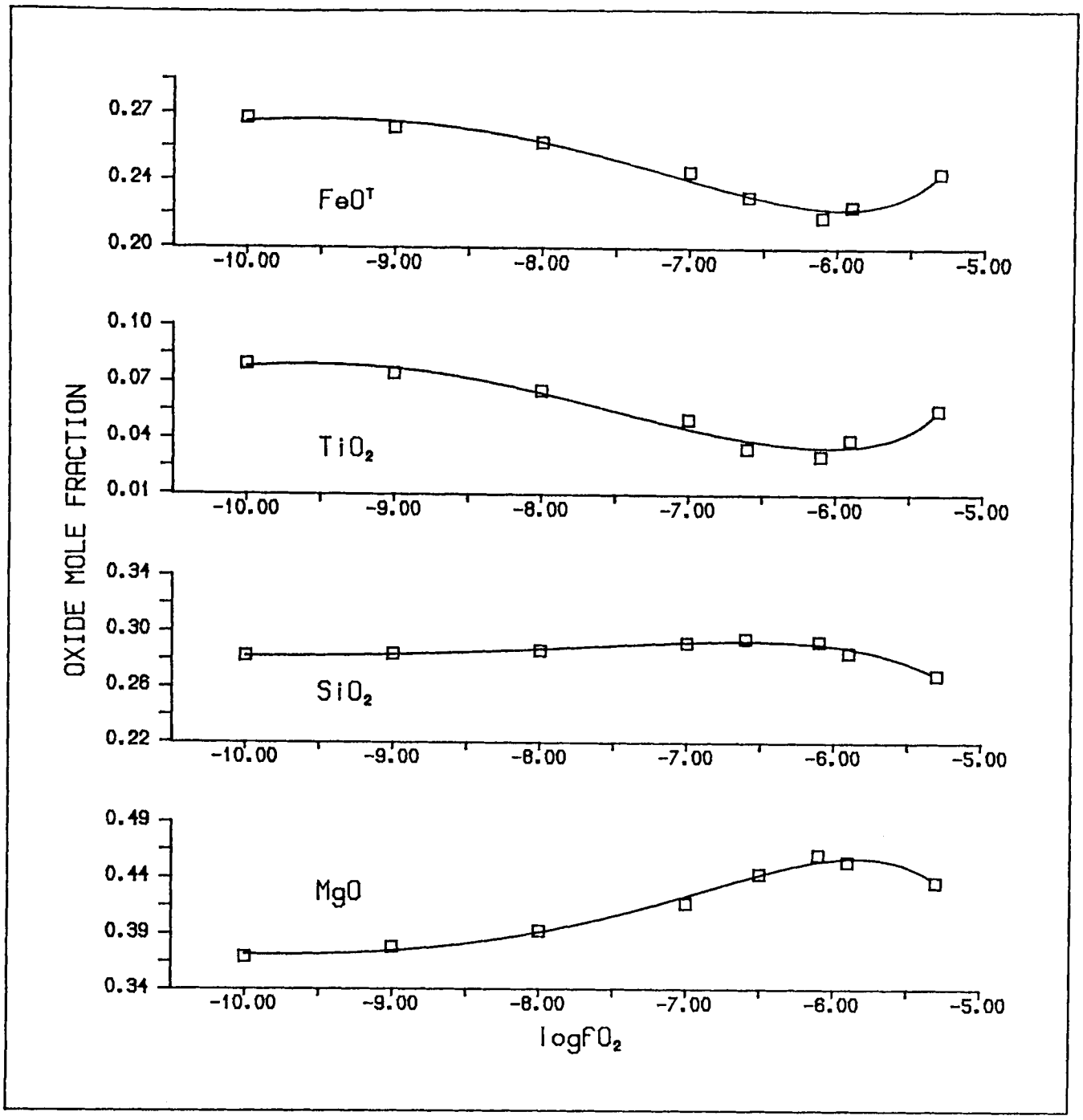

Fig. 6.1 *Bulk composition of residue (non-molten or solid part of charge) as a function of oxygen fugacity. Original total bulk composition (melt + solid) is A in* Table 4.11. *Maximum depletion, in terms of decreasing FeO and TiO_2, and increasing MgO contents, occurs at an oxygen fugacity of just above 10^{-6} bar and coincides with that of maximum degree of partial melting (**Figs. 5.4 - 5.6**). Points are calculated by the method stated in the text. Curves are drawn from an empirical fit of the calculated points.*

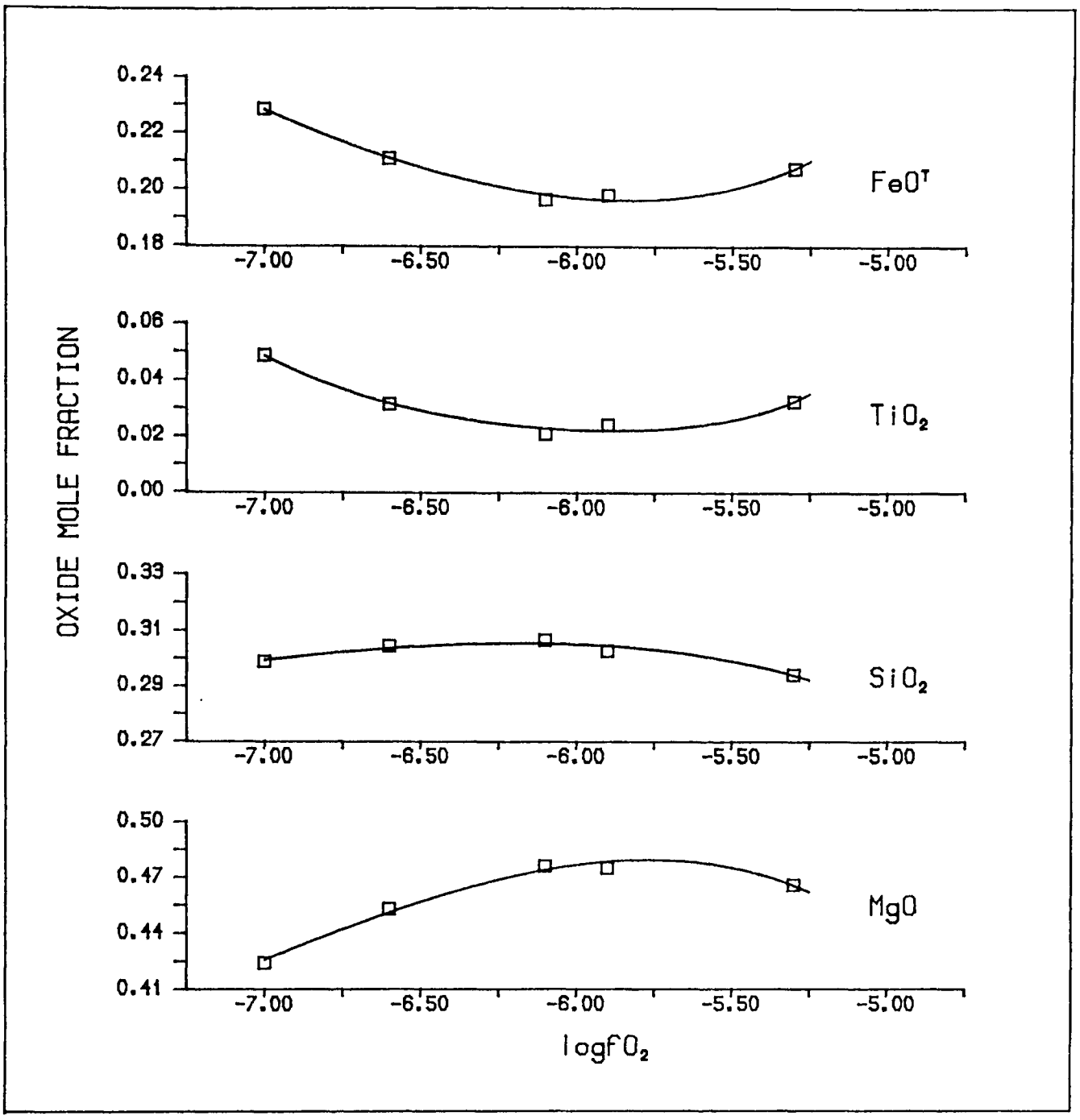

Fig. 6.2 *Bulk composition of residue as function of oxygen fugacity. Original bulk composition is D in* Table 4.11. *The depletion pattern is shown similar to that in* ***Fig 6.1****, despite the difference in original bulk composition.*

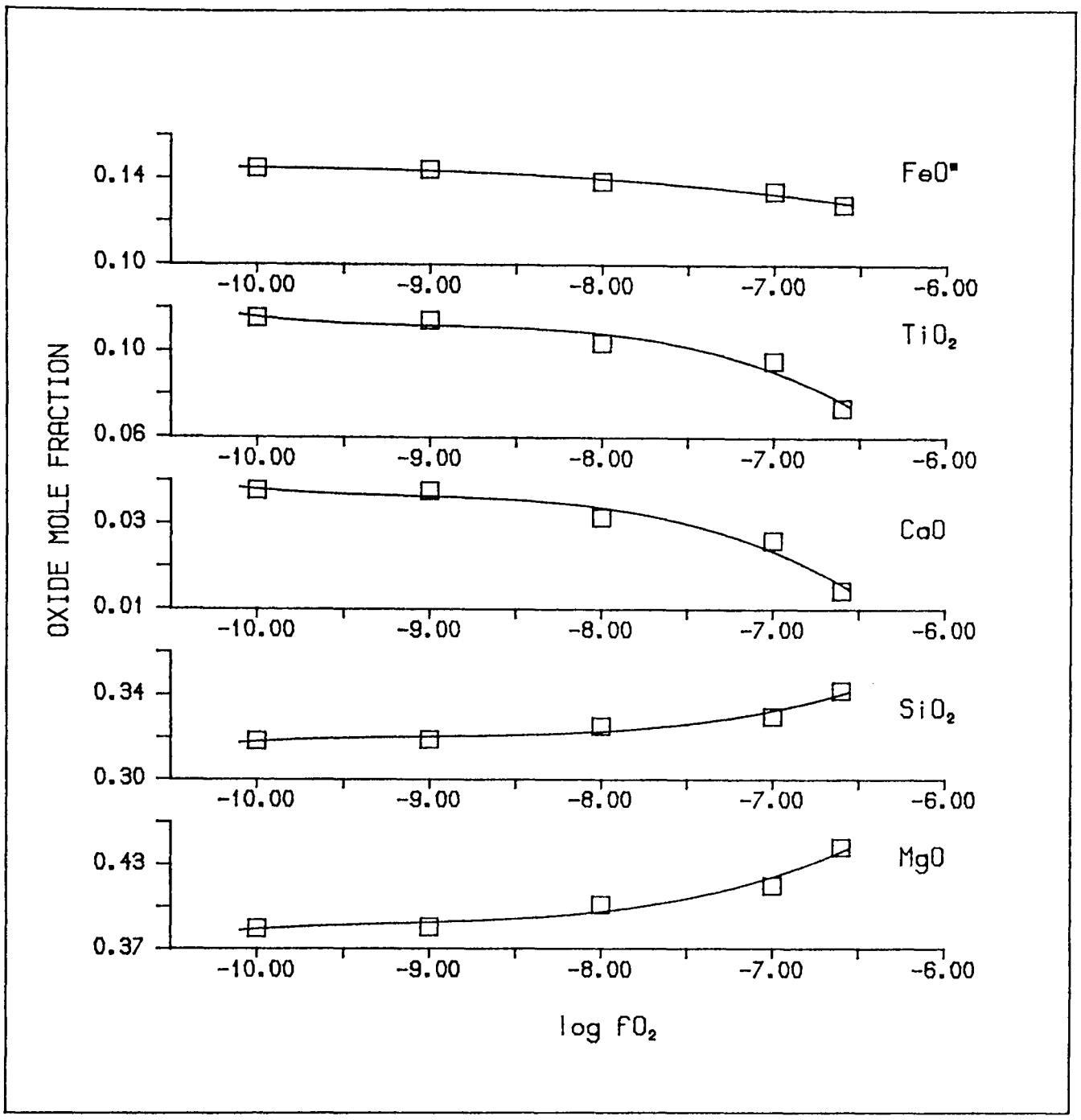

Fig. 6.3 *Bulk composition of residue as function of oxygen fugacity. Original bulk composition is as that in* Table 4.12.

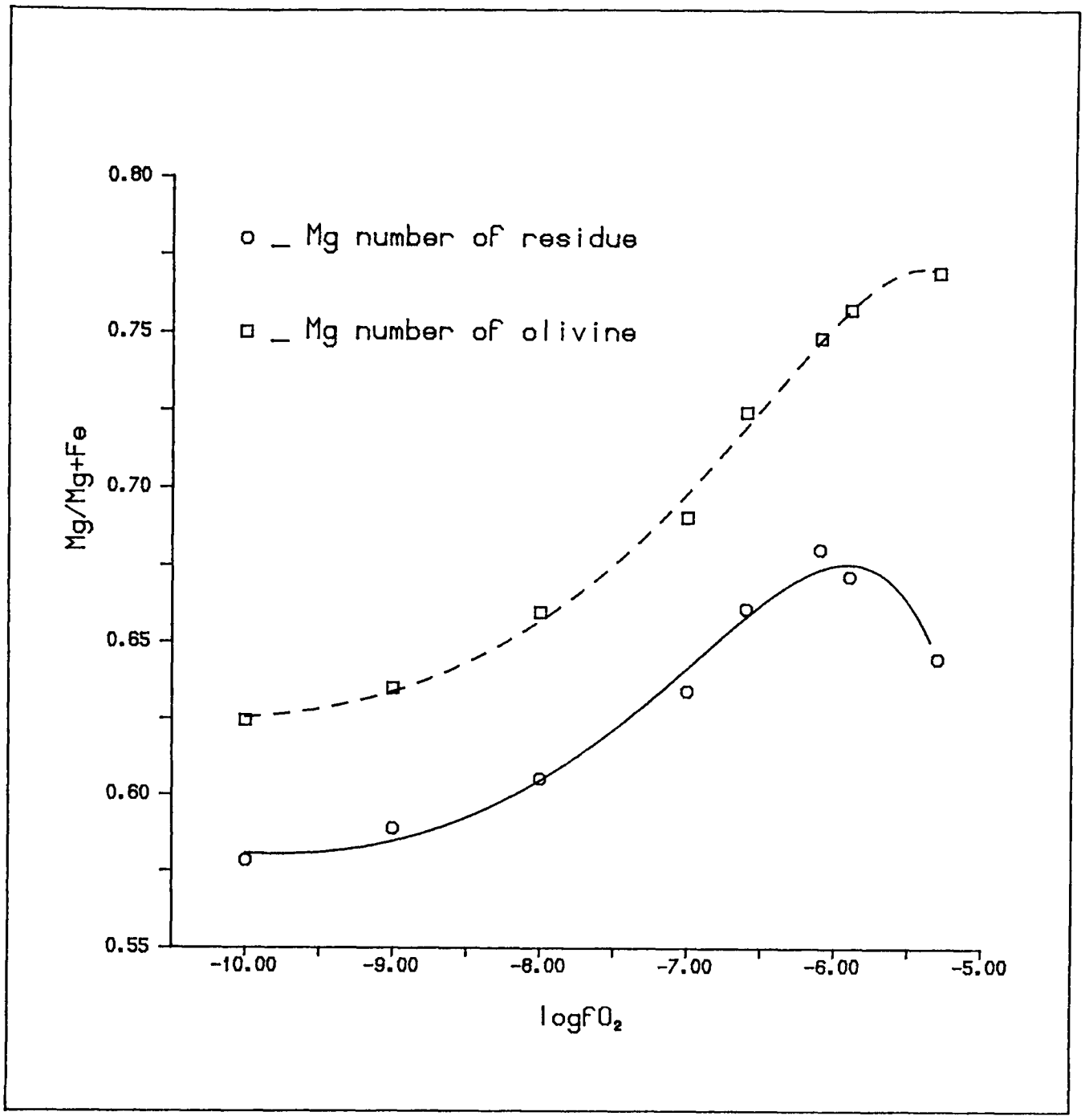

Fig. 6.4 *Effect of oxygen fugacity on Mg number of residue (original bulk composition is A in* Table 4.11*). Mg number of olivine is also shown in this diagram (dashed line). Commonly, the Mg numbers of both olivine and "whole rock" have been used as an index for degree of depletion caused by partial melting. The different trends of the two Mg numbers at extremely oxidizing conditions indicates that using the Mg-number of olivine as an index may be hazardous. Maximum depletion occurs at a high but intermediate oxygen fugacity represented by the highest Mg number of the residue bulk.*

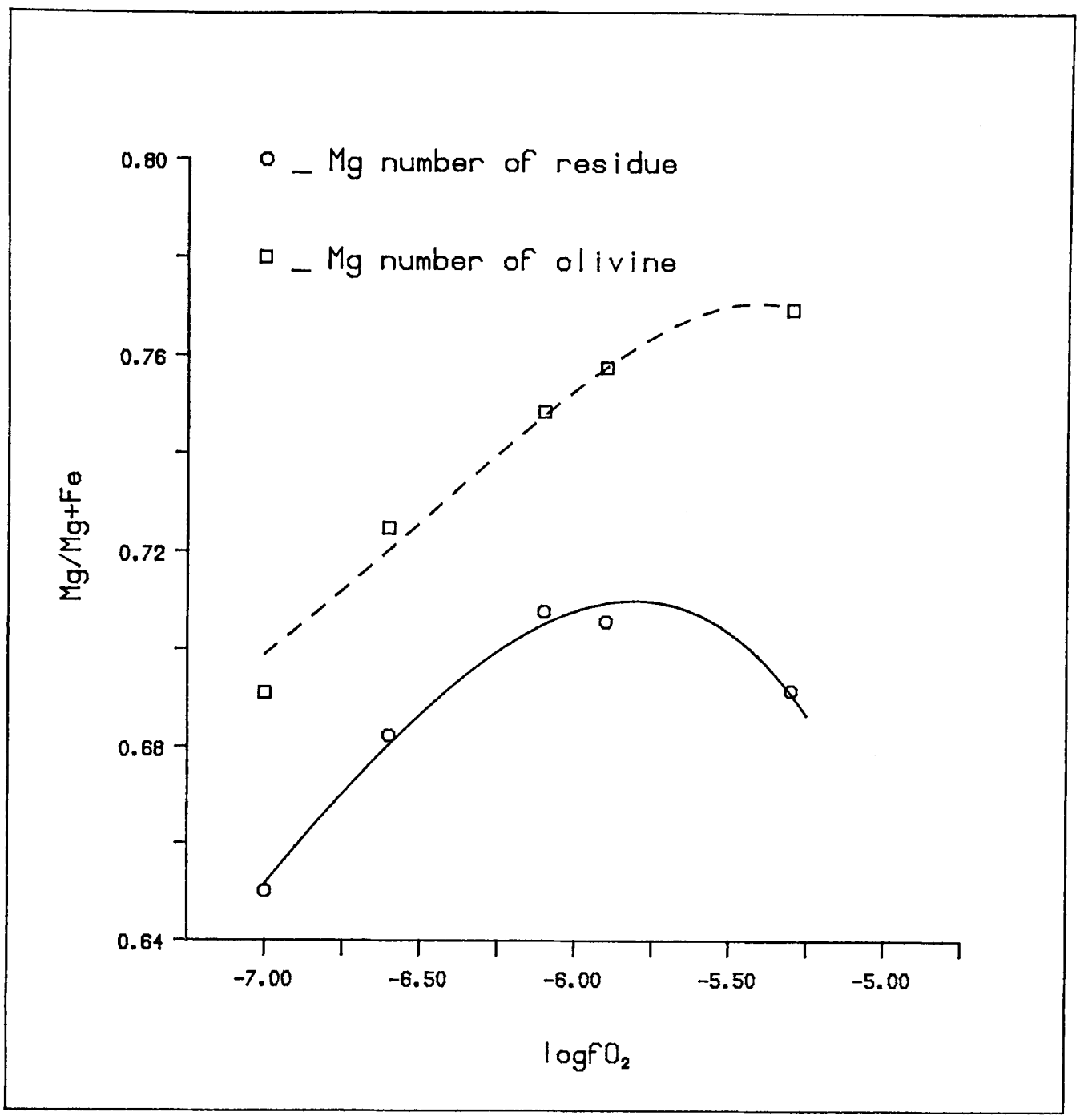

Fig. 6.5 *Effect of oxygen fugacity on Mg number of the residue and Mg-number of olivine (original composition is D in* Table 4.11*). The depletion pattern is shown similar to* ***Fig 6.4****.*

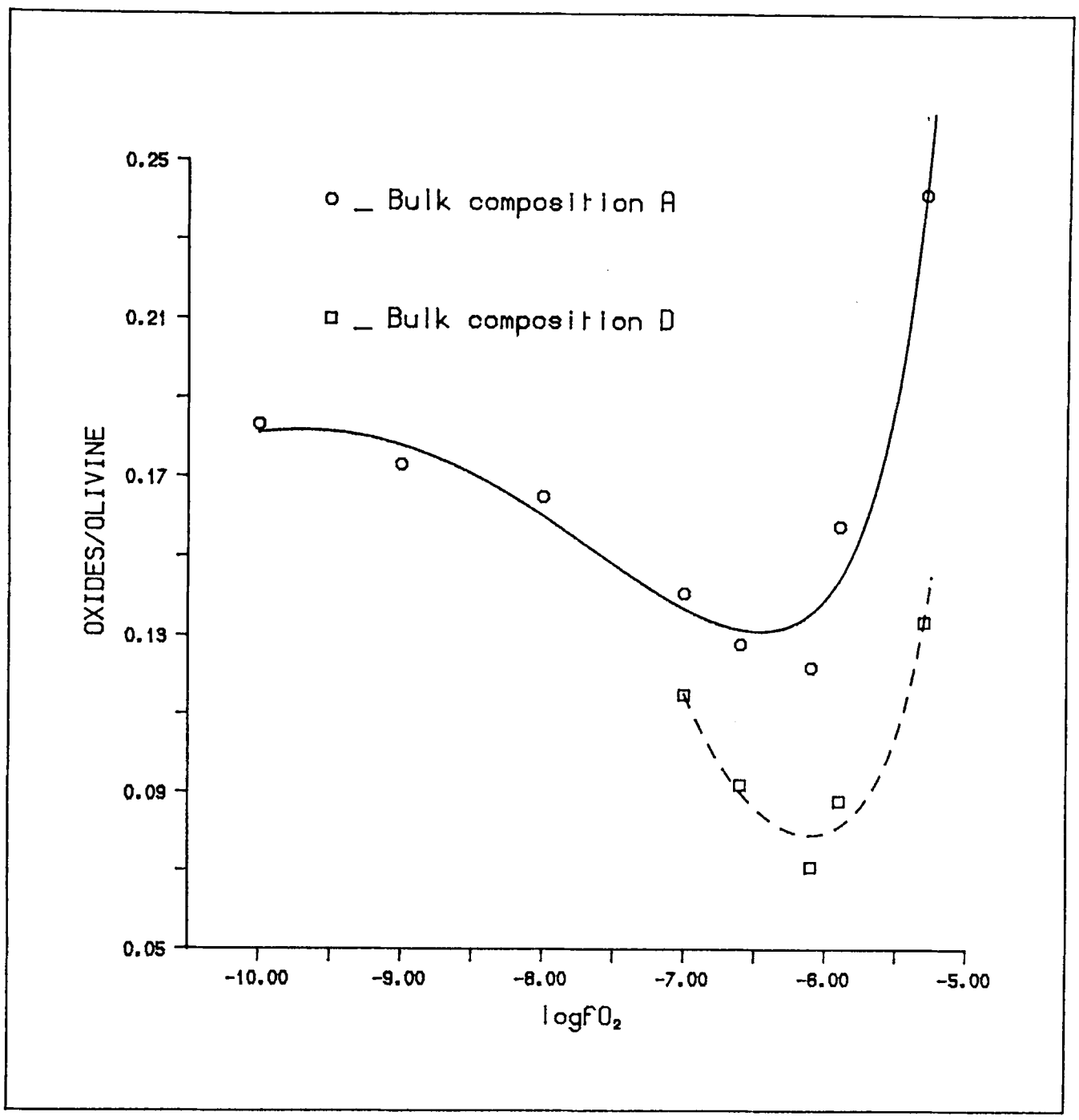

Fig. 6.6 *Effect of oxygen fugacity on the relative quantity (mole fractions) of oxide phases (sum of ilmenite and ulvospinel), and silicate (olivine), expressed as oxides/olivine. The minima near log* $fO_2 = -6$ *are close to the maximum depletion, as given by the Mg-number of the residue in* ***Figs. 6.4*** *and* ***6.5****. Bulk compositions A,D refer to* Table 4.11.

The correlation of changing FeO, TiO_2, MgO and SiO_2 (***Figs. 6.1*** and ***6.2*** shows that the Mg-number depletion pattern is obviously sympathetic to the Ti content in the residue, and therefore, is related to the relative quantity of solid oxide (IL+USP) and silicate (OL) phases in the concerned chemical system. Sums of solid oxides to olivine ratio have been calculated in Table 6.1 and plotted in ***Fig. 6.6***. Error estimation is from

$$\text{ERROR} = \frac{X_{IL}\sigma_{OL} + X_{USP}\sigma_{OL} + X_{OL}\sigma_{IL} + X_{OL}\sigma_{USP}}{X_{OL}^2} \qquad (6.2)$$

X_{IL}, X_{USP} and X_{OL} are mole fractions of ilmenite, ulvospinel and olivine respectively, σ_{IL}, σ_{USP} and σ_{OL} are the related standard errors.

Comparison of ***Fig. 6.6*** with ***Figs. 6.4*** and ***6.5*** shows that the maximum depletion in the residue is related to the maximum depletion of oxide, or more exactly, the depletion of ilmenite (***Fig. 5.4*** and ***5.5***).

The relative enrichment of Fe in the bulk solid (residue) composition at relatively reducing conditions is also related to the relative enrichment of Fa end-member in the coexisting olivine (***Fig. 6.4***). Depletion during redox melting (by oxidation) at relatively reducing conditions (log fO_2 < -6.2) is achieved by the preferential dissolution of ilmenite and Fa end-member in olivine with increasing oxygen fugacity, despite the fact that precipitation of ulvospinel occurs (***Fig. 5.4*** and ***5.5***). For highly oxidizing conditions (log fO_2 > 5.8), however, depletion during redox melting (by reduction) is achieved by dissolution of both ilmenite and ulvospinel with decrease in oxygen fugacity (***Figs. 5.4-5.6***). Across the interval near log fO_2 of -6.0 where redox melting changes from an oxidation process to a reduction process, the olivine shows no change in trends, and becomes both less abundant and richer in Fo with increasing fO_2 (***Figs. 5.2, 5.4*** and ***5.5***).

Although the common concept about depletion (in terms of major element

characteristics) holds its strength in that a larger degree of partial melting corresponds to a higher degree of residue bulk depletion, the melting and depletion relationship is not symmetric for phase compositions. At extremely oxidizing conditions, the composition of the coexisting melt becomes significantly more dependent on the redox state, poorer in TiO_2 and FeO, richer in SiO_2 and MgO with increasing fO_2. Thus, the elemental geochemistry (compatibility, incompatibility) during redox melting (at highly oxidizing conditions) may need more serious reconsideration.

6.2. Extended summary

The processes of redox partial melting are basically determined by the relationship amongst silicates, oxides, and melt at different oxygen fugacities, in a similar way to the simple system Fe-Si-O discussed in Chapter 1. Unlike the simple system, the addition of the components Mg and Ti, results in extensive solid solution in the coexisting phases, and extremely wide stability fields of both silicate and oxide phases of geological interests. Instead of abrupt assemblage transitions, change in oxygen fugacity causes continuous variation in the compositions of these solid solutions. The major chemical trend for olivine is the depletion of Fe end member with increase in oxygen fugacity, whilst for oxides, it is the enrichment of compositions in Fe^{+3} or Mg rich end members. The liquid composition remains reasonably constant over a wide range of relatively reducing conditions but changes considerably at more oxidizing conditions, where Mg, Si increase, and Fe, Ti decrease with increase in oxygen fugacity.

In general, the response of each phase to the change in oxygen fugacity is sensitive, and the scale of mass redistribution caused by change in oxygen fugacity is significant. The change in degree of partial melting with redox conditions is one of the consequences of the mass redistribution, because not only the compositions but also the proportions of the phases change.

In the melting assemblages considered, olivine and ulvospinel show a single trend

with increase in oxygen fugacity, i.e. olivine dissolution and ulvospinel precipitation respectively. Ilmenite shows a double trend, at relative reducing conditions, ilmenite dissolves and decreases in amount with increase in oxygen fugacity, but at extremely oxidizing conditions, ilmenite (rich in Fe_2O_3) is precipitated with increasing oxygen fugacity.

The degree of partial melting is, therefore, determined by the overall effect of precipitation and dissolution of the coexisting solid phases. For some of the geologically appropriate compositions, at relatively reducing conditions, the dissolution of olivine and ilmenite exceeds the precipitation of ulvospinel, and the net effect is a larger degree partial melting with increase in oxygen fugacity. At extremely oxidizing conditions, however, the precipitation of ilmenite and ulvospinel exceeds the dissolution of olivine, and increase in oxygen fugacity results in a smaller degree partial melting. A set of general partial melting and residue depletion relationships, using bulk composition A (Chapter 4) in the system Mg-Fe-Ti-Si-O, are illustrated in ***Fig. 6.7***; curves are fitted with empirical equations.

Differentiating the equations represented by curves in ***Fig. 6.7***, the rate of change or sensitivity of dissolution, precipitation, and amount of partial melting as the result of change in oxygen fugacity at different redox states can be calculated. At relatively reducing conditions, ***Fig. 6.8*** shows that olivine and ilmenite reach their highest dissolution rate at about 0.5 log fO_2 unit below NNO buffer if subject to oxidation, and thus result in a maximum rate of melt productivity in oxidation melting.

With log fO_2 = -7.25 equivalent to QFM at 1300°C, 1atm (extrapolated from Myers and Eugster, 1983), then, change in oxygen fugacity within QFM±1 logfO_2 unit can produce 63% of the total integrated amount of partial melt caused by oxidation melting over a range of oxygen fugacities going from highly reduced to log fO_2 of approximately -6.2. That is 63% of the maximum amount of partial melting (32% of total "rock") in ***Fig. 6.7***; or 63% of the total area under the curve in ***Fig. 6.9***.

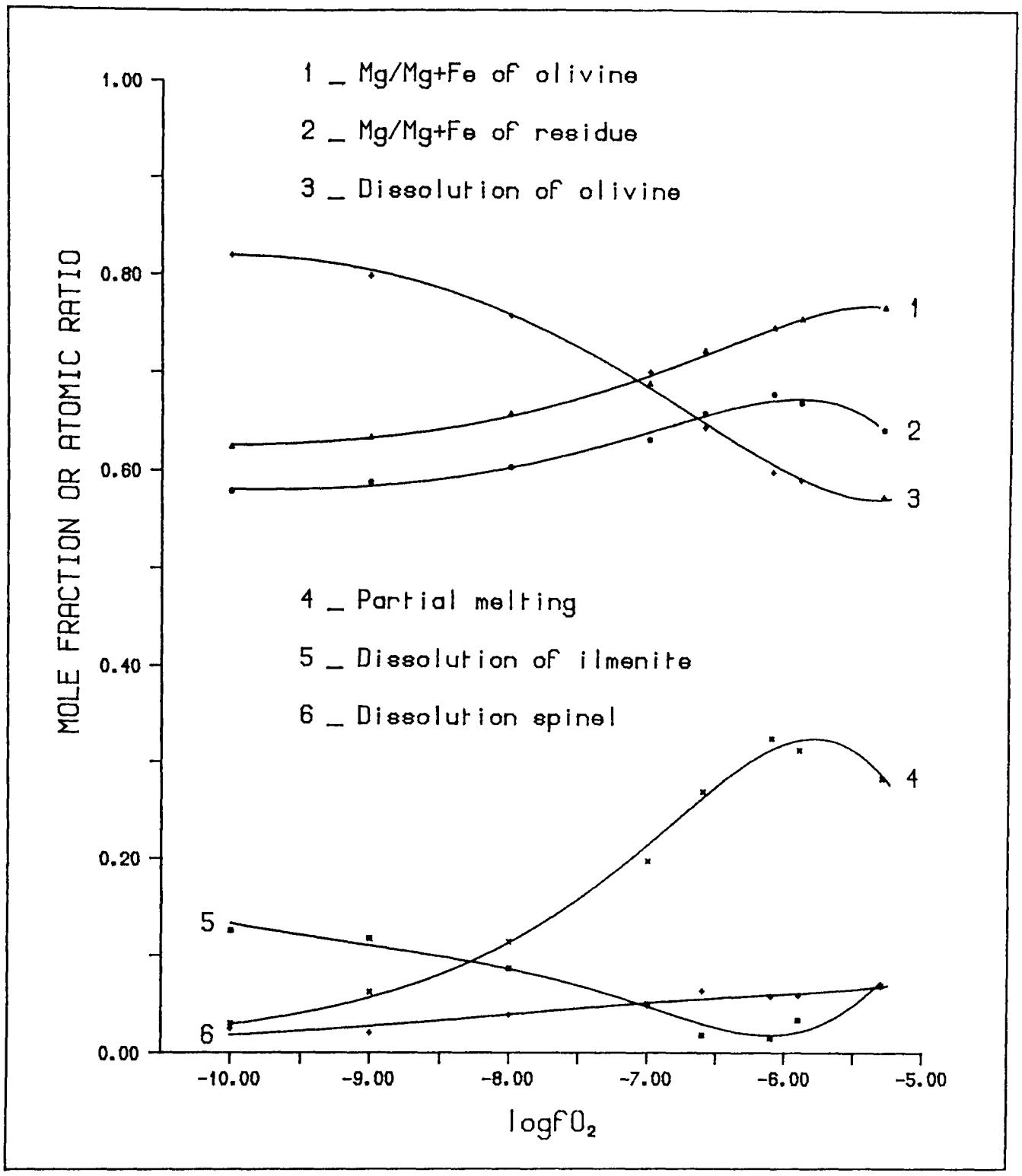

Fig. 6.7 *Summary of redox melting and residue depletion relationships (constant T=1300°C and P=1atm). At relatively reducing conditions, increased melting occurs with oxidation as the result of dissolution of olivine (3) and ilmenite (5). At oxidizing conditions (log* fO_2 *> -6.0), increased melting with reduction as the result of dissolution of ilmenite (5) and ulvospinel (6). The degree of depletion (as shown by Mg/(Mg+Fe) of solid residue) is sympathetic to degree of partial melting. Mg/(Mg+Fe) of olivine should not be used independently as an depletion indicator.*

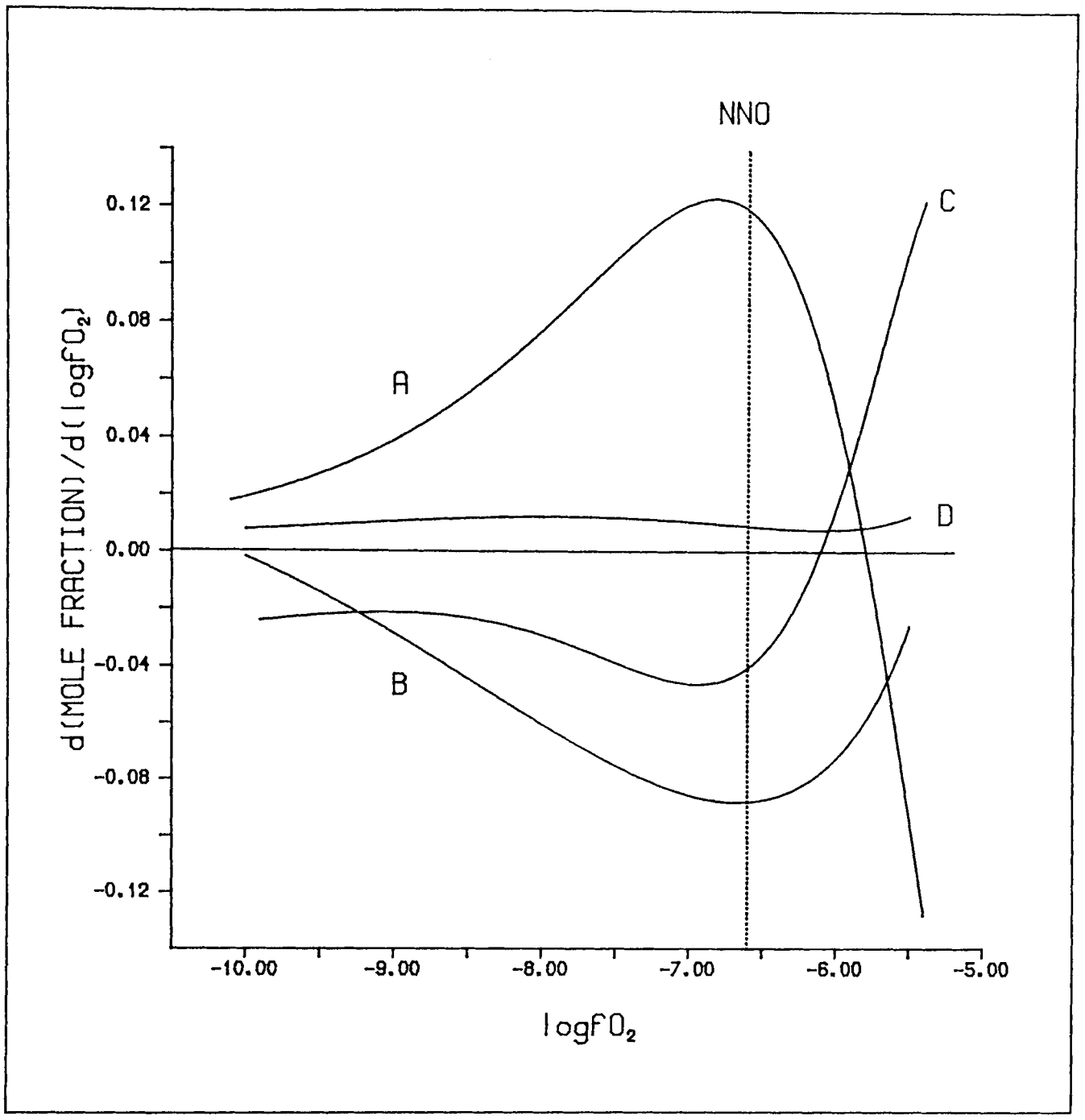

Fig. 6.8 *Sensitivity of redox melting to change of oxygen fugacity. A: partial melting. B: dissolution of olivine. C: dissolution of ilmenite. D: dissolution of ulvospinel. A maximum melting rate with oxidation exists at about half log fO_2 unit below NNO as the result of large dissolution rates of both olivine and ilmenite. A maximum reduction melting rate is expected to exist at more oxidizing conditions as the result of dissolution of ilmenite and ulvospinel.*

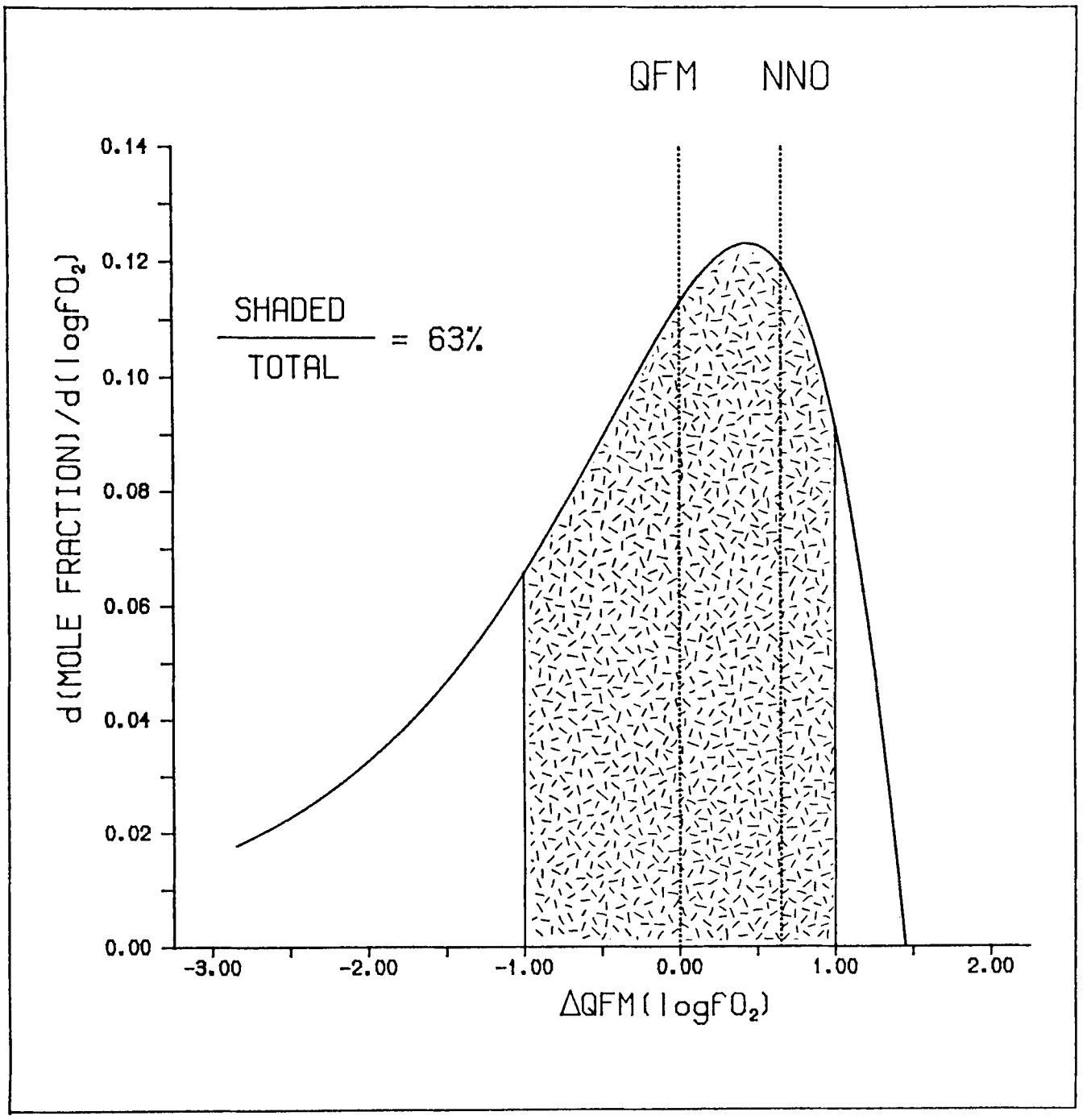

Fig. 6.9 *Melt productivity of oxidation melting. The curve in this diagram is a section (+) of curve A in* ***Fig. 6.8****, i.e. the differentiation of curve 4 (partial melting) in* ***Fig. 6.7****. The shaded area represents the quantity of melt produced by oxidation within QFM± 1 logfO_2 unit. Up to 63% of the melt, which it is possible to generate in oxidation melting, is generated in the oxygen fugacity range of QFM± 1 logfO_2 unit (see text).*

CHAPTER 7

A COMPARISON WITH PREVIOUS EXPERIMENTAL WORK

A further examination of the experimental data set of this study will be given by comparison with other data sets and testing the consistency between different data sets of experimental or theoretical analyses.

However, there are difficulties in performing the comparison between different data sets, either because the data are not collected at the same experimental conditions (P, T etc.) or the data are not from the same chemical system. The data sets only become comparable on the condition that minor factors are neglected; for example, the effects of Si on the phase relations of Mg-Fe-Ti oxides in system Mg-Fe-Ti-Si-O is neglected, and thus, the relations between the Mg-Fe-Ti oxides in the system Mg-Fe-Ti-Si-O should be the same as those in system Mg-Fe-Ti-O.

Data from the same experimental conditions (1300°C, 1atm) are rather sparse. To the author's knowledge, there are two other independent data sets (Taylor, 1964; Woermann, *et al.*, 1969) available. Taylor's experiments were carried out in the system Fe-Ti-O with the technique of thermogravimetry to measure the gain or loss of oxygen from a given bulk composition (fixed Fe/Ti ratio) at different oxygen fugacities. The compositions of coexisting phases were not obtained from direct analyses of individual phases, but from deductions of a series of experiments. Therefore, the actual stoichiometry of the coexisting phases is not well known (Andersen and Lindsley, 1988). However, from their tie-line positions between coexisting ilmenite and ulvospinel binary solid solutions, the coexisting pairs show oxidized character relative to those of this study.

Woermann *et al.* (1969) conducted a series of experiments in the system Mg-Fe-Ti-O, and the ilmenite (solid solution, coexisting with ulvospinel solid solution)

compositions at different oxygen fugacities were given in a diagram of IL-GK-HM ternary solid solution (***Fig. 7.1***). Their data on the composition of the binary IL-HM join at different oxygen fugacities are very similar to those of Taylor (1964), but significantly more oxidized than the data of this study (***Fig. 7.1***). Since they gave neither the detailed descriptions of the experimental technique and the analytical procedures for the coexisting phases, nor the actual compositions of the coexisting phases and the error involved in the calculation procedures, it is very difficult to judge the reliability of their results.

The relatively oxidized character of the determined ilmenite compositions in these early experiments was also shown by comparison with the experimental results of Katsura *et al.* (1976), and Spencer and Lindsley (1981). Partially based on the data of Katsura *et al.* (1976) at high temperature, Andersen and Lindsley (1988) developed solid solution models for ilmenite and ulvospinel solid solutions and calibrated the IL_{SS}-USP_{SS} geothermometer and oxygen barometer. It is shown in Table 7.1 that the compositions of IL+USP pairs expected from this newly calibrated geothermometer and oxygen barometer at 1300°C and 1atm, are close to those observed in this study, thus, indicating some degree of consistency between the data sets of Katsura *et al.* (1976) (at 1100°C and 1200°C) and the present study (at 1300°C).

Table 7.1 A COMPARISON BETWEEN EXPERIMENTALLY DETERMINED AND CALCULATED COMPOSITIONS OF IL+USP PAIRS

log fO_2	This study	Calculated
-9.0	$IL_{97.9}USP_{96.0}$	$IL_{96.7}USP_{90.2}$
-8.0	$IL_{94.3}USP_{88.3}$	$IL_{93.8}USP_{83.0}$
-7.0	$IL_{85.3}USP_{75.0}$	$IL_{86.0}USP_{72.0}$
-6.6	$IL_{79.5}USP_{65.6}$	$IL_{78.0}USP_{64.0}$

Rawson and Irvine (1979-1980) performed experiments on the Mg-Fe^{2+} partitioning between olivine and ulvospinel solid solutions at 1067°C and 1167°C and various oxygen fugacities. Partially based on these partitioning data, O'Neill and Wall (1987)

calibrated a Mg-Fe^{2+} exchange geothermometer between olivine and multi-component spinel. Using this calibrated geothermometer, with the compositional data of the coexisting olivine and ulvospinel of this study as input, the equilibrium temperatures estimated by the geothermometer are calculated. The results show that the calculated temperatures are in reasonable agreement with the experimentally controlled temperature (***Fig. 7.2***). Thus, the two data sets (Rawson and Irvine, 1979-1980, and present study) may be regarded as consistent.

Similarly, Andersen and Lindsley (1979) carried out experiments on the Mg-Fe^{2+} partitioning between olivine and ilmenite solid solutions. Based on the acquired partitioning data, they developed a Margules model for ilmenite ternary solid solution and calibrated the coexisting olivine and ilmenite as a geothermometer (Andersen and Lindsley, 1979, 1981). Using this geothermometer (Andersen and Lindsley, 1981), with the compositional data of coexisting olivine and ilmenite of this study as input, the estimated equilibrium temperatures are calculated, and shown in ***Fig. 7.3***. It is obvious that there are large discrepancies between the estimated value and the actual experimentally controlled temperature, especially at oxidizing conditions. The low temperatures calculated for IL+OL assemblages (***Fig. 7.3***), show some similarity with the calculated result of two pyroxene geothermometry on ferric rich natural samples (Andersen and Lindsley, 1981). There may be two reasons for the apparently very low temperatures yielded by this thermometer. Firstly, the data set of Andersen and Lindsley (1979) is largely restricted to lower temperatures (only one experiment above 1000°C), and all ilmenites have low contents of haematite (less then 6 mole%). Secondly, they used a molecular model to describe the solid solution of ilmenite, and such a model may be not sufficient in characterizing the thermodynamic behaviour of this solid solution at conditions beyond those experimentally calibrated; i.e., extrapolation to the non-calibrated conditions (eg. ferric rich) with a molecular model is not reliable.

Because of the limited data available in the literature which contain reliable

information on the compositions of coexisting phases in the pertinent systems at the same controlled experimental conditions, there is no obvious conflict with the results of present study. The self-consistency of the present data is regarded as strong evidence for their validity. Data acquired at different conditions can not be used as a *standard* for testing the credibility of the present data set, since the testing involves an *extrapolation* from a *model*. On the contrary, the present data set may be used as a *standard* to test the *extrapolations* or as part of a data base to develop new models.

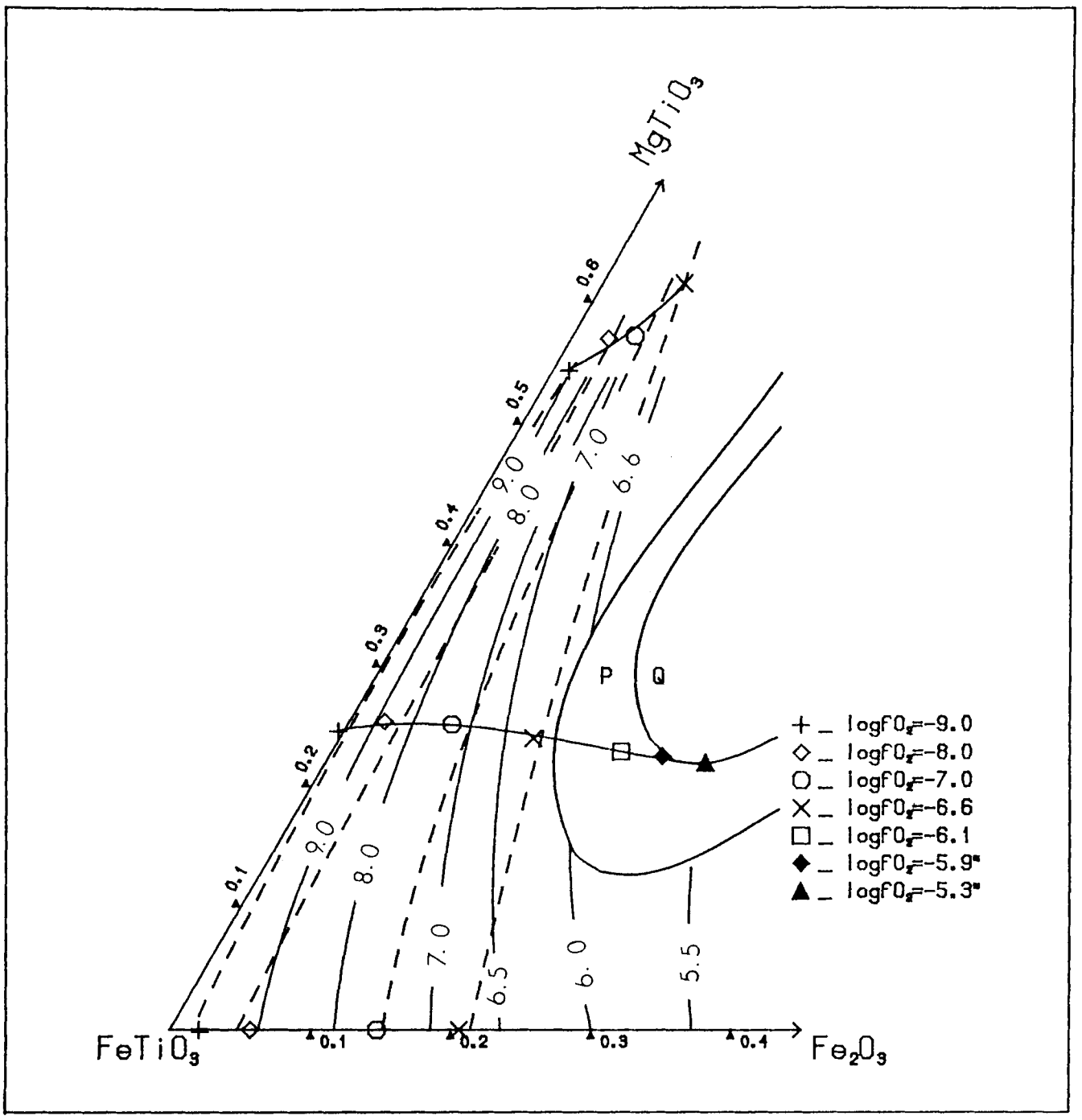

Fig. 7.1 *A comparison between two independent data sets. Solid lines: compositions of ilmenite at different oxygen fugacities, adopted from Woermann et al. (1969b). Oxygen isobars are indicated by the numbers at the lower portion of the graph. Dashed lines: this study. oxygen isobars are at the upper portion of the graph. Symbols on the bottom line (on edge of triangle) are for ilmenites in the assemblage IL+USP+LQ in the system Fe-Ti-Si-O. Symbols on the middle curve are for the ilmenite in the assemblage IL+USP+OL+LQ in the system Mg-Fe-Ti-Si-O. Symbols on the upper curve are for the ilmenites in the assemblage IL+USP+OL+PEROV+LQ in the system Mg-Fe-Ca-Ti-Si-O. Solid curves P and Q (adopted from Woermann et al., 1969b) represent the possible position of the solvus in the ternary solid solution (see chapter 3 and 5). For Fe-rich compositions, the data of Woermann et al. (1969b) show oxidized character relative to this study, but are similar to those of Taylor (1964) for the IL-HM join.*

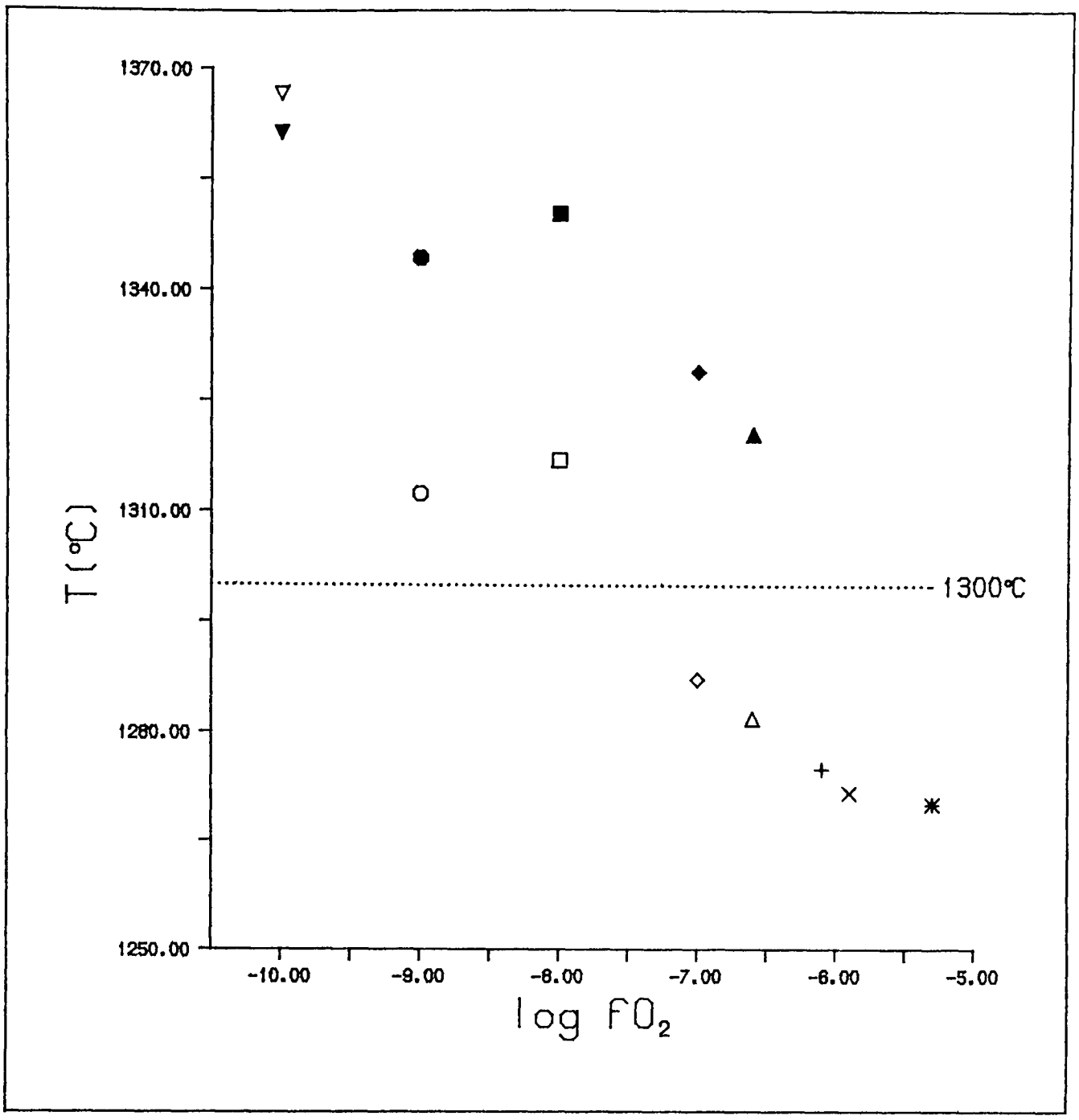

Fig. 7.2 *A comparison between the calculated temperature (determined by the geothermometer of O'Neill and Wall, 1987) and the experimentally controlled temperature (1300°C) in this study. X-axis is the experimentally controlled oxygen fugacity (reflecting ferric content in USP). Open symbols are calculated from OL+USP pairs in the assemblage IL+USP+OL+LQ in the system Mg-Fe-Ti-Si-O. Solid symbols are from the OL+USP pairs in the assemblage IL+USP+OL+PEROV+LQ in the system Mg-Fe-Ca-Ti-Si-O. The pair (open and solid symbols) is from same run at each oxygen fugacity. Dotted line represents the experimentally controlled temperature. The discrepancies are reasonably small between the calculated and the experimentally determined temperatures, and may indicate the general agreement between the two data sets of Rawson and Irvine (1979-1980), and present study, though still suggest that the geothermometer of O'Neill and Wall (1987) needs more refinement.*

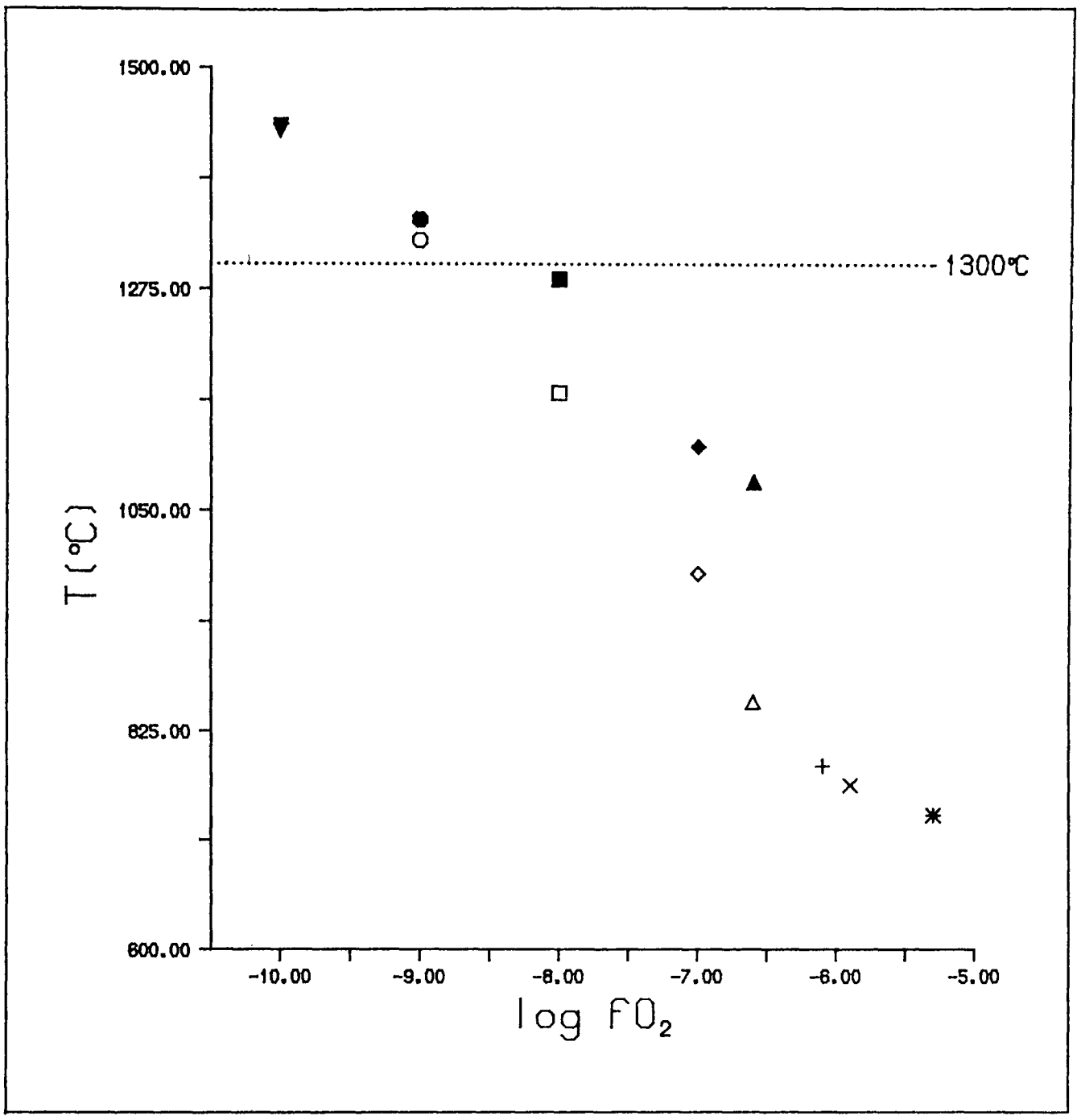

Fig. 7.3 *A comparison between the calculated temperature (determined by the geothermometer of Andersen and Lindsley, 1981) and the experimentally controlled temperature (1300° C) in this study. X-axis is the experimentally controlled oxygen fugacity (reflect ferric content in IL). Open symbols are calculated from OL+IL pairs in the assemblage IL+USP+OL+LQ in system Mg-Fe-Ti-Si-O. Solid symbols are from the OL+IL pairs in the assemblage IL+USP+OL+PEROV+LQ in system Mg-Fe-Ca-Ti-Si-O. The pair (open and solid symbols) is from same runs at each oxygen fugacity. Dotted line represents the experimentally controlled temperature. The reasonable small discrepancies between the calculated and the experimentally determined temperatures at relatively reducing conditions (log fO_2 = -9.0) suggest that Andersen and Lindsley's (1981) model may be valid for ferric poor compositions, but erroneous for ferric rich compositions. A serious recalibration of this geothermometer may be needed.*

CHAPTER 8

GEOLOGICAL IMPLICATIONS: A DISCUSSION

8.1. The fO_2 character of basalts and redox partial melting

For most `non-subduction` related basaltic magmatism, the generation of magma has been mostly attributed to mantle diapir adiabatic upwelling. In this adiabatic upwelling model, the solidus of upwelling mantle peridotite intersects with adiabatic geotherms as a result of adiabatic depressurisation and partial melting occurs. However, such a model does not require oxygen fugacity as a necessary parameter, and therefore, the oxygen fugacity of basalt is often considered indifferent to the melting processes, and the redox character of magma as predefined by the redox state of the mantle source.

Results from mantle xenolith studies have usually shown that the redox state of the Earth's upper mantle is heterogeneous, and ranges from IW, defined by the precipitation of Ni-Fe alloy to well above NNO; though the methodology used in these redox state studies, (e.g. intrinsic fO_2 measurement: Arculus and Delano, 1981; Arculus *et al.*, 1984; geothermometry and oxygen barometry from equilibrium mantle assemblage: Haggerty and Tompkins, 1983; O'Neill and Wall, 1987) is in as much controversy as the results. Possibly, a view of homogeneous redox state of the mantle is more unrealistic than that of heterogeneous state, since the mantle peridotites do not contain any efficient buffer assemblage for oxygen fugacity and there is evidence suggesting that the Earth's upper mantle is subject to a secular evolution towards oxidation. The proposed EMOG* assemblage (Eggler and Baker, 1982) as a potential buffer is not widely accepted due to the solid solution effect and the scant appearance of elemental carbon and primary carbonate in mantle xenoliths. While evidence supporting a secular evolution of the upper mantle towards oxidation prevails, its redox state should not develop to a specific value, and thus a range of oxygen fugacity in the

* Assemblage enstatite (MgSiO3) + magnesite (MgCO3) + olivine (Mg2SiO4) + graphite. representing the reaction Mg2SiO4 + C + O2 = MgSiO3 + MgCO3.

mantle is to be expected. Thus, adiabatic upwelling of mantle diapirs of variable redox state possibly generate basalts with different oxygen fugacities.

However, oxygen fugacity study of the most common tholeiitic basalts shows a relatively narrow range of oxygen fugacity, near QFM. With a heterogeneous mantle, a simple adiabatic upwelling model may not be satisfactory in interpreting this phenomenon. Therefore, oxygen fugacity as an intensive variable should be considered in a magma genesis model with a view to preferentially generating melt at redox states near QFM.

A recent study (Taylor and Green, 1988) on the effects of volatiles on magma genesis has shown that change of gas species in system Peridotite-C-H-O can strongly influence the solidus position of a peridotite. Therefore, redox partial melting has been suggested as an important mechanism for magma generation. In this established redox melting model (Taylor and Green, 1988; Foley, 1988) gas species in the system C-H-O from mantle outgassing are essential. The volatile phase from deep mantle is thought to be very reduced and dominated with CH_4, but becomes oxidized with ascent. The oxidized fluid phase is H_2O and CO_2 rich and drastically decreases the solidus of a mantle peridotite. Nevertheless, the experiments carried out by Taylor and Green (1988) are at C-H-O fluid saturated conditions, and so far, there has not been a reliable estimation on the absolute abundance of these C-H-O species in the mantle. The extremely restricted occurrence of carbonatite and the absence of elemental carbon and hydrous minerals in most of the common mantle xenoliths, and the low concentration of H_2O and CO_2 in common basalts, cast serious doubt on the roles of C-H-O fluid on extensive melting.

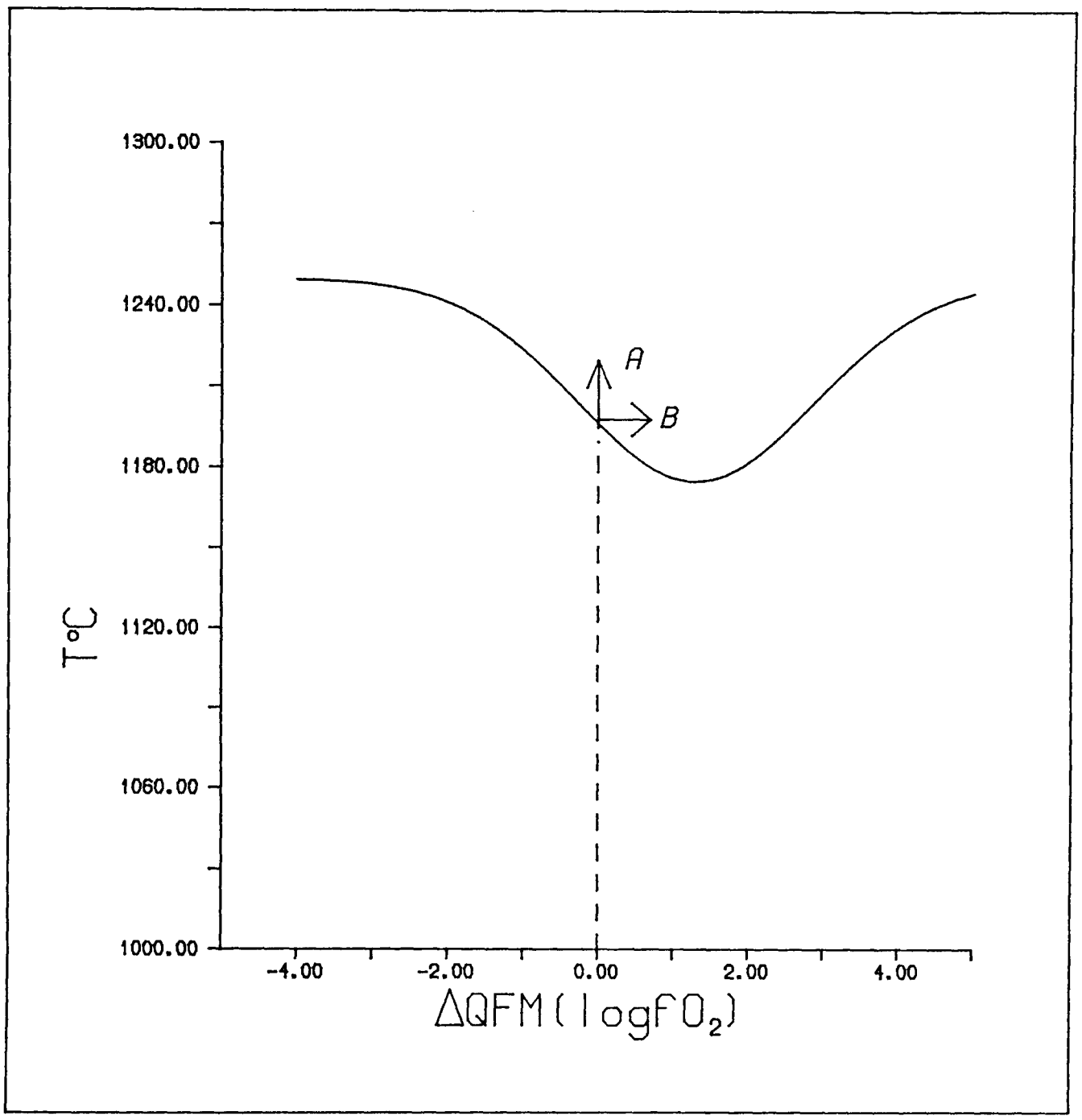

Fig. 8.1 *Hypothetical solidus of peridotite as a function of oxygen fugacity. Solid curve: the solidus. A: temperature perturbation. B: redox perturbation. Redox perturbation may be more important for magmatism on the evolved Earth.*

The possibility of redox melting, however, is not restricted to redox volatile-induced partial melting but also includes Fe^{3+}/Fe^{2+} induced partial melting. The Fe^{+3}/ Fe^{+2} induced partial melting has been illustrated in Chapter 1 (***Fig. 1.1, 1.2***) with a simple system Fe-Si-O, in which the fayalite-magnetite cotectic represents a thermal trough, oxidation and reduction across this thermal trough result in possible melting. The conclusion drawn from analysis of the simple system holds in the more complicated systems Mg-Fe-Ti-Si-O and Mg-Fe-Ca-Ti-Si-O of this study (Chapter 4). For simplicity, mantle peridotite may be viewed as a pseudo-binary system, and change of oxygen fugacity will result in change of Fe^{3+}/Fe^{2+} ratio, and may result in decrease of solidus temperature for a peridotite (***Fig. 8.1***). Clearly, mantle melting will depend on redox state in the absence as well as the presence of volatiles.

Confidence in the possibility of the existence of redox melting in mantle processes can, at least, be justified from the following two facts:

1. The absolute abundance of iron in the Earth's upper mantle which can be reliably estimated from mantle xenoliths, varies from 7-11 wt% (total iron as FeO).

2. Subduction of oxidized oceanic crust supplies a transport mechanism for more oxidized oceanic crust reaching the more reduced portion of the Earth's upper mantle. Oxygen combined with ferric iron is non-volatile, and devolatization during subduction will not change the oxidized character of the oceanic crust.

While evidence supports the idea that redox state can strongly influence the degree of partial melting, igneous petrologists may be interested in the melt productivity of redox perturbation at different redox states. An estimate of this productivity can be derived by differentiation of the melt-logfO_2 function which is an empirical regression of the experimental data presented in this study. The derived function $dM/d(\log fO_2)$ (M: degree of partial melting) has been graphically shown in Chapter 6 (***Fig. 6.8, 6.9***) for

assemblage IL+USP+OL+LQ in simple system Mg-Fe-Ti-Si-O. Interestingly, the maximum melt productivity is at an oxygen fugacity about 0.5logfO_2 unit lower than NNO, ie. near QFM, which is the typical redox state of the most common basalts. The coincidence between the oxygen fugacity value of the maximum melt productivity and that of most common basalts may not be fortuitous. A detailed analysis on the processes of magma segregation from source region can further support the possibility that the typical oxygen fugacity can be produced through redox partial melting.

Over the past few years, the processes involved in extraction of magma from mantle have been subjected to intensified study. Recent reviews have been given by Ribe (1987b) and McKenzie (1985). These studies can be basically divided into two related parts, (1) the geometry of melt distribution in the crystalline framework, and (2) expulsion of the melt from the framework.

Beere's study (1978) shows that the melt network forms a stable three-dimensional interconnected network at all melt fractions if the dihedral angle is less than 60°. For basic silicate melts, the dihedral angle is less than 60° (Waff and Bulau, 1979; Toramaru and Fujii, 1986), thus, the silicate melt in the mantle forms an interconnected network if textural equilibrium can be achieved.

Calculation on the fluid dynamical processes involved in the expulsion of melt from the crystaline matrix by compaction (McKenzie 1984) demonstrates that basic melt can separate quickly from the partially molten mantle, and the melt fraction present in the mantle during melting is likely to be very small, 1% for picritic basalt.

For a given redox perturbation ΔfO_2, for example, oxidation, which generates melt fraction more than 0.01 in the mantle over a time span Δt, if Δt is sufficiently long, then, the generated melt can not be retained in the mantle, and melt segregation will happen simultaneously as melting advances. Obviously, the melt produced at later stage should be relatively oxidized. If there is no mixing happening between the melt generated at different stages, then, the quantities of basalts with different oxygen

fugacities will have a distribution pattern similar to ***Fig. 6.9***, though this Figure is derived from analysis of `batch melting`. If mixing does happen, then, the distribution pattern should be tighter around the maximum value, simply because the greatest volume of melt is produced at the maximum.

Therefore, if redox state of the Earth's upper mantle is to be incorporated in a magma genesis model, such a model is likely to portray a dynamic process, in which redox state perturbation, or more specifically, the secular development of the Earth's upper mantle towards oxidation, is the cause of partial melting. On the other hand, if P and T perturbation can not generate the oxygen fugacity character of the common basalts (QFM) from the heterogeneous (redox state) mantle, then these perturbations are likely to be the results of magmatism rather than the cause of it (see Chapter 9, future work).

8.2. Redox reaction in subduction related processes

Arc volcanism is related to the subduction of oceanic crust into the Earth's upper mantle. Although there is evidence supporting the three component model, ie. the involvement of MORB-like mantle wedge, subducted slab, and sediments (Ellam and Hawkesworth, 1988), the melting processes and the evolution of arc volcanism is still not clear. The prevailing hypothesis is that the dehydration of the slab causes partial melting in the mantle wedge and POAM (plagioclase, olivine, amphibole, and magnetite) fractionation at relatively high oxygen fugacity causes the calc-alkaline volcanism. However, there have been warnings on the study of arc related volcanism that the redox state may be much more complicated than the assumed conditions of near NNO (Gill, 1981); and the effects of redox state and redox reaction on partial melting in arc environments are basically conjectural (Arculus and Powell, 1986). Ironically, island arcs are the most sensitive localities for redox reaction, because this is the environment of first encounter between the relatively oxidized oceanic crust and the mantle wedge, which is believed to be MORB-like, and therefore, with redox character

near QFM. A reexamination of island arc volcanism in terms of redox partial melting is appropriate therefore.

Despite the fact that there has not been a precise estimate of the oxygen fugacity of arc volcanic rock series, the general temporal evolution trend from tholeiitic to calc-alkaline magmatism in arcs indicates a secular evolution toward oxidation (Gill, 1981). The elevated oxygen fugacity has been mostly attributed to the influx of slab derived fluid. High level assimilation may not be responsible for the elevated oxygen fugacity, since xenoliths from arc volcanism indicate oxidizing environments (Arculus and Wills, 1980; Conrad and Kay, 1984). It is highly likely that there is an inversion in the oxygen fugacity versus depth profile; with the top portion of slab representing the highest oxygen fugacity, if the slab is the only source of oxygen.

At the initial stage of subduction, if the mantle wedge is treated as equivalent to MORB or residue of MORB, not only chemically but also physically, then portions of the mantle wedge should be at conditions near or at their solidus. Oxidation of mantle wedge as a result of introduction of slab derived substance at these conditions favours partial melting, and obviously, combined with the effects of the slab-released fluid phase, partial melting can occur in spite of the possible temperature drop in the thermal regime. If partial melting, melt segregation, and source depletion occur simultaneously, then the mantle wedge is likely to continuously approach a state of equilibrium with the incoming slab derived material, and therefore will undergo continuous chemical modification. Models in which the mantle wedge is considered to be a source with constant chemistry as a result of vigorous convection within the mantle (Arculus and Powell, 1986) may be not satisfactory. Arc volcanism shows a strong temporal character, and the continuous supply of oceanic crust may be regarded as a constant source, thus emphasizing the likely importance of temporal variation in the wedge component. Even if convection does exist in the mantle wedge, the speed of homogenization by convection is unlikely to exceed the rate of subduction. Consequently, the evolution of the mantle wedge will be towards oxidation, in

conjunction with the tholeiitic series being replaced by the calc-alkaline series. Some of the depleted character of the calc-alkaline series may represent the depleted character of the wedge, eg. HREE (heavy rare earth elements) depletion, higher Mg-number, Ni and Cr.

Although the oxidized oceanic crust has been considered as an important component in subduction related volcanism, its direct contribution to partial melt and the geochemistry of the volcanic products is not thoroughly understood. One of the major characteristic of the calc-alkaline series rock is the LILE (large iron lithophile elements) enrichment relative to HFSE (high field strength elements). While rejecting the wedge (which is expected to become progressively oxidized during arc evolution) as a possible site for a residual HFSE-rich phase, partial melting of the subducted slab has been excluded from the recently developed model due to the typical high LILE/HFSE ratio in arc volcanism (Arculus and Powell 1986; Ellam and Hawkesworth 1988). Thus, the slab involvement in arc volcanism is believed to be the supply of IRS fluid (cf. Gill, 1981), which causes the enrichment of LILE relative to HFSE in the wedge and subsequent partial melting.

However, unlike the mantle wedge, the subducted slab is initially highly oxidized, and partial melting of oceanic crust under very high oxygen fugacities is unknown. If redox state can strongly influence the relative quantities of the coexisting phases, it is plausible that the dominating existence of oxides, eg. ilmenite, as residual phases in the slab at very high oxygen fugacity, (Chapter 6, ***Fig 6.4***), is responsible for the depletion of HFSE. Therefore, partial melting of slab may not produce a trace element signature different from the observed (high LILE/HFSE).

At an early stage of arc development, larger degree partial melting may occur in both the mantle wedge and the subducted slab due to (1) the higher reducing capacity of the wedge, (2) sudden influx of IRS fluid in the wedge, and (3) the possible higher initial temperature of the wedge. As the wedge is progressively oxidized and depleted,

* Fluid released during slab dehydration, which will be rich in incompatible trace elements, in radiogenic Sr and He and possibly Nd and Pb, and in silica.

the reducing capacity of the wedge decreases, thus the degree of partial melting of both the wedge and subducted slab decreases despite the possible existence of a higher concentration of IRS fluid. This small degree of partial melt from slab may be relatively silica rich, saturated with volatiles and with high concentration of LILE and REE, and therefore, in effect, similar to the IRS (Gill, 1981) fluid. Infiltration or ascent of this silicate melt and IRS fluid, which are highly oxidizing, causes further partial melting along the path, partially due to the redox reaction. Ascent of the generated magma may be principally a reduction process due to the reversed redox profile, and therefore, dissolution of primary oxides is a major reaction. This may account for the absence of oxide phenocrysts in calc-alkaline rocks.

Although there have been numerical modelling of subduction-related back-arc spreading (eg. Toksoz and Hsui 1978), the chemical reaction in the back-arc spreading induced by the subduction of oceanic crust is not clear. Even whether the subducted slab participates in partial melting is in question. The most widely accepted hypothesis is that the slab involvement in arc volcanism is the supply of IRS fluid which is enriched in LILE relative to HFSE. Based on the assumption that the contribution from slab is characterized by the high LILE/HFSE ratio in the generated magma, the possibility of a contribution of the concurrent subduction to the generation of Lau and North Fiji back-arc basin basalt has been excluded (Volpe, et al. 1988; Ewart and Hawkesworth, 1987). However, if redox reaction is considered, melting of the subducted slab becomes possible, and the trace element and Sr-Nd isotopic character of Lau Basin basalt may be attributed to the mixing of MORB and slab. Therefore, back-arc volcanism and the opening of back-arc basin may be caused by the extensive or complete redox reaction between the concurrently subducted slab and MORB-like mantle (behind the wedge) due to the high efficiency of convection in the back-arc mantle (encounter with Asthenosphere?).

Melting controlled by redox state, unlike melting caused by P, T perturbations, has a maximum degree of partial melting at a given P, and T. When this maximum

amount of melt is extracted, the residue is subjected to maximum depletion. Therefore, the secular development towards oxidation of the wedge contributes to the generation of depleted lithosphere. If accretion of arc is the major process of continent growth, then, during its formation, subcontinental lithosphere should have experienced an episode of oxidation and depletion. This oxidized and depleted subcontinental lithosphere may be preserved, especially beneath the relatively young continents.

Subduction beneath this depleted continental lithosphere will not cause significant melting, if any, of the subducted slab due to the elevated solidus of the slab at highly oxidizing conditions. Therefore, the oxidized oceanic crust may be preserved and transported to deep regions of the Earth's mantle. Once the slab detaches from the depleted subcontinental lithosphere and encounters the relatively reduced portion of the mantle, redox partial melting occurs. Therefore, deep source magmatism may also be subduction related. Thus if back-arc spreading is partially caused by redox melting, then so, by analogy, might continental rifting.

8.3. Oxides enrichment in some layered intrusions

The discussion in Chapter 6 suggests that oxygen fugacity can strongly influence the bulk composition (or proportion) of the coexisting solid phases. Such a composition is basically determined by the oxide/silicate ratio of the solid phases (***Fig. 6.6***). Therefore, change in oxygen fugacity during crystallization of mafic intrusions may result in enrichment in oxide minerals in particular precipitation bands. One possible mechanism for significant oxide enrichment is oxidation at high oxygen fugacities. At this condition, oxides precipitate, and silicate dissolves. An increase in the proportion of oxides caused by oxidation is associated with the coexisting silicates showing high MgO contents (eg. Morse 1980). Fe-Ti oxides enrichment in Kiglapait mafic intrusion (Morse, 1980) may be used as one example.

8.4. Redox reaction in kimberlite and melilitite genesis

In the previous sections, some large scale geological phenomena have been discussed in terms of redox reaction. Although it seems to be convenient to involve a redox mechanism in interpreting these phenomena, the finger prints of redox reactions on a smaller scale phenomenon (eg. hand specimen), may not be easy to detect or separate from other effects. After all, we principally observe the products of redox reactions which normally have more than enough time to reach equilibrium. Therefore, the initial state of the redox reaction and the progression of events in redox reaction are not preserved, and hence, beyond observation. In addition, where changes in the natural system may be observed, it may be difficult to distinguish compositional variations caused by redox effects from those due to magma differentiation and mixing.

Unlike other igneous processes, kimberlites and their associated rocks (eg. melilitites, lamproites) are well known for their explosive emplacement character. Although the process (rapid?) of generating kimberlite magma is uncertain, the rapid ascent and solidification enable kimberlite magma to carry large quantities of macrocrysts and mantle xenoliths without significant modification of their original chemistry. Therefore, evidence of mantle environments and processes may be reconstructed with the data from kimberlites and associated rocks.

References on kimberlite petrology numerous. The nature and variation of Mg-rich ilmenite and olivine, which are most bearing on this study, have recently been reviewed by Haggerty and Tompkins (1984), Shee (1984), and Moore (1987, 1988). One of the important characters of kimberlites revealed by these studies is the extreme variation in chemistry on the individual grain and hand specimen scales. Phases of different sources and/or generations appear to be physically mixed within one specimen, and chemical reactions between these phases are seen at different stages of attaining equilibrium. If redox reaction did contribute to partial melting, and magma generation was a rapid process, then, the finger prints of redox reaction (intermediate states

towards equilibrium, or even initial oxidants and reductants) may be preserved in the rapidly erupted kimberlite magmas.

The olivine populations in kimberlites and the nature of their zonations have recently been summarized by Moore (1988),

> '*... Two chemically distinctive olivine populations are present in all of the kimberlites studied. The dominant olivine population, which includes large rounded olivines and smaller euhedral crystals, is Mg-rich relative to late-stage rim compositions (of all crystals). It is ..., reflecting Rayleigh-type crystallization during magma evolution. The most Mg-rich of these olivines are considered to be similar to those in the mantle source rock. The second compositional population, generally very subordinate, though markedly more abundant in the megacryst-rich Monastery kimberlite, is Fe-rich relative to rim compositions. This group of olivines crystallized from evolved liquids in equilibrium with iron rich megacryst, both entrained by the kimberlite magma during ascent...*'

Moore (1988) suggested that olivine could be used as a monitor of the magma evolution path of kimberlites and melilitites. The implication of the above statement is that only the most Mg-rich olivine may have contributed to the generation of *primary* kimberlite magma, other olivines are either products of crystallization (implying solidification) or entrained megacrysts and their fragments (xenocrystic); and the observed kimberlites represent highly evolved products.

Although Moore (1988) placed emphasis on mixing of olivine populations from different states of fractional crystallization, he also noticed (Moore, 1988; Moore and Erlank, 1979) that different olivine populations were formed in different redox environments. The Fe-rich olivine population was believed to be formed at reducing conditions.

Zonation of ilmenite macrocrysts in kimberlite has also been discussed in many publications (eg. Shee, 1984; Haggerty and Tompkins, 1984; Moore, 1987). Microprobe

analyses (Shee, 1984) show that the rims of ilmenite are enriched in magnesium relative to the their cores, while the ferric contents of the rims are either the same as those in the cores or are higher. Comparing with the experimentally determined oxygen isobars (***Fig. 3.2***) the core to rim composition change may be the result of oxidation (Shee, 1984; Moore, 1987). Detailed study of the ilmenite cores suggests that the cores in some cases (e.g. Haggerty and Tompkins, 1984) were initially highly oxidized, some of them had compositions at the HM-rich limb of the solvus in the ternary solid-solution IL-GK-HM (Haggerty and Tompkins, 1984; Haggerty *et al.*, 1985). These initially oxidized cores were substantially reduced at some stage of kimberlite (or melilitite) magma evolution, and this process was ambiguously termed high temperature `subsolidus` reduction by Haggerty and Tompkins (1984) and Haggerty *et al.* (1985). Texture evidence from ilmenite macrocrysts in olivine melilitites from Namaqualand-Bushmanland (Haggerty *et al.*, 1985) indicates that such a reduction process possibly happened at an early stage of melilitite magma evolution, but Haggerty *et al.* (1985) also suggested that these ilmenite macrocrysts were of xenocrystic origin (and therefore, accidental inclusions which should not have any significance in the generation of the melilitite magma).

However, it is interesting that all kimberlites and melilitites should have sampled the similar sets of macrocrysts if the macrocrysts are indeed xenocrysts. Since the entrainment of xenocrysts might be expected to be a random process, the systematic co-appearance of the reduced Fe-rich olivine population, the Mg-rich olivine (oxidized?) population, and the oxidized ilmenite macrocrysts may suggest that such a co-appearance is a source feature of kimberlite and melilitite magma.

The fundamental premise of Moore's (1988) hypothesis, that normal zonation of Mg-rich olivine population was formed during an extended period of Rayleigh-type crystallization (implying solidification), can be easily questioned. Zoned crystals and reaction rims are not exclusively formed during solidification processes. The formation of zonations or reaction rims only represents the precipitation or modification of

particular phases with specific compositions, while other phases, or the same phases with different compositions might be dissolving, and the overall amount of melt increasing. Thus, zonations and reaction rims may supply information on redox reaction, with the core compositions representing the initial redox states, and partial melting.

Therefore, the evidence from the macrocrysts in kimberlite and melilitite may indicate a specific situation in which there is a interaction between relatively reduced (e.g. Fe-rich olivine) and relatively oxidized (e.g. initial ilmenite macrocrysts) mantle material, and such a situation is fundamentally important with the viewpoint of redox reaction and redox partial melting.

It is highly reasonable to group together the Mg-rich olivine with ilmenite macrocrysts, since for a given bulk composition the olivine becomes Mg-rich at higher oxygen fugacities (Chapter 6). Therefore, Mg-rich character of olivine does not necessarily indicate that its source was depleted, nor that it had a necessarily higher temperature of formation (Chapter 6).

Mixing of the relatively reduced material (left side of ***Fig. 6.7***) with the relatively oxidized material (right side of ***Fig. 6.7***) will result in the reduction and dissolution of ilmenite macrocrysts, dissolution of Fe-rich olivines, and precipitation of olivines with intermediate compositions. Therefore, normal zoning of the Mg-rich macrocrysts can certainly occur during reduction melting of the oxidized material. The dissolution of ilmenite macrocrysts is possibly a slow process, and ulvospinel is formed as lamellae in the host of ilmenite to maintain the equilibrium between the oxides with the newly formed redox environment. Therefore, the `subsolidus` reduction of Haggerty and Tompkins (1984) and Haggerty *et al.* (1985) may not be a real subsolidus reaction.

redox reduction of the existing melt may result in over saturation of olivine in the melt, fast crystallization of olivine from such melt will produce an idiomorphic morphology which is characteristic of olivine phenocrysts in kimberlites and melilitites.

Such a fast crystallization mechanism may also explain the large numbers of inclusions in these phenocryst olivines and the formation of reversed zoning of some Fe-rich olivines. Fluctuation in redox state by changing the proportion of oxidized and reduced material in the `mixed` magma will result in possible fluctuation in zoning pattern, this may explain the `unusual hopper` olivine described from olivine melilitites by Moore and Erlank (1979).

The ilmenite macrocrysts (which were firstly reduced, to develop ulvospinel lamellae) in olivine melilitite from Namaqualand-Bushmanland, show reaction rims of Mg-titanomagnetite, which was inferred to result from oxidation (Haggerty *et al.*, 1985). The present study supports such a conclusion. Unlike the Si-free system (eg. Fe-Mg-Ti-O), oxidation of ilmenite+ulvospinel pairs in the silicate-bearing situation will result in the dissolution of ilmenite and precipitation of spinels (Chapter 6). Therefore, the reaction rim of ilmenite macrocrysts (Haggerty *et al.*, 1985) may represent a later stage oxidation with a slight decrease in temperature. This later stage oxidation may correspond to the reversed zoning in the edge of normal `hopper` olivines in these rocks.

The above interpretation on the kimberlite and melilitite magma genesis relies on the premise that the macrocrysts in kimberlites were not xenocrysts, thus they represent the magma source character, which involves a mixture of relatively reduced and relatively oxidized material. Following this premise, the kimberlite magma represents the heterogeneous products of initial stage redox melting of mantle rocks.

The relatively oxidized material in the above discussion may be from subducted ancient oceanic crust which has experienced a very complicated history (eg. continental margin volcanism). Similarly, the relatively reduced material may also have passed a very complicated but unknown history. The possible involvement of subducted slab in the generation of kimberlite magma has been speculated on (eg. Helmstaedt and Gurney, 1984). If such an involvement is true, the redox melting mechanism may play an

important role in kimberlite magma formation, and such a mechanism is also likely to be important for other continental alkaline series rocks. A systematic study on the relationship between calcalkaline and alkaline magmas and the evolution of subducted oceanic crust is clearly important.

8.5. A further discussion on reduction melting

The experiments carried out in this study are in very simple systems, therefore, the results may not be representative of more complicated real geological situations. The silicate (olivine) in the experiments is almost ferric free, thus, its stability shows a single trend as oxygen fugacity changes. Although olivine can be representative of other ferric free phases (eg. orthopyroxene), it is totally inadequate to represent ferric bearing silicates (eg. omphacitic pyroxene). The ferric rich silicates are believed to be stable in alkaline rich bulk compositions, and thus, form possible thermal barriers (and thermal troughs between these barriers) at specific oxygen fugacities (Seifert, O'Neill, per. comm.). The alkaline-rich situation may be pertinent to subducted slab situation due to both the possible involvement of alkaline rich sediments and reaction between oceanic crust and sea water (spilitite). Therefore, the alkaline enriched bulk compositions may be involved in reduction melting of subducted slab.

The possible existence of more than one thermal trough in the entire redox regime may suggest that while the magma source development (in terms of redox state) may be continuous, the melt generation can be discontinuous, and thus contribute to the diversity of igneous rocks.

CHAPTER 9

CONCLUDING REMARKS AND PROPOSED FURTHER RESEARCH

9.1. Experimental results

Detailed summary on the experimental results has been given in Chapter 6. However, the major conclusions will be restated in this section.

1. In systems Mg-Fe-Ti-Si-O and Mg-Fe-Ca-Ti-Si-O, the compositions of coexisting phases (in assemblages IL+USP+OL+LQ and IL+USP+OL+PEROV+LQ respectively) are strongly dependent on oxygen fugacity at constant temperature (1300°C) and pressure (1atm).

2. Proportions of the coexisting phases (including melt) are also sensitive to change of oxygen fugacity, thus redox perturbation can result in partial melting.

3. Maximum degree of partial melting leading to the maximum depletion of the solid residue occurs at about 0.5 log fO_2 unit above NNO in the assemblage IL+USP+OL+LQ in system Mg-Fe-Ti-Si-O.

4. Maximum melt productivity as the result of unit increase in log fO_2 exists at about 0.5 log fo_2 unit below NNO, that is near QFM which is typical oxygen fugacity of common basalts.

9.2. Concluding remarks on redox partial melting

Due to the reconnaisance nature of this study and the necessarily restricted extent of the studies in P-T and chemical space, the following concluding remarks must be very tentative with respect to the wider importance of redox melting.

1. It is almost certain that some part of the Earth's upper mantle is in a reduced redox state (eg. below or near QFM). If these parts are at or near their solidus

temperature, then, oxidation of these parts will cause partial melting.

2. The commonly observed oxygen fugacity distribution character of tholeiitic basalts (i.e. near QFM) may not just reflect the redox state of the source region, but more the process of magma generation and extraction. The relationships between melt productivity and redox state demonstrated in this thesis provide an explanation of the QFM character of tholeiitic basalts, which is not simply dependent on a uniform source redox state.

3. If the redox state of the Earth's upper mantle is heterogeneous, and if P-T perturbation can not generate the QFM character of common basalts, then, redox perturbation (oxidation) may be accepted as the major cause of basaltic magmatism on the evolved Earth.

4. Magma source should not be regarded as a closed system with constant bulk chemistry. For tholeiitic magmatism, partial melting, melt extraction, and source depletion are simultaneous and continuous. A magma source can be a large area which contains both relatively fertile and relatively depleted portions. For tholeiitic basalts, its major element chemistry is determined by the source portions where there is maximum melt productivity.

5. Oxidation may contribute partially to the depletion of the mantle wedge underlying arcs and the subcontinental lithospheric mantle. Thus, oxidation plays important roles in continental growth and stabilization.

6. Recycling of oceanic crust is not a simple recycle, it involves at least redox reaction which may be responsible for various types of magmatism. However, subduction of the oxidized oceanic crust beneath the oxidized and depleted subcontinental lithospheric mantle will not result in extensive melting of the crust, due to the elevated solidus temperature of the highly oxidized oceanic crust.

7. Transport of the oxidized crustal material to the deep mantle makes it possible

that deep source magmatism is also caused by subduction-related redox reaction. The involvement of the subducted slab in kimberlite magma formation is supported by the redox reaction mechanism. Thus, the generation of kimberlite magma may represent an initial stage of redox melting of mantle rock and subducted slab.

8. Reverse to melting process, oxidation may be responsible for the enrichment of Fe-Ti oxides in some layered mafic igneous intrusions during solidification.

9. The possible existence of more than one thermal trough on the solidus of a magma source within the entire redox regime may result in the discontinuity in generation of magma whose source development, however, may be continuous. Thus, fractionation is not necessary (and hence, intermediate members, as well) for producing magmas with significant difference in major element chemistry from simple source (eg. MORB+SLAB?).

9.3. Proposed further research

In this study the melt productivity as the result of redox perturbation has been described as a function of $\log fO_2$ at 1300°C, ie.

$$\left.\frac{\partial M}{\partial(\log fO_2)}\right|_{T=1300\,^{\circ}C} = F_O(\log fO_2) \tag{9.1}$$

If data at different temperatures are available, the melt productivity as result of redox perturbation can be described as a function of T and $\log fO_2$ (***Fig. 9.1***), i.e.

$$\frac{\partial M}{\partial(\log fO_2)} = F_O(T, \log fO_2) \tag{9.2}$$

Obviously, at different temperatures, the redox state at which the melt productivity is maximum should satisfy the condition

$$\frac{\partial^2 M}{\partial (\log fO_2)^2} = \frac{\partial F_O(T, \log fO_2)}{\partial (\log fO_2)} = 0 \tag{9.3}$$

If the T-logfO_2 relationship defined by the above equation is close to QFM (eg. ***Fig. 9.1***), then, redox perturbation is possibly responsible for the generation of basaltic magma, which has the typical oxygen fugacity near QFM. So far, the T-logfO_2 relationship has been determined only at 1300°C in a relatively simple system Mg-Fe-Ti-Si-O.

Similarly, thermal perturbation can also be described as a function of T and logfO_2, i.e.

$$\begin{cases} \dfrac{\partial M}{\partial T} = F_T(T, \log fO_2) \\ \log fO_2 = \psi(T, X_i) \end{cases} \tag{9.4}$$

Therefore, the temperatures, at which the melt productivity is the maximum (if the maximum does exist) at different redox states, should satisfy the relationship

$$\begin{cases} \dfrac{\partial^2 M}{\partial T^2} = \dfrac{\partial F_T(T, \log fO_2)}{\partial T} = 0 \\ \log fO_2 = \psi(T, X_i) \end{cases} \tag{9.5}$$

If T-logfO_2 relationship defined by the above equation is close to QFM, then, thermal perturbation is likely to be the cause of magmatism, but if not, thermal perturbation, which can be observed in mantle xenoliths, is likely to be the result of magmatism.

Therefore, the relative importance of redox perturbation and thermal perturbation in tholeiitic magma genesis can be distinguished through the observation of state control on the effect of different state perturbations (***Fig. 9.1***), which requires extension

of the experiments reported in this thesis to a wider range of T conditions (and possibly P and bulk compositions).

Experiments at different temperatures on more complicated bulk compositions, especially alkaline-bearing compositions are required for understanding the behaviour of subducted slab.

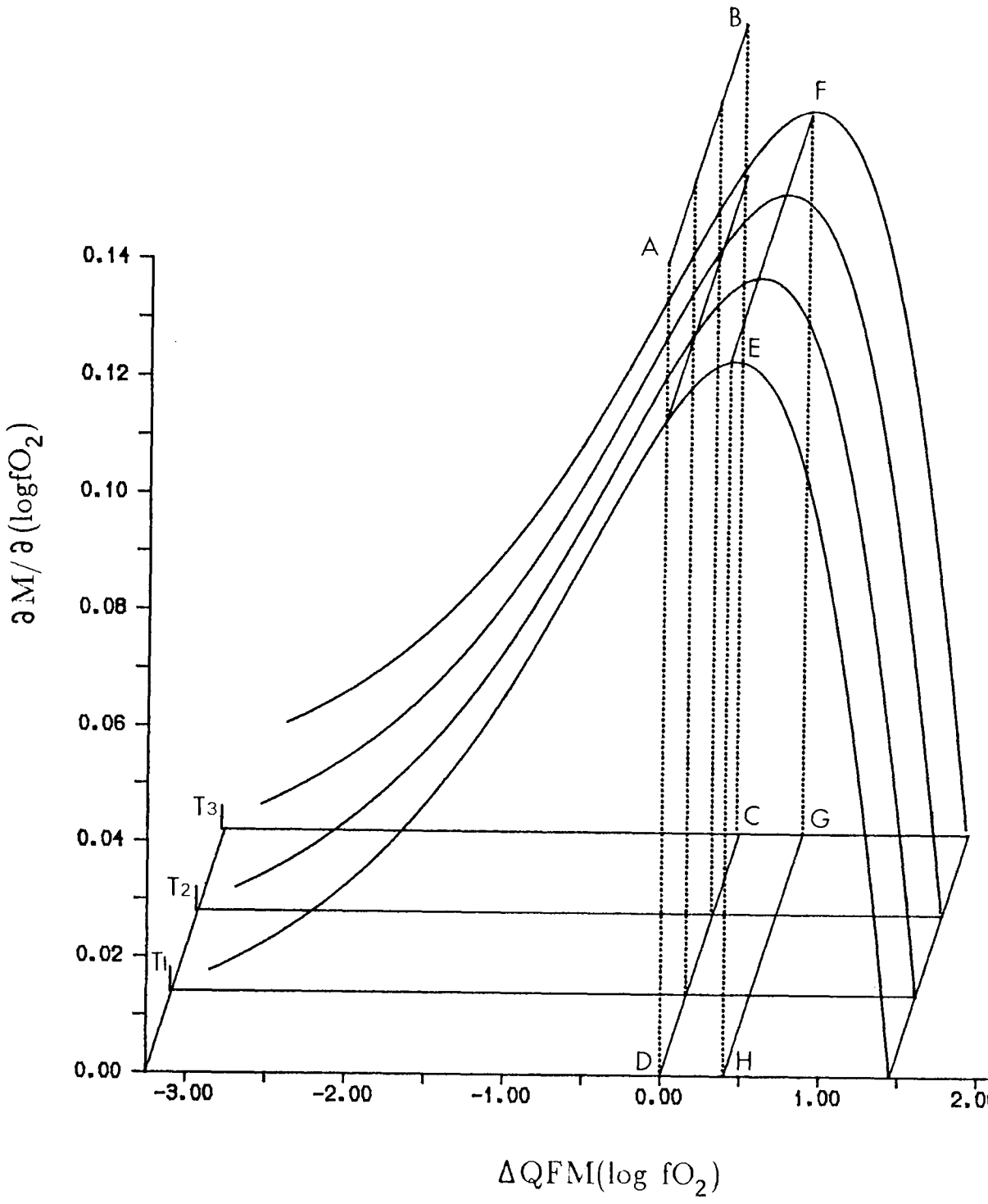

Fig. 9.1 *Hypothetical diagram for melt productivity of redox perturbation as a function of temperature and oxygen fugacity. Plane ABCD represents QFM. The maximum melt productivity at different temperatures is represented by the curve EF, and its projection, GH, on to the plane T-logfO_2 characterizes the T-logfO_2 relationship defined by equation (9.3). If the projection GH is close to CD (QFM), then, redox perturbation is likely to be responsible for the generation of basaltic magma.*

REFERENCES

Andersen, D. J. and Lindsley, D. H. (1981) A valid Margules formulation for an asymmetric ternary solution: revision of the olivine-ilmenite thermometer, with applications. Geochim. Cosmochim. Acta. 45:847-853.

Arculus, R. J. (1985) Oxidation status of the mantle: past and present. Ann. Rev. Earth. Planet. Sci. 13:75-97.

Arculus, R. J., Dawson, J. B., Mitchell, R. H. Gust, D. A. and Holmes, R. D. (1984) Oxidation state of the upper mantle recorded by megacryst ilmenites in kimberlites and type A and B spinel lherzolites. Contrib. Mineral. Petrol. 85:85-94.

Arculus, R. J. and Delano, J. W. (1981) Intrinsic oxygen fugacity measurements: techniques and results for spinels from upper mantle peridotite and megacryst assemblages. Geochim. Cosmochim. Acta. 45:899-913.

Arculus, R. J. and Delano, J. W. (1987) Oxidation state of the upper mantle: present conditions, evolution, and controls. In: Mantle xenoliths. Nixon, P. H. (ed) pp 549-598

Arculus, R. J. and Powell, R. (1986) Source component mixing in the region of arc magma generation. J. Geophys. Res. 91:5913-5926.

Arculus, R. J. and Wills, K. J. A. (1980) The petrology of plutonicblocks and inclusions from the the Lesser Antilles arc. J. Petrology. 21:743-99.

Basaltic Volcanism Study Project (1981). Basaltic Volcanism on the terrestrial planets. Pergamon Press, Inc., New York. 1286pp.

Beere, W. (1975) A unifying theory of the stability of penetrating liquid phases and sinitering pores. Acta Metal. 23:131-138.

Biggar, G. M. (1972) Revised temperature calibration and scale. In: Progress in experimental petrology. Report No2 of Natural Environmental Research Council, UK. pp 86.

Biggar, G. M. (1974) Phase equilibrium studies of the chilled margins of some layered intrusions. Contr. Mineral. Petrol. 46:159-167.

Biggar, G. M. (1977) Some disadvantages of $Pt_{95}Au_5$ as a container for m lt n silicates. Mineral. Mag. 41:555-556.

Bishop, F. C. (1980) The distribution of Fe^{+2} and Mg between coexisting ilmenite and pyroxene with applications to geothermometry. Amer J. Scien. 280: 46-77.

Bowen, C. W. and Schairer, J. F. (1932) The system FeO-SiO_2. Am. J. Sci. 24:177-213.

Bowen, C. W. and Schairer, J. F. (1935) The system MgO-FeO-SiO_2. Am. J. Sci. 29:151-217.

Buddington, A. F. and Lindsley, D. H. (1964) Iron-titanium oxide minerals and synthetic equivalents. J. Petrol. 5:310-357.

Christie, D. M., Carmicael, S. E. and C. H. Langmuir (1986) Oxidation states of Mid-ocean ridge basalt glasses. Earth Planet. Sci. Lett. 79:397-411.

Colby, J. (1971) Magic IV, a new improved version of MAGIC. Proc. of the VIth Nat. Conf. of EPASA, PIttsburgh.

Conrad, W. K. and Kay, R. W. (1984) Ultramafic and mafic inclusions from Adak Island: crystallization history, and implications for the nature of primary magmas and crustal evolution in the Aleutian Arc. J. Petrology. 25:88-125.

Deines, P., Nafziger, N. H., Ulmer, G. C. and Woermann, E. (1974) Temperature-oxygen fugacity tables for selected gas mixtures in the system C-H-O at one atmosphere total pressure. Bul. Earth Mineral Scie. Exp. Station. No.88. Pennsylvania State Univ.

Ellam, R. M. and Hawkesworth, C. J. (1988) Elemental and isotopic variations in subduction related basalts: evidence for a three component model. Contrib. Mineral. Petrol. 98:72-80.

Eggler, D. H. and Baker, D. R. (1982) Reduced volatiles in the system C-O-H: implication to mantle melting, fluid formation and diamond genesis. In: Akimoto, S. and Manghnani, M. H. (eds.) High pressure research in geophysics. Tokyo: Centre for Acd. Publ. Japan. PP237-250.

Ewart, A. and Hawkesworth, C. J. (1986) The Pleistocene-recent Tonga-Kermadec arc lava: interpretation of new isotopic and rare earth datain terms of a depleted mantle source model. J. Petrol. 28:495-530.

Foley, S. F. (1988) The genesis of continental basic alkline magmas: an interpretation in terms of redox melting. J. Petrol. Special Volume 1988. 139-162.

Frost, B. R., Lindsley, D. H. and Anderson, D. J. (1988) Fe-Ti oxide-silacate equilibria: Assemblage with fayalitic olivine. Amer. Mineral. 73:727-740.

Fujii,N., Osamura,K. and Takahashi,E. (1986) Effect of water saturation on the distribution of partial melt in the olivin-pyroxene-plagioclase system. J. Geophy. Res. 91:9253-9259.

Gill, J. (1981) Orogenic andesites and plate tectonics. Springer-Verlag Berlin.Heidelberg.New York.

Haggerty, S. E. (1978) The redox state of the planetary basalt. Geophys. Res. Ltte. 5:443-446.

Haggerty, S. E., Moore, A. E. and Erlank, A. J. (1985) Macrocryst Fe-Ti oxides in olivine melilitites fron Namaqualand-Bushmanland, South Africa. Contrib. Mineral. Petrol. 91:163-170.

Haggerty, S. E. and Tompkins, L. A. (1983) Redox state of the Earth's upper mantle from kimberlitic ilmenites. Nature 303:295-300.

Haggerty, S. E. and Tompkins, L. A. (1984) Subsolidus reactions in kimberlitic ilmenites: exsolution, reduction and the redox state of the mantle. In: J. Kornprobst (ed.) Proc. 3rd Int. Kim. Conf. Vol 1. pp 323-358.

Hamilton, D. L. and Anderson, G. M. (1967) Effects of water and oxygen pressures on the crystallization of basaltic magmas. In: Basalts. Hess and Poldervaart (ed.) Vol. 1 pp445-482.

Hamilton, D. L., Burnman, C. W. and Osborn, E. F. (1964) The solubility of water and effects of oxygen fugacity and water content on crystallization of mafic magmas. J. Petrol. 5:21-39.

Harris, P. G (1957) Zone refining and the origin of potassic basalts. Geochim. et Cosmochim. Acta. 12:195-208.

Helmstaedt, H. and Gurney, J. J. (1984) Kimberlites of South Africa - Are they related to subduction process? In: J. Kornprobst (ed.) Proc. 3rd Int. Kim. Conf. Vol 1. pp 425-434.

Hill, R. and Roeder, P. (1974) The crystallization of spinel from basaltic liquid as a fuction of oxygen fugacity. J. Geol. 82:709-729.

Hughes, C. J. (1982) Petrogenesis of igneous rocks. in Igneous Petrology Elsevier Scientific Pub. Comp. 445-472.

Hunter, R. H. (1987) Texture equilibrium in layered igneous rocks. in Origins of Igneous Layering. Parsons(ed.) D.Reidel Pub. Comp. 473-503.

Jaques,A.L. and Green, D. H. (1979) Determination of liquid composition in high pressure melting of peridotite. Am. Mineral. 64:1312-1321.

Johannes, W. and Bode, B. (1978) Loss of iron to the Pt-container in melting experiments with basalts and a method to reduce it. Contrib. Mineral. Petrol. 67:221-225.

Kennedy, G. C. (1955) Some aspects of the role of water in rock melt. In: Poldervaart, Arie (ed.) Crust of the Earth. Geo. Sci. Am. Spe. Paper 62:762p.

Kooten, G. K. V. (1980) Mineralogy, petrology, and geochemistry of an ultrapotassic basaltic suite, central Sierra Nevada, California, U.S.A.. J. Petrol. 21:651-684.

Lindsley, D. H. (1963) Fe-Ti oxides in rocks as thermometers and oxygen barometers. Carnegie Inst. of Washington, Year Book 62, pp 60-66.

MacGregor, I. D. (1965) The effect of pressure on the minimum melting composition in the system MgO-SiO_2-TiO_2. Carnegie Inst. Washington Year Book 64, 135-139.

MacGregor, I. D. (1969) The system MgO-SiO_2-TiO_2 and its bearing on the distribution of TiO_2 in basalts. Am. J. Sci.(Schairer Vol.)267A:342-363.

Mattioli, G. S. and Wood, B. J. (1986) Upper mantle oxygen fugacity recorded by spinel lherzolites. Nature 322:626-628.

Mckenzie, D. (1985a) ^{230}Th-^{238}U disequilibrium and the melting processes beneath ridge axes. Earth Planet.Sci. Lett. 72:149-151.

McKenzie, D. (1985b) The extraction of magma from the crust and mantle. Earth Planet. Sci. Lett. 74:81-91.

McKenzie, D. (1984) The generation and compaction of partially molten rock. J. Petrol. 25:713-765.

Moore, A. E. (1987) A model for the origin of ilmenite in kimberlite and diamond: implications for the genesis of the discrete nodule (megacryste) sute. Contrib. Mineral. Petrol. 95:245-253.

Moore, A. E. (1988) Olivine: a monitor of Magma evolutionary paths in kimberlites and olivine melilitites. Contrib. Mineral. Petrol. 99:238-248.

Moore, A. E. and Erlank, A. J. (1979) Unusual olivine zoning- evidence for complex physico-chemical changes during the evolution of olivine melilitite and kimberlite magmas. Contrib. Mineral. Petrol. 70:391-405.

Morse, S. A. (1980) Kiglapait mineralogy II: Fe-Ti oxide minerals and the activities of oxygen and silica. J. Petrol. 21:685-719.

Myers, J. and Eugster, H. P. (1983) The system Fe-Si-O: oxygen buffer calibration to 1500K. Contrib. Mineral. Petrol. 82:75-90.

Nehru, C. E. and Wyllie, P. J. (1975) Composition of Glasses from St. Pauls peridotite partially melted at 20kb. J. Geol. 83:455-471.

O'Neill, H. S. C. and Wall, V. J. (1987) The olivine-orthopyroxene-spinel oxygen geobarometer, the nickel precipitation curve, and the oxygen fugacity of the Earth's upper mantle. J. Petrol. 28:1169-1191.

O'Neill, H. S. C. Pownceby, M. I. and Wall, V. J. (1988) Ilmenite-rutile-iron and Ulvospinel-ilmenite-iron equilibria and the thermochemistry of ilmenite ($FeTiO_3$) and ulvospinel (Fe_2TiO_4). Geochim. Cosmochim. Acta 52:2065-2072.

Osborn, E. F. (1959) Role of oxygen pressure in the crystallization and differentiation of basaltic magma. Am. J. Sci. 13:147-155.

Osborn, E. F. and Muan, A. (1960) In: Phase equilibrium diagrams of oxide systems, Plate 6. Pub. the Amer Ceramic Soci and the Edward Orton.

Petric, A. and Jacob, K. T. (1982) Thermodynamic properties of Fe_3O_4-FeV_2O_4 and Fe_3O_4-$FeCr_2O_4$ spinel solid solutions. J. Am. Ceram. Soc. 65:117-123.

Petric, A., Jacob, K. T. and Alcock, C. B. (1981) Thermodynamic properties of Fe_3O_4 - $FeAl_2O_4$ spinel solid solutions. J. Am. Ceram. Soc. 64:632-639.

Presnall, D. C. (1966) The join Forsterite-diopside-iron oxides and its bearing on the crystallization of basaltic and ultramafic magmas. Am. J. Sci. 264:753-809.

Ribe, N. M. (1985a) The generation and composition of partial melts in the Earth's mantle. Earth Planet. Sci. Lett. 73:361-376.

Ribe, N. M. (1986) Melt segregation driven by dynamic forcing. Geophys. Res. Lett. 13:1462-1465.

Ribe, N. M. (1987a) A stagnation-point flow model for melt extraction from a mantle plume. J. Geophy. Res. 92:6437-6443.

Ribe, N. M. (1987b) Theory of melt segregation' a review. J. Vocanol. Geoth Res. 33:241-253.

Roeder, P. L. and Emslie, R. F (1970) Olivine-Liquid Equilibrium. Contrb. Mineral. Petrol. 29:275-289.

Roeder, P. L. and Osborn, E. F. (1966) Experimental data for the system MgO-FeO-Fe_2O_3-$Ca_2Al_2O_8$-SiO_2 and their petrologic implications. Am. J. Sci. 246:428-480.

O Rowson, S. A. and Irvine, T. N. (1980) Mg-Fe^{2+} partitioning between olivine and ferrian ulvospinel. Carnegie Inst. of Wacshington, Year Book, 79:332-337.

Shee, S. R. (1984) The oxide minerals of the Wesselton Mine Kimberlite, Kimberley, South Africa. In: Kornprobst J. (ed), Proc. 3rd Int. Kim. Conf. Vol. 1 pp 97-108.

Shi, P., Harte, B. and Biggar, G. M. (1989) Redox partial melting. Terra Abstr. EUG V Strasbourg. Vol. 1 No. 1 pp269.

Simons, B. and Woermann, E. (1978) Iron titanium oxides in equilibrium with metallic iron. Contrib. Mineral. Petrol. 66:81-89.

Speidel, D. H. (1964) El ement distribution among coexisting phases in the system MgO-FeO-Fe_2O_3-SiO_2-TiO_2 as a function of temperature, oxygen fugacity, and bulk composition: Pa. State Univ. Ph.D. Thesis.

Speidel, D. H. (1970) Effect of Magnesium on iron-titanium oxides. Am. J. Sci. 268:341-353.

Spiengelman, M. and Mckenzie, D. (1987) Simple 2-D Models for melt extraction at mid ocean ridges and island arcs. Earth Planet. Sci. Lett. 87:137-152.

Taylor, W. R. and Green, D. H. (1988) Measurement of reduced peridotite-C-O-H solidus and implications for redox melting of the mantle. Nature 332:349-332.

Thomson, R. N. (1975) Primary basalts and magma genesis. II. Snake River Plain, Idaho, USA. Contrib. Mineral. Petrol. 52:213-232.

Toksoz, M. N. and Husi, A. T. (1978) Numerical studies on back-arc convection and the formation of marginal basin. In: Numerical Modelling in Geodynamics, Toksoz, M. N. (ed.). Tectonophysics, 50:177-196.

Toramaru, A. and Fujii, N. (1986) Connectivity of a melt Phase in a partially molten peridotite. J. Geophy. Res. 91:9236-9252.

Ulmer, G. C. et al.(1987) The mantle redox state: an unfinished story. Geol. Soc. Am. Spec. Pap. 215:5-23.

Volpe, A. M., Macdougall, J. D., and Hawkins, J. W. (1988) Lau Basin basalts (LBB): trace element and Sr-Nd isotope evidence for heterogeneity in backarc basin mantle. Earth Planet. Sci. Lett. 90:174-186.

Waff,H.S. and Bulau,J.R. (1979) Equilibrium fluid distribution in an ultramafic partial melt under hydrostatic stress conditions. J. Geophy. Res. 84:6109-6114.

Waff, H. S. and Bulau, J. R. (1982) Experimental determination of near-equilibrium textures in partially molten silicates at high pressures. Adv. Earth Planet. Sci. 12:229-236.

Walker, D. Jurewicz, S. and Watson, E. B. (1985) Experimental observation of an isothermal transition from orthocumulus to adcumulus texture. EOS 66:362.

Woermann, E., Brezny, B. and Muan, A. (1969a) Phase equilibria in the system MgO-iron oxide-TiO_2 in air. Am. J. Sci. 267A(Schairer Vol.):463-479.

Woermann, E., Hirschberg, A., and Lamprecht, A (1969b) *Forsch. Niner.* 47:79-80.

Woermann, E. and Lamprecht, A. (1970) *Hochtemperaturgleichgewichte im system* MgO-FeO-SiO_2-TiO_2. Naturwissenschaften 57:191.

Wyllie, P. J. (1978) Mantle fluid compositions buffered in peridotite-CO_2-H_2O by carbonates, amphibole, and phlogopite. J. Geology. 86:687-713.

Wyllie, P. J. (1979) Magmas and volatile components. Amer. Mineral. 64:469-500.

Yoder, H. S. (1976) Zone melting. in Generation of Basaltic Magma. National Academy of Science. Washington,D.C. 115-117.

Yoder, H. S. and Tilley, C. E. (1961) Simple basalt systems. Carnegie Inst. Washington Year Book. 60:106-113.

Yoder, H. S.and Tilley, C. E. (1962) Origin of basalt magmas: An experimental study of natural and synthetic rock systems. J. Petrol. 3:342-532.

APPENDICES

I. SOME CALCULATION PROCEDURES

I.I. Ferrous and ferric recalculation for ilmenite

The ferric and ferrous iron contents of the rhombhedral phase in this study were calculated with assumed stoichiometry of R_2O_3.

Calculation procedure:

1. Probe analyses (in oxide weight percent, Fe as FeO) were recalculated to molar number,

$$X_{SiO2} = Wt_{SiO2}/60.058$$

$$X_{FeO} = Wt_{FeO}/71.846$$

$$X_{TiO2} = Wt_{TiO2}/79.899$$

$$X_{MgO} = Wt_{MgO}/40.311$$

$$X_{CaO} = Wt_{CaO}/56.079$$

2. The molar numbers of TiO_2 and SiO_2 were summed together,

$$X_T = X_{TiO2}+X_{SiO2}$$

so were the molar numbers of FeO^*, MgO, and CaO,

$$X_F = X_{FeO}+X_{MgO}+X_{CaO}$$

3. Then, the ferric molar number is

$$X_{FC} = X_F-X_T$$

and the ferrous molar number is

$$X_{FS} = X_F-X_{FC}$$

4. Transfer molar number to weight percent

$$Wt_{FC} = X_{FC} \cdot 0.5 \cdot 159.692$$

$$Wt_{FS} = X_{FS} \cdot 71.846$$

An example of recalculated result:

MgO	SiO_2	CaO	TiO_2	FeO		
0.1044	0.0002	0.0004	0.5088	0.3830*		
MgO	SiO_2	CaO	TiO_2	FeO	Fe_2O_3	TOTAL
0.1044	0.0002	0.0004	0.5088	0.2711	0.1244	1.0094

* Probe analysis

I.II. Ferrous and ferric recalculation for ulvospinel

The spinel phase in this study was recalculated with assumed stoichiometry of R_3O_4.

Calculation procedure:

1. As section A1.1.1
2. As section A1.1.2
3. The ferric molar number is

$$X_{FC} = X_F - 2X_T$$

and the ferrous molar number is

$$X_{FS} = X_F - X_{FC}$$

4. As section A1.1.4

An example of recalculated result:

MgO	SiO_2	CaO	TiO_2	FeO		
0.1057	0.0012	0.0005	0.2817	0.5880		
MgO	SiO_2	CaO	TiO_2	FeO	Fe_2O_3	TOTAL
0.1057	0.0012	0.0005	0.2817	0.4097	0.1982	0.9970

I.III. Ferrous and ferric recalculation for pseudobrookite

The orthorhombic phase in this study was recalculated with assumed stoichiometry of R_3O_5.

Calculation procedure:

1. As section A1.1.1
2. Calculate the molar number of TiO_2 which is combined to iron oxides.

$$X_{TF} = X_{TiO2}+X_{SiO2}-(X_{MgO}+X_{CaO})\bullet 2$$

3. The ferric molar number is

$$X_{FC} = [X_F-(X_F+X_{TF})/3]\bullet 2$$

and the ferrous molar number is

$$X_{FS} = X_F-X_{FC}$$

4. As section A1.1.4

An example of recalculated result:

MgO	SiO_2	CaO	TiO_2	FeO		
0.0640	0.0009	0.0000	0.5973	0.3113		
MgO	SiO_2	CaO	TiO_2	FeO	Fe_2O_3	TOTAL
0.0640	0.0009	0.0000	0.5973	0.1029	0.2316	0.9968

I.IV. Calculation of cation numbers

With assumed stoichiometry, the cation numbers are dependent on the oxygen anion numbers, OX, specified. The rombhedral phase is calculated based on 3 oxygen per structure formulae, the spinel 4, olivine 4, quartz 2, orthopyroxene 6,

and pseudobrookite 5.

Calculation procedure:

1. calculation of oxygen molar number.

$$X_{OMg} = Wt_{MgO}/40.311$$

$$X_{OFe2+} = Wt_{FeO}/71.846$$

$$X_{OFe3+} = (Wt_{Fe2O3}/159.692)\cdot 3$$

$$X_{OSi} = (Wt_{SiO2}/60.805)\cdot 2$$

$$X_{OTi} = (Wt_{TiO2}/79.899)\cdot 2$$

$$X_{OCa} = Wt_{CaO}/56.079$$

$$Total = X_{OMg}+X_{OFe2+}+X_{OFe3+}+X_{OSi}+X_{OTi}+X_{OCa}$$

2. Calculation of cation numbers.

With given oxygen number, OX, per structure formulae, cation number were calculated as follows,

$$X_{Mg} = X_{OMg}\cdot OX/Total$$

$$X_{Fe2+} = X_{OFe+2}\cdot OX/Total$$

$$X_{Fe3+} = X_{OFe+3}\cdot OX\cdot 2/3/Total$$

$$X_{Si} = X_{OSi}\cdot OX/2/Total$$

$$X_{Ti} = X_{OTi}\cdot OX/2/Total$$

$$X_{Ca} = X_{OCa}\cdot OX/Total$$

TABLE A2.1 ELECTRON MICROPROBE ANALYSES OF PHASES IN ASSEMBLAGE IL+USP+LQ AT $\log fO_2$=-9.0

Wt%	IL	USP	LQ	Pt-Fe
MgO	0.00(0.00)	0.00(0.00)	0.00(0.00)	------
SiO_2	0.03(0.02)	0.08(0.02)	10.22(0.51)	------
TiO_2	50.62(0.19)	33.74(0.12)	33.85(0.68)	------
FeO	45.55(0.18)	62.04(0.16)	54.38(0.50)	------
Fe_2O_3	2.12(0.39)	2.59(0.21)	------	------
SUM	98.32	98.45	98.44	
CAT/OXY	2/3	3/4	--	--
Mg	0.0000	0.0000	------	------
Si	0.0008	0.0030	------	------
Ti	0.9788	0.9601	------	------
Fe^{2+}	0.9794	1.9631	------	------
Fe^{3+}	0.0410	0.0738	------	------
SUM	2.0000	3.0000	------	------
#	5	4	5	0

is the number of analyses. IL=Ilmenite. OL=Olivine. USP=Ulvospinel. LQ=Glass. Standard deviation in paretheses. Ferric iron calculated from assumed stoichiometry.

TABLE A2.1 ELECTRON MICROBROBE ANALYSES OF PHASES IN ASSEMBLAGE IL+USP+LQ AT $logfo_2$=-9.0 (Cont.)

Wt%	IL	USP	LQ	Pt-Fe
MgO	2.99(0.04)	2.74(0.02)	2.06(0.04)	------
SiO_2	0.01(0.01)	0.09(0.01)	15.06(0.39)	------
TiO_2	54.29(0.14)	35.70(0.08)	33.20(0.91)	------
FeO	43.40(0.02)	60.12(0.11)	49.60(1.08)	------
Fe_2O_3	0.00(0.00)	1.26(0.12)	------	------
SUM	100.69	99.91	99.92	------
CAT/OXY	2/3	3/4	--	--
Mg	0.1093	0.1488	------	------
Si	0.0003	0.0033	------	------
Ti	1.0003	0.9794	------	------
Fe^{2+}	0.8894	1.8339	------	------
Fe^{3+}	0.0000	0.0346	------	------
SUM	1.9993	3.0000	------	------
#	4	6	5	0

is the number of analyses. IL=Ilmenite. OL=Olivine. USP=Ulvospinel. LQ=Glass. Standard deviation in paretheses. Ferric iron calculated from assumed stoichiometry.

TABLE A2.1 ELECTRON MICROPROBE ANALYSES OF PHASES IN ASSEMBLAGE IL+USP+LQ AT logfO_2=-9.0 (Cont.)

Wt%	IL	USP	LQ	Pt-Fe
MgO	5.97(0.07)	5.46(0.07)	4.93(0.15)	------
SiO_2	0.01(0.01)	0.10(0.01)	18.37(1.09)	------
TiO_2	54.44(0.19)	35.19(0.25)	28.42(0.93)	------
FeO	38.32(0.25)	55.27(0.33)	47.69(1.61)	------
Fe_2O_3	1.44(0.22)	3.32(0.36)	------	------
SUM	100.18	99.34	99.29	------
CAT/OXY	2/3	3/4	--	--
Mg	0.2145	0.2927	------	------
Si	0.0002	0.0034	------	------
Ti	0.9867	0.9517	------	------
Fe^{2+}	0.7724	1.6625	------	------
Fe^{3+}	0.0261	0.0897	------	------
SUM	1.9999	3.0000	------	------
#	4	6	5	0

is the number of analyses. IL=Ilmenite. OL=Olivine. USP=Ulvospinel. LQ=Glass. Standard deviation in paretheses. Ferric iron calculated from assumed stoichiometry.

TABLE A2.2 ELECTRON MICROPROBE ANALYSES OF PHASES IN ASSEMBLAGE IL+USP+LQ AT $\log fO_2$=-8.0

Wt%	IL	USP	LQ	Pt-Fe
MgO	0.00(0.00)	0.00(0.00)	0.00(0.00)	Wt_{Fe}%:
SiO_2	0.03(0.01)	0.10(0.01)	13.19(0.92)	13.09(0.07)
TiO_2	49.52(0.24)	31.14(0.12)	34.53(1.00)	Wt_{Pt}%:
FeO	44.57(0.23)	59.85(0.13)	51.16(1.07)	87.34(0.30)
Fe_2O_3	5.98(0.33)	8.01(0.18)	------	
SUM	100.10	100.10	98.88	100.43
CAT/OXY	2/3	3/4	--	Mole Fract.
Mg	0.0000	0.0000	------	X_{Fe}:
Si	0.0008	0.0037	------	0.3436
Ti	0.9423	0.8828	------	X_{Pt}
Fe^{2+}	0.9431	1.8865	------	0.6564
Fe^{3+}	0.1139	0.2271	------	
SUM	2.0001	3.0001	------	1.0000
#	4	4	4	6

is the number of analyses. IL=Ilmenite. OL=Olivine. USP=Ulvospinel. LQ=Glass. Standard deviation in paretheses. Ferric iron calculated from assumed stoichiometry.

TABLE A2.2 ELECTRON MICROPROBE ANALYSES OF PHASES IN ASSEMBLAGE IL+USP+LQ AT $\log fO_2$=-8.0 (Cont.)

Wt%	IL	USP	LQ	Pt-Fe
MgO	1.37(0.03)	1.31(0.01)	1.12(0.04)	Wt_{Fe}%:
SiO_2	0.01(0.01)	0.10(0.02)	12.49(0.08)	13.12(0.05)
TiO_2	50.84(0.05)	31.89(0.08)	33.31(0.04)	Wt_{Pt}%:
FeO	43.28(0.08)	58.54(0.02)	52.48(0.34)	86.96(0.23)
Fe_2O_3	4.44(0.28)	7.34(0.28)	------	
SUM	99.94	99.18	99.39	100.08
CAT/OXY	2/3	3/4	--	Mole Fract.
Mg	0.0512	0.0726	------	X_{Fe}:
Si	0.0003	0.0035	------	0.3451
Ti	0.9579	0.8935	------	X_{Pt}:
Fe^{2+}	0.9069	1.8246	------	0.6549
Fe^{3+}	0.0837	0.2059	------	
SUM	2.0000	3.0001	------	1.0000
#	4	3	3	4

is the number of analyses. IL=Ilmenite. OL=Olivine. USP=Ulvospinel. LQ=Glass. Standard deviation in paretheses. Ferric iron calculated from assumed stoichiometry.

TABLE A2.2 ELECTRON MICROPROBE ANALYSES OF PHASES IN ASSEMBLAGE IL+USP+LQ AT $\log fO_2$=−8.0 (Cont.)

Wt%	IL	USP	LQ	Pt-Fe
MgO	2.56(0.03)	2.41(0.09)	2.55(0.13)	Wt_{Fe}%:
SiO_2	0.02(0.01)	0.11(0.01)	16.73(0.38)	12.91(0.09)
TiO_2	51.58(0.26)	32.10(0.08)	29.01(0.55)	Wt_{Pt}%:
FeO	41.85(0.15)	57.17(0.13)	51.75(0.22)	87.28(0.21)
Fe_2O_3	3.97(0.11)	7.72(0.23)	------	
SUM	99.98	99.51	100.05	100.18
CAT/OXY	2/3	3/4	--	Mole Fract.
Mg	0.0947	0.1325	------	X_{Fe}:
Si	0.0005	0.0040	------	0.3406
Ti	0.9624	0.8890	------	X_{Pt}:
Fe^{2+}	0.8684	1.7607	------	0.6594
Fe^{3+}	0.0741	0.2139	------	
SUM	2.0001	3.0001	------	1.0000
#	4	4	4	6

is the number of analyses. IL=Ilmenite. OL=Olivine. USP=Ulvospinel. LQ=Glass. Standard deviation in paretheses. Ferric iron calculated from assumed stoichiometry.

TABLE A2.2 ELECTRON MICROPROBE ANALYSES OF PHASES IN ASSEMBLAGE IL+USP+LQ AT logfO_2=-8.0(Cont.)

Wt%	IL	USP	LQ	Pt-Fe
MgO	4.08(0.03)	3.75(0.09)	3.78(0.05)	Wt_{Fe}%:
SiO_2	0.02(0.01)	0.11(0.01)	16.18(0.23)	12.95(0.05)
TiO_2	52.84(0.46)	32.57(0.01)	30.39(0.03)	Wt_{Pt}%:
FeO	40.27(0.40)	55.53(0.19)	48.96(0.03)	87.29(0.39)
Fe_2O_3	3.31(0.40)	7.49(0.16)	------	
SUM	100.52	99.45	99.31	100.25
CAT/OXY	2/3	3/4	--	Mole Fract.
Mg	0.1483	0.2040	------	X_{Fe}:
Si	0.0005	0.0041	------	0.3414
Ti	0.9691	0.8931	------	X_{Pt}:
Fe^{2+}	0.8214	1.6933	------	0.6586
Fe^{3+}	0.0608	0.2056	------	
SUM	2.0001	3.0001	------	1.0000
#	4	4	3	5

is the number of analyses. IL=Ilmenite. OL=Olivine. USP=Ulvospinel. LQ=Glass. Standard deviation in paretheses. Ferric iron calculated from assumed stoichiometry.

TABLE A2.2 ELECTRON MICROPROBE ANALYSES OF PHASES IN ASSEMBLAGE IL+USP+LQ AT $\log fO_2$=-8.0 (Cont.)

Wt%	IL	USP	LQ	Pt-Fe
MgO	5.39(0.06)	4.91(0.05)	5.05(0.06)	Wt_{Fe}%:
SiO_2	0.02(0.01)	0.12(0.01)	17.68(0.18)	12.77(0.09)
TiO_2	52.60(0.43)	32.49(0.35)	28.73(0.37)	Wt_{Pt}%:
FeO	37.70(0.46)	53.69(0.50)	48.18(0.12)	87.67(0.12)
Fe_2O_3	4.37(0.53)	8.32(0.48)	------	
SUM	100.08	99.53	99.67	100.44
CAT/OXY	2/3	3/4	--	Mole Fract.
Mg	0.1949	0.2646	------	X_{Fe}:
Si	0.0005	0.0042	------	0.3372
Ti	0.9597	0.8827	------	X_{Pt}:
Fe^{2+}	0.7650	1.6223	------	0.6628
Fe^{3+}	0.0798	0.2262	------	
SUM	1.9999	3.0000	------	1.0000
#	4	6	4	5

is the number of analyses. IL=Ilmenite. OL=Olivine. USP=Ulvospinel. LQ=Glass. Standard deviation in paretheses. Ferric iron calculated from assumed stoichiometry.

TABLE A2.3 ELECTRON MICROPROBE ANALYSES OF PHASES IN ASSEMBLAGE IL+USP+OL+LQ AT $\log fO_2$=−8.0

Wt%	IL	USP	OL	LQ	Pt-Fe
MgO	9.87(0.04)	9.37(0.14)	38.20(0.11)	7.71(1.00)	Wt_{Fe}%:
SiO_2	0.02(0.00)	0.12(0.01)	38.23(0.21)	20.78(0.48)	12.59(0.09)
TiO_2	55.29(0.30)	33.75(0.12)	0.43(0.11)	28.77(0.61)	Wt_{Pt}%:
FeO	32.09(0.29)	47.85(0.52)	23.32(0.10)	38.01(0.37)	87.54(0.03)
Fe_2O_3	3.23(0.40)	8.07(0.42)	------	------	
CaO	0.05(0.01)	0.04(0.01)	0.22(0.00)	5.00(0.22)	
SUM	100.55	100.20	100.40	100.28	100.13
CAT/OX	2/3	3/4	3/4	--	Mole Fract.
Mg	0.3436	0.4897	1.4899	------	X_{Fe}:
Si	0.0005	0.0042	0.9886	------	0.3344
Ti	0.9711	0.8894	0.0083	------	X_{Pt}:
Fe^{2+}	0.6268	1.4024	0.5104	------	0.6656
Fe^{3+}	0.0568	0.2129	------	------	
Ca	0.0013	0.0015	0.0061	------	
SUM	2.0001	3.0001	3.0036	------	1.0000
#	4	4	5	3	5

is the number of analyses. IL=Ilmenite. OL=Olivine. USP=Ulvospinel. LQ=Glass. Standard deviation in paretheses. Ferric iron calculated from assumed stoichiometry.

TABLE A2.3 ELECTRON MICROPROBE ANALYSES OF PHASES IN ASSEMBLAGE IL+USP+OL+LQ AT $\log fO_2$=-8.0(Cont.)

Wt%	IL	USP	OL	LQ	Pt-Fe
MgO	11.13(0.04)	10.56(0.09)	40.11(0.28)	7.19(0.49)	Wt_{Fe}%:
SiO_2	0.03(0.01)	0.11(0.02)	38.36(0.19)	21.18(0.74)	12.73(0.13)
TiO_2	54.88(0.34)	33.21(0.16)	0.44(0.10)	28.36(0.81)	WT_{Pt}%:
FeO	29.38(0.26)	45.40(0.24)	20.91(0.10)	32.46(0.67)	87.25(0.33)
Fe_2O_3	4.61(0.27)	9.68(0.16)	------	------	
CaO	0.13(0.01)	0.10(0.01)	0.52(0.03)	9.83(0.57)	
SUM	100.16	99.06	100.34	98.88	99.98
CAT/OX	2/3	3/4	3/4	--	Mole Fract.
Mg	0.3855	0.5479	1.5497	------	X_{Fe}:
Si	0.0007	0.0038	0.9828	------	0.3376
Ti	0.9590	0.8694	0.0085	------	X_{Pt}:
Fe^{2+}	0.5710	1.3216	0.4532	------	0.6624
Fe^{3+}	0.0806	0.2535	------	------	
Ca	0.0032	0.0038	0.0144	------	
SUM	2.0000	3.0000	3.0086	------	1.0000
#	4	4	4	5	6

analyses number of analyses. IL=Ilmenite. OL=Olivine. USP=Ulvospinel. LQ=Glass. Standard deviation in paretheses. Ferric iron calculated from assumed stoichiometry.

TABLE A2.3 ELECTRON MICROPROBE ANALYSES OF PHASES IN ASSEMBLAGE IL+USP+OL+LQ AT $\log fO_2$=-8.0(Cont.)

Wt%	IL	USP	OL	LQ	Pt-Fe
MgO	14.32(0.09)	14.49(0.07)	44.71(0.22)	8.88(0.23)	Wt_{Fe}%:
SiO_2	0.03(0.01)	0.08(0.01)	39.72(0.16)	19.28(0.35)	12.32(0.05)
TiO_2	56.95(0.47)	35.47(0.07)	0.27(0.08)	32.65(0.73)	Wt_{Pt}%:
FeO	25.50(0.62)	41.81(0.16)	15.68(0.18)	28.48(0.55)	87.85(0.19)
Fe_2O_3	3.67(0.46)	8.48(0.19)	------	------	
CaO	0.17(0.01)	0.13(0.01)	0.57(0.02)	11.36(0.51)	
SUM	100.64	100.56	100.95	100.65	100.07
CAT/OX	2/3	3/4	3/4	--	Mole Fract.
Mg	0.4825	0.7212	1.6737	------	X_{Fe}:
Si	0.0007	0.0027	0.9858	------	0.3324
Ti	0.9682	0.8907	0.0051	------	X_{Pt}:
Fe^{2+}	0.4821	1.1674	0.3293	------	0.6676
Fe^{3+}	0.0624	0.2131	------	------	
Ca	0.0041	0.0048	0.0153	------	
SUM	2.0000	2.9999	3.0092	------	1.0000
#	4	4	4	3	5

is the number of analyses. IL=Ilmenite. OL=Olivine. USP=Ulvospinel. LQ=Glass. Standard deviation in paretheses. Ferric iron calculated from assumed stoichiometry.

TABLE A2.3 ELECTRON MICROPROBE ANALYSES OF PHASES IN ASSEMBLAGE IL+USP+OL+LQ AT $\log fO_2$=-8.0(Cont.)

Wt%	IL	USP	OL	LQ	Pt-Fe
MgO	15.52(0.11)	15.09(0.14)	45.21(0.08)	7.08(0.72)	Wt_{Fe}%:
SiO_2	0.02(0.01)	0.07(0.01)	39.60(0.19)	20.30(1.21)	12.40(0.11)
TiO_2	56.74(0.50)	35.27(0.07)	0.46(0.03)	32.76(1.91)	Wt_{Pt}%:
FeO	23.05(0.44)	40.33(0.09)	14.25(0.13)	23.72(0.55)	87.93(0.22)
Fe_2O_3	4.43(0.42)	8.91(0.21)	------	------	
CaO	0.26(0.01)	0.29(0.04)	0.97(0.03)	16.52(1.00)	
SUM	100.02	99.96	100.49	100.28	100.34
CAT/OX	2/3	3/4	3/4	--	Mole Fract.
Mg	0.5215	0.7512	1.6922	------	X_{Fe}:
Si	0.0005	0.0024	0.9826	------	0.3301
Ti	0.9620	0.8857	0.0087	------	X_{Pt}:
Fe^{2+}	0.4346	1.1265	0.2992	------	0.6699
Fe^{3+}	0.0751	0.2238	------	------	
Ca	0.0063	0.0105	0.0262	------	
SUM	2.0000	3.0001	3.0099	------	1.0000
#	4	4	4	4	4

is the number of analyses. IL=Ilmenite. OL=Olivine. USP=Ulvospinel. LQ=Glass. Standard deviation in paretheses. Ferric iron calculated from assumed stoichiometry.

TABLE A2.3 ELECTRON MICROPROBE ANALYSES OF PHASES IN ASSEMBLAGE IL+USP+OL+LQ AT $\log fO_2$=−8.0(Cont.)

Wt%	IL	USP	OL	LQ	Pt-Fe
MgO	17.75(0.04)	18.97(0.35)	48.32(0.54)	7.68(0.84)	Wt_{Fe}%:
SiO_2	0.02(0.01)	0.07(0.01)	40.28(0.55)	17.40(0.35)	12.08(0.08)
TiO_2	58.55(0.36)	36.48(0.60)	0.32(0.09)	37.05(0.80)	Wt_{Pt}%:
FeO	20.66(0.37)	35.57(0.48)	10.37(0.31)	22.35(0.54)	88.12(0.21)
Fe_2O_3	3.28(0.18)	8.72(0.14)	------	------	
CaO	0.30(0.02)	0.25(0.05)	0.82(0.03)	16.25(0.48)	
SUM	100.56	100.06	100.11	100.74	100.20
CAT/OX	2/3	3/4	3/4	--	Mole Fract.
Mg	0.5842	0.9186	1.7822	------	X_{Fe}:
Si	0.0004	0.0022	0.9849	------	0.3238
Ti	0.9723	0.8912	0.0059	------	X_{Pt}:
Fe^{2+}	0.3815	0.9663	0.2146	------	0.6762
Fe^{3+}	0.0545	0.2131	------	------	
Ca	0.0071	0.0086	0.0217	------	
SUM	2.0000	3.0000	3.0093	------	1.0000
#	4	4	4	5	5

is the number of analyses. IL=Ilmenite. OL=Olivine. USP=Ulvospinel. LQ=Glass. Standard deviation in paretheses. Ferric iron calculated from assumed stoichiometry.

TABLE A2.4 ELECTRON MICROPROBE ANALYSES OF PHASES IN ASSEMBLAGE IL+USP+LQ AT $\log fO_2=-7.0$

Wt%	IL	USP	LQ	Pt-Fe
MgO	0.00(0.00)	0.00(0.00)	0.00(0.00)	Wt_{Fe}%:
SiO_2	0.02(0.01)	0.12(0.01)	14.05(0.23)	10.26(0.09)
TiO_2	44.40(0.18)	26.19(0.10)	29.30(0.13)	Wt_{Pt}%:
FeO	39.94(0.12)	55.11(0.12)	55.66(0.09)	89.99(0.14)
Fe_2O_3	15.30(0.26)	17.18(0.25)	------	
SUM	99.66	98.60	99.00	100.25
CAT/OXY	2/3	3/4	--	Mole Fract.
Mg	0.0000	0.0000	------	X_{Fe}:
Si	0.0005	0.0045	------	0.2849
Ti	0.8526	0.7495	------	X_{Pt}:
Fe^{2+}	0.8529	1.7541	------	0.7151
Fe^{3+}	0.2940	0.4919	------	
SUM	2.0000	3.0000	------	1.0000
#	4	3	3	4

is the number of analyses. IL=Ilmenite. OL=Olivine. USP=Ulvospinel. LQ=Glass. Standard deviation in paretheses. Ferric iron calculated from assumed stoichiometry.

TABLE A2.4 ELECTRON MICROPROBE ANALYSES OF PHASES IN ASSEMBLAGE IL+USP+LQ AT logfO_2=-7.0 (Cont.)

Wt%	IL	USP	LQ	Pt-Fe
MgO	1.23(0.01)	1.38(0.03)	1.41(0.03)	Wt_{Fe}%:
SiO_2	0.01(0.01)	0.12(0.02)	15.62(0.39)	10.37(0.08)
TiO_2	45.42(0.15)	27.35(0.03)	29.12(0.49)	Wt_{Pt}%:
FeO	38.67(0.12)	54.24(0.16)	52.88(0.15)	89.78(0.28)
Fe_2O_3	14.85(0.35)	16.05(0.09)	------	
SUM	100.18	99.14	99.02	100.15
CAT/OXY	2/3	3/4	--	Mole Fract.
Mg	0.0461	0.0768	------	X_{Fe}:
Si	0.0003	0.0045	------	0.2875
Ti	0.8592	0.7695	------	X_{Pt}:
Fe^{2+}	0.8135	1.6973	------	0.7125
Fe^{3+}	0.2811	0.4520	------	
SUM	2.0002	3.0001	------	1.0000
#	5	3	3	5

is the number of analyses. IL=Ilmenite. OL=Olivine. USP=Ulvospinel. LQ=Glass. Standard deviation in paretheses. Ferric iron calculated from assumed stoichiometry.

TABLE A2.4 ELECTRON MICROPROBE ANALYSES OF PHASES IN ASSEMBLAGE IL+USP+LQ AT logfO_2=-7.0 (Cont.)

Wt%	IL	USP	LQ	Pt-Fe
MgO	2.44(0.02)	2.79(0.04)	2.71(0.07)	Wt_{Fe}%:
SiO_2	0.01(0.01)	0.12(0.01)	14.43(1.73)	10.27(0.05)
TiO_2	46.33(0.09)	27.82(0.08)	31.25(2.60)	Wt_{Pt}%:
FeO	37.34(0.09)	52.65(0.11)	51.16(0.29)	90.25(0.24)
Fe_2O_3	14.02(0.10)	16.28(0.14)	------	
SUM	100.14	99.66	99.55	100.25
CAT/OXY	2/3	3/4	--	Mole Fract.
Mg	0.0906	0.1533	------	X_{Fe}:
Si	0.0003	0.0044	------	0.2845
Ti	0.8682	0.7702	------	X_{Pt}:
Fe^{2+}	0.7782	1.6213	------	0.7155
Fe^{3+}	0.2629	0.4509	------	
SUM	2.0002	3.0001	------	1.0000
#	4	5	4	4

is the number of analyses. IL=Ilmenite. OL=Olivine. USP=Ulvospinel. LQ=Glass. Standard deviation in paretheses. Ferric iron calculated from assumed stoichiometry.

TABLE A2.4 ELECTRON MICROPROBE ANALYSES OF PHASES IN ASSEMBLAGE IL+USP+LQ AT logfO_2=-7.0(Cont.)

Wt%	IL	USP	LQ	Pt-Fe
MgO	3.68(0.05)	3.91(0.03)	------	Wt_{Fe}%:
SiO_2	0.03(0.00)	0.14(0.02)	------	10.32(0.07)
TiO_2	48.04(0.12)	28.36(0.03)	------	Wt_{Pt}%:
FeO	36.68(0.15)	51.45(0.02)	------	89.94(0.20)
Fe_2O_3	11.66(0.27)	15.76(0.15)	------	
SUM	100.09	99.62	------	100.27
CAT/OXY	2/3	3/4	--	Mole Fract.
Mg	0.1353	0.2128	------	X_{Fe}:
Si	0.0007	0.0049	------	0.2862
Ti	0.8910	0.7786	------	X_{Pt}:
Fe^{2+}	0.7566	1.5708	------	0.7139
Fe^{3+}	0.2164	0.4329	------	
SUM	2.0000	3.0000	------	1.0000
#	5	3	0	5

is the number of analyses. IL=Ilmenite. OL=Olivine. USP=Ulvospinel. LQ=Glass. Standard deviation in paretheses. Ferric iron calculated from assumed stoichiometry.

TABLE A2.4 ELECTRON MICROBROBE ANALYSES OF PHASES IN ASSEMBLAGE IL+USP+LQ AT $logfo_2$=−7.0 (Cont.)

Wt%	IL	USP	LQ	Pt–Fe
MgO	7.00(0.11)	7.00(0.14)	8.38(0.07)	Wt_{Fe}%:
SiO_2	0.02(0.00)	0.13(0.01)	22.11(0.11)	10.11(0.01)
TiO_2	50.90(0.07)	29.43(0.05)	25.51(0.12)	Wt_{Pt}%:
FeO	33.33(0.18)	47.74(0.16)	44.36(0.18)	90.36(0.27)
Fe_2O_3	9.36(0.26)	15.49(0.16)	------	
SUM	100.61	99.79	100.36	100.47
CAT/OXY	2/3	3/4	--	Mole Fract.
Mg	0.2495	0.3714	------	X_{Fe}:
Si	0.0005	0.0047	------	0.2811
Ti	0.9152	0.7878	------	X_{Pt}:
Fe^{2+}	0.6665	1.4212	------	0.7189
Fe^{3+}	0.1684	0.4149	------	
SUM	2.0001	3.0000	------	1.0000
#	4	3	3	4

is the number of analyses. IL=Ilmenite. OL=Olivine. USP=Ulvospinel. LQ=Glass. Standard deviation in paretheses. Ferric iron calculated from assumed stoichiometry.

TABLE A2.5 ELECTRON MICROPROBE ANALYSES OF PHASES IN ASSEMBLAGE IL+USP+OL+LQ AT $\log fO_2$=-7.0

Wt%	IL	USP	OL	LQ	Pt-Fe
MgO	9.50(0.07)	9.24(0.01)	39.20(0.12)	8.82(0.15)	Wt_{Fe}%:
SiO_2	0.02(0.01)	0.12(0.01)	38.24(0.14)	22.06(0.82)	10.12(0.12)
TiO_2	52.59(0.16)	30.25(0.12)	0.48(0.10)	27.67(0.00)	Wt_{Fe}%:
FeO	30.33(0.27)	45.07(0.11)	22.39(0.16)	37.58(1.03)	90.42(0.31)
Fe_2O_3	8.37(0.29)	15.35(0.18)	------	------	
CaO	0.04(0.01)	0.04(0.01)	0.18(0.02)	4.47(0.08)	
SUM	100.85	100.07	100.62	100.28	100.54
CAT/OX	2/3	3/4	3/4	--	Mole Fract.
Mg	0.3315	0.4810	1.5268	------	X_{Fe}:
Si	0.0005	0.0040	0.9874	------	0.2810
Ti	0.9258	0.7943	0.0020	------	X_{Pt}:
Fe^{2+}	0.5938	1.3160	0.4894	------	0.7190
Fe^{3+}	0.1475	0.4034	------	------	
Ca	0.0010	0.0014	0.0051	------	
SUM	2.0001	3.0001	3.0107	------	1.0000
#	5	3	4	2	9

is the number of analyses. IL=Ilmenite. OL=Olivine. USP=Ulvospinel. LQ=Glass. Standard deviation in paretheses. Ferric iron calculated from assumed stoichiometry.

TABLE A2.5 ELECTRON MICROPROBE ANALYSES OF PHASES IN ASSEMBLAGE IL+USP+OL+LQ AT $\log fO_2$=-7.0 (Cont.)

Wt%	IL	USP	OL	LQ	Pt-Fe
MgO	11.07(0.05)	10.63(0.08)	41.01(0.15)	8.16(0.74)	Wt_{Fe}%:
SiO_2	0.02(0.01)	0.10(0.01)	38.64(0.30)	24.41(0.61)	10.10(0.04)
TiO_2	52.63(0.27)	30.16(0.38)	0.32(0.01)	25.44(0.13)	Wt_{Pt}%:
FeO	27.49(0.28)	42.74(0.60)	19.78(0.05)	32.15(0.54)	90.20(0.22)
Fe_2O_3	8.86(0.22)	16.27(0.50)	------	------	
CaO	0.09(0.01)	0.09(0.01)	0.37(0.01)	9.99(0.74)	
SUM	100.16	99.99	100.30	100.16	100.30
CAT/OX	2/3	3/4	3/4	--	Mole Fract.
Mg	0.3844	0.5484	1.5785	------	X_{Fe}:
Si	0.0005	0.0035	0.9859	------	0.2812
Ti	0.9220	0.7847	0.0062	------	X_{Pt}:
Fe^{2+}	0.5356	1.2367	0.4271	------	0.71.89
Fe^{3+}	0.1553	0.4236	------	------	
Ca	0.0023	0.0032	0.0103	------	
SUM	2.0001	3.0001	3.0070	------	1.0001
#	4	4	5	4	4

is the number of analyses. IL=Ilmenite. OL=Olivine. USP=Ulvospinel. LQ=Glass. Standard deviation in paretheses. Ferric iron calculated from assumed stoichiometry.

TABLE A2.5 ELECTRON MICROPROBE ANALYSES OF PHASES IN ASSEMBLAGE IL+USP+OL+LQ AT $\log fO_2$=-7.0(Cont.)

Wt%	IL	USP	OL	LQ	Pt-Fe
MgO	13.37(0.21)	13.21(0.01)	44.13(0.29)	9.11(0.26)	Wt_{Fe}%:
SiO_2	0.02(0.01)	0.08(0.02)	39.89(0.08)	19.65(0.00)	9.92(0.05)
TiO_2	55.10(0.17)	31.73(0.01)	0.31(0.05)	30.61(0.03)	Wt_{Pt}%:
FeO	25.57(0.48)	40.32(0.09)	15.93(0.05)	29.36(0.62)	90.20(0.10)
Fe_2O_3	6.91(0.45)	14.97(0.06)	------	------	
CaO	0.13(0.00)	0.11(0.01)	0.48(0.02)	10.67(0.51)	
SUM	101.10	100.44	100.74	99.41	100.12
CAT/OX	2/3	3/4	3/4	--	Mole Fract.
Mg	0.4524	0.6656	1.6557	------	X_{Fe}:
Si	0.0005	0.0028	0.9922	------	0.2776
Ti	0.9406	0.8067	0.0057	------	X_{Pt}:
Fe^{2+}	0.4854	1.1401	0.3354	------	0.7225
Fe^{3+}	0.1180	0.3809	------	------	
Ca	0.0032	0.0039	0.0130	------	
SUM	2.0001	3.0000	3.0020	------	1.0001
#	4	2	4	2	4

is the number of analyses. IL=Ilmenite. OL=Olivine. USP=Ulvospinel. LQ=Glass. Standard deviation in paretheses. Ferric iron calculated from assumed stoichiometry.

TABLE A2.5 ELECTRON MICROBROBE ANALYSES OF PHASES IN ASSEMBLAGE IL+USP+OL+LQ AT $logfo_2$=−7.0(Cont.)

Wt%	IL	USP	OL	LQ	Pt-Fe
MgO	15.19(0.06)	15.24(0.06)	45.68(0.16)	7.19(0.07)	Wt_{Fe}%:
SiO_2	0.02(0.01)	0.08(0.01)	39.58(0.15)	20.43(1.95)	9.92(0.08)
TiO_2	55.22(0.26)	32.02(0.25)	0.47(0.09)	33.36(0.93)	Wt_{Pt}%:
FeO	22.35(0.24)	37.36(0.30)	13.48(0.14)	23.42(2.13)	90.36(0.12)
Fe_2O_3	7.26(0.33)	15.51(0.28)	------	------	
CaO	0.20(0.02)	0.17(0.01)	0.77(0.02)	15.53(1.16)	
SUM	100.23	100.38	99.98	99.93	100.28
CAT/OX	2/3	3/4	3/4	--	Mole Fract.
Mg	0.5114	0.7575	1.7116	------	X_{Fe}:
Si	0.0005	0.0025	0.9832	------	0.2773
Ti	0.9379	0.8030	0.0089	------	X_{Pt}:
Fe^{2+}	0.4221	1.0419	0.2834	------	0.7227
Fe^{3+}	0.1234	0.3891	------	------	
Ca	0.0048	0.0060	0.0207	------	
SUM	2.0001	3.0000	3.0078	------	1.0000
#	4	4	4	4	4

is the number of analyses. IL=Ilmenite. OL=Olivine. USP=Ulvospinel. LQ=Glass. Standard deviation in paretheses. Ferric iron calculated from assumed stoichiometry.

TABLE A2.5 ELECTRON MICROPROBE ANALYSES OF PHASES IN ASSEMBLAGE IL+USP+OL+LQ AT $\log fO_2$=−7.0(Cont.)

Wt%	IL	USP	OL	LQ	Pt-Pt
MgO	16.87(0.08)	17.65(0.16)	47.29(0.17)	9.24(0.30)	Wt_{Fe}%:
SiO_2	0.01(0.01)	0.08(0.01)	39.53(0.17)	18.38(0.41)	9.70(0.09)
TiO_2	57.06(0.39)	33.37(0.19)	0.37(0.03)	33.81(0.81)	Wt_{Pt}%:
FeO	20.91(0.43)	35.01(0.41)	11.19(0.16)	23.27(0.69)	90.44(0.22)
Fe_2O_3	5.93(0.55)	14.47(0.44)	------	------	
CaO	0.26(0.04)	0.19(0.01)	0.80(0.02)	14.64(0.98)	
SUM	101.04	100.77	99.18	99.34	100.14
CAT/OX	2/3	3/4	3/4	--	Mole Fract.
Mg	0.5570	0.8592	1.7691	------	X_{Fe}:
Si	0.0002	0.0025	0.9803	------	0.2724
Ti	0.9504	0.8197	0.0069	------	X_{Pt}:
Fe^{2+}	0.3873	0.9564	0.2349	------	0.7276
Fe^{3+}	0.0988	0.3556	------	------	
Ca	0.0062	0.0067	0.0215	------	
SUM	1.9999	3.0001	3.0127	------	1.0000
#	4	3	4	3	9

is the number of analyses. IL=Ilmenite. OL=Olivine. USP=Ulvospinel. LQ=Glass. Standard deviation in paretheses. Ferric iron calculated from assumed stoichiometry.

TABLE A2.6 ELECTRON MICROPROBE ANALYSES OF PHASES IN ASSEMBLAGE IL+USP+LQ AT $\log fO_2$=-6.6

Wt%	IL	USP	LQ	Pt
MgO	0.00(0.00)	0.00(0.00)	0.00(0.00)	Wt_{Fe}%:
SiO_2	0.02(0.01)	0.14(0.01)	15.03(1.74)	8.53(0.10)
TiO_2	41.41(0.28)	23.07(0.14)	28.75(1.56)	Wt_{Pt}%:
FeO	37.26(0.27)	52.54(0.14)	51.16(0.30)	91.72(0.23)
Fe_2O_3	21.42(0.60)	23.80(0.23)	------	
SUM	100.11	99.55	94.90	100.25
CAT/OXY	2/3	3/4	--	Mole Fract.
Mg	0.0000	0.0000	------	X_{Fe}:-
Si	0.0005	0.0052	------	0.2452
Ti	0.7940	0.6561	------	X_{Pt}--
Fe^{2+}	0.7945	1.6615	------	0.7548
Fe^{3+}	0.4110	0.6772	------	
SUM	2.0000	3.0000	------	1.0000
#	5	4	3	4

is the number of analyses. IL=Ilmenite. USP=Ulvospinel. LQ=Glass. Standard deviation in paretheses. Ferric iron calculated from assumed stoichiometry.

TABLE A2.6 ELECTRON MICROPROBE ANALYSES OF PHASES IN ASSEMBLAGE IL+USP+LQ AT $\log fO_2$=-6.6 (Cont.)

Wt%	IL	USP	LQ	Pt-Fe
MgO	2.07(0.03)	2.41(0.07)	2.85(0.20)	Wt_{Fe}%:
SiO_2	0.01(0.01)	0.14(0.02)	19.18(1.04)	8.34(0.03)
TiO_2	43.12(0.11)	24.17(0.19)	26.11(0.93)	Wt_{Pt}%:
FeO	35.10(0.19)	49.82(0.32)	51.87(0.33)	91.76(0.14)
Fe_2O_3	20.16(0.29)	22.95(0.37)	------	
SUM	100.16	99.49	100.00	100.16
CAT/OXY	2/3	3/4	--	Mole Fract.
Mg	0.0771	0.1336	------	X_{Fe}:
Si	0.0003	0.0051	------	0.2408
Ti	0.8102	0.6744	------	X_{Pt}:
Fe^{2+}	0.7334	1.5460	------	0.7592
Fe^{3+}	0.3791	0.6409	------	
SUM	2.0001	3.0000	------	1.0000
#	4	4	4	5

is the number of analyses. IL=Ilmenite. USP=Ulvospinel. LQ=Glass. Standard deviation in paretheses. Ferric iron calculated from assumed stoichiometry.

TABLE A2.6 ELECTRON MICROPROBE ANALYSES OF PHASES IN ASSEMBLAGE IL+USP+LQ AT $\log fO_2$=−6.6 (Cont.)

Wt%	IL	USP	LQ	Pt-Fe
MgO	3.03(0.05)	3.61(0.04)	4.18(0.26)	Wt_{Fe}%:
SiO_2	0.03(0.01)	0.14(0.01)	21.53(1.70)	8.25(0.05)
TiO_2	43.67(0.15)	24.96(0.11)	24.34(1.55)	Wt_{Pt}%:
FeO	33.90(0.17)	48.94(0.20)	50.02(0.54)	91.76(0.33)
Fe_2O_3	19.55(0.22)	22.55(0.15)	------	
SUM	100.18	100.20	100.06	100.14
CAT/OXY	2/3	3/4	--	Mole Fract.
Mg	0.1123	0.1966	------	X_{Fe}:
Si	0.0007	0.0052	------	0.2389
Ti	0.8164	0.6851	------	X_{Pt}:
Fe^{2+}	0.7048	1.4937	------	0.7611
Fe^{3+}	0.3657	0.6194	------	
SUM	1.9999	3.0000	------	1.0000
#	4	4	4	6

is the number of analyses. IL=Ilmenite. USP=Ulvospinel. LQ=Glass. Standard deviation in paretheses. Ferric iron calculated from assumed stoichiometry.

TABLE A2.6 ELECTRON MICROPROBE ANALYSES OF PHASES IN ASSEMBLAGE IL+USP+LQ AT $\log fO_2$=-6.6 (Cont.)

Wt%	IL	USP	LQ	Pt0-Fe
MgO	4.65(0.03)	5.67(0.05)	6.27(0.07)	Wt_{Fe}%:
SiO_2	0.03(0.01)	0.16(0.01)	19.28(0.28)	8.04(0.04)
TiO_2	44.69(0.42)	26.34(0.17)	26.16(1.01)	Wt_{Pt}%:
FeO	31.93(0.39)	46.94(0.19)	46.45(0.83)	91.65(0.52)
Fe_2O_3	18.86(0.54)	20.66(0.33)	------	
SUM	100.16	99.77	98.36	99.69
CAT/OXY	2/3	3/4	--	Mole Fract.
Mg	0.1702	0.3046	------	X_{Fe}:
Si	0.0007	0.0055	------	0.2346
Ti	0.8251	0.7142	------	X_{Pt}:
Fe^{2+}	0.6556	1.4152	------	0.7654
Fe^{3+}	0.3484	0.5605	------	
SUM	2.0000	3.0000	------	1.0000
#	4	3	4	7

is the number of analyses. IL=Ilmenite USP=Ulvospinel. LQ=Glass. Standard deviation in paretheses. Ferric iron calculated from assumed stoichiometry.

TABLE A2.6 ELECTRON MICROPROBE ANALYSES OF PHASES IN ASSEMBLAGE IL+USP+LQ AT $\log fO_2$=-6.6 (Cont.)

Wt%	IL	USP	LQ	Pt-Fe
MgO	6.32(0.09)	7.33(0.03)	8.01(0.30)	Wt_{Fe}%:
SiO_2	0.01(0.01)	0.15(0.00)	20.46(1.72)	7.96(0.08)
TiO_2	46.36(0.15)	27.20(0.08)	26.22(1.86)	Wt_{Pt}%:
FeO	30.43(0.19)	45.19(0.13)	44.77(0.11)	91.62(0.23)
Fe_2O_3	17.43(0.34)	19.99(0.16)	------	
SUM	100.55	99.86	99.36	99.59
CAT/OXY	2/3	3/4	--	Mole Fract.
Mg	0.2274	0.3887	------	X_{Fe}:
Si	0.0002	0.0051	------	0.2328
Ti	0.8415	0.7274	------	X_{Pt}:
Fe^{2+}	0.6143	1.3440	------	0.7672
Fe^{3+}	0.3166	0.5349	------	
SUM	2.0000	3.0001	------	1.0000
#	6	3	3	8

is the number of analyses. IL=Ilmenite. USP=Ulvospinel. LQ=Glass. Standard deviation in paretheses. Ferric iron calculated from assumed stoichiometry.

TABLE A2.7 ELECTRON MICROPROBE ANALYSES OF PHASES IN ASSEMBLAGE IL+USP+OL+LQ AT $\log fO_2$=−6.6

Wt%	IL	USP	OL	LQ	Pt-Fe
MgO	8.50(0.07)	8.84(0.01)	39.65(0.23)	7.95(0.51)	Wt_{Fe}%:
SiO_2	0.02(0.01)	0.14(0.01)	38.14(0.11)	22.77(0.89)	7.93(0.04)
TiO_2	49.90(0.21)	27.69(0.07)	0.43(0.01)	27.13(0.64)	Wt_{Pt}%:
FeO	29.70(0.21)	43.28(0.11)	21.62(0.05)	38.04(0.28)	92.21(0.21)
Fe_2O_3	12.90(0.29)	19.92(0.11)	------	------	
CaO	0.04(0.01)	0.04(0.01)	0.17(0.00)	4.19(0.30)	
SUM	101.06	99.91	100.01	100.08	100.14
CAT/OX	2/3	3/4	3/4	--	Mole Fract.
Mg	0.2988	0.4631	1.5410	------	X_{Fe}:
Si	0.0005	0.0047	0.9828	------	0.2311
Ti	0.8850	0.7319	0.0085	------	X_{Pt}:
Fe^{2+}	0.5858	1.2721	0.4715	------	0.9689
Fe^{3+}	0.2289	0.5268	------	------	
Ca	0.0010	0.0015	0.0048	------	
SUM	2.0000	3.0001	3.0086	------	1.0000
#	4	4	3	4	4

is the number of analyses. IL=Ilmenite. OL=Olivine. USP=Ulvospinel. LQ=Glass. Standard deviation in paretheses. Ferric iron calculated from assumed stoichiometry.

TABLE A2.7 ELECTRON MICROPROBE ANALYSES OF PHASES IN ASSEMBLAGE IL+USP+OL+LQ AT $\log fO_2$=-6.6(Cont.)

Wt%	IL	USP	OL	LQ	Pt-Fe
MgO	10.42(0.02)	10.63(0.05)	41.81(0.22)	9.41(0.09)	Wt_{Fe}%:
SiO_2	0.02(0.01)	0.13(0.01)	39.12(0.09)	20.19(0.21)	7.70(0.07)
TiO_2	50.96(0.09)	28.06(0.12)	0.32(0.06)	28.59(0.15)	Wt_{Pt}%:
FeO	27.21(0.40)	40.80(0.27)	18.01(0.03)	34.33(0.24)	92.07(0.09)
Fe_2O_3	12.24(0.16)	20.10(0.21)	------	------	
CaO	0.05(0.01)	0.06(0.01)	0.29(0.01)	6.91(0.05)	
SUM	100.90	99.78	99.55	99.98	99.77
CAT/OX	2/3	3/4	3/4	--	Mole Fract.
Mg	0.3616	0.5503	1.6034	------	X_{Fe}:
Si	0.0005	0.0044	0.9944	------	0.2261
Ti	0.8923	0.7329	0.0062	------	X_{Pt}:
Fe^{2+}	0.5299	1.1849	0.3875	------	0.7739
Fe^{3+}	0.2145	0.5254	------	------	
Ca	0.0013	0.0022	0.0079	------	
SUM	2.0001	3.0001	3.0014	------	1.0000
#	4	4	5	4	4

is the number of analyses. IL=Ilmenite. OL=Olivine. USP=Ulvospinel. LQ=Glass. Standard deviation in paretheses. Ferric iron calculated from assumed stoichiometry.

TABLE A2.7 ELECTRON MICROPROBE ANALYSES OF PHASES IN ASSEMBLAGE IL+USP+OL+LQ AT $\log fO_2$=-6.6 (Cont.)

Wt%	IL	USP	OL	LQ	Pt-Fe
MgO	12.62(0.07)	12.69(0.20)	43.99(0.24)	7.93(0.40)	Wt_{Fe}%:
SiO_2	0.02(0.01)	0.11(0.01)	39.35(0.30)	20.19(0.71)	7.62(0.05)
TiO_2	52.65(0.13)	29.06(0.04)	0.37(0.06)	31.30(0.83)	Wt_{Pt}%:
FeO	24.75(0.13)	38.69(0.25)	15.29(0.09)	30.47(0.51)	92.02(0.17)
Fe_2O_3	10.91(0.08)	19.81(0.13)	------	------	
CaO	0.10(0.01)	0.10(0.01)	0.44(0.02)	10.28(0.43)	
SUM	101.05	100.46	99.44	100.17	99.64
CAT/OX	2/3	3/4	3/4	--	Mole Fract.
Mg	0.4303	0.6432	1.6690	------	X_{Fe}:
Si	0.0005	0.0035	0.9897	------	0.2243
Ti	0.9056	0.7430	0.0072	------	X_{Pt}:
Fe^{2+}	0.4734	1.1000	0.3254	------	0.7757
Fe^{3+}	0.1878	0.5068	------	------	
Ca	0.0025	0.0035	0.0119	------	
SUM	2.0001	3.0000	3.0032	------	1.0000
#	5	3	4	3	4

is the number of analyses. IL=Ilmenite. OL=Olivine. USP=Ulvospinel. LQ=Glass. Standard deviation in paretheses. Ferric iron calculated from assumed stoichiometry.

TABLE A2.7 ELECTRON MICROBROBE ANALYSES OF PHASES IN ASSEMBLAGE IL+USP+OL+LQ AT $logfo_2$=−6.6(Cont.)

Wt%	IL	USP	OL	LQ	Pt-Fe
MgO	14.99(0.13)	15.56(0.17)	46.63(0.24)	8.28(0.83)	Wt_{Fe}%:
SiO_2	0.02(0.01)	0.08(0.01)	39.71(0.31)	19.24(0.33)	7.52(0.05)
TiO_2	54.85(0.17)	30.27(0.07)	0.36(0.01)	33.80(0.40)	Wt_{Pt}%:
FeO	22.40(0.32)	35.35(0.21)	12.30(0.09)	25.57(1.16)	92.12(0.29)
Fe_2O_3	8.67(0.42)	19.18(0.30)	------	------	
CaO	0.17(0.01)	0.15(0.01)	0.62(0.01)	13.37(1.05)	
SUM	101.10	100.59	99.62	100.25	99.64
CAT/OX	2/3	3/4	3/4	--	Mole Fract.
Mg	0.5018	0.7714	1.7431	------	X_{Fe}:
Si	0.0004	0.0029	0.9843	------	0.2218
Ti	0.9264	0.7571	0.0068	------	X_{Pt}:
Fe^{2+}	0.4207	0.9832	0.2580	------	0.7782
Fe^{3+}	0.1465	0.4800	------	------	
Ca	0.0041	0.0054	0.0168	------	
SUM	1.9999	3.0000	3.0090	------	1.0000
#	4	4	4	3	4

is the number of analyses. IL=Ilmenite. OL=Olivine. USP=Ulvospinel. LQ=Glass. Standard deviation in paretheses. Ferric iron calculated from assumed stoichiometry.

TABLE A2.7 ELECTRON MICROPROBE ANALYSES OF PHASES IN ASSEMBLAGE IL+USP+OL+LQ AT $\log fO_2$=−6.6(Cont.)

Wt%	IL	USP	OL	LQ	Pt-Fe
MgO	16.91(0.07)	17.53(0.11)	47.83(0.33)	7.40(0.69)	Wt_{Fe}%:
SiO_2	0.01(0.01)	0.10(0.01)	40.62(0.23)	18.06(0.87)	7.33(0.04)
TiO_2	55.71(0.23)	31.05(0.10)	0.40(0.02)	35.81(1.12)	Wt_{Pt}%:
FeO	19.70(0.14)	32.98(0.03)	10.77(0.07)	23.47(1.23)	92.22(0.10)
Fe_2O_3	8.81(0.15)	18.69(0.14)	------	------	
CaO	0.22(0.06)	0.20(0.03)	0.69(0.02)	14.65(1.02)	
SUM	101.36	100.55	100.31	99.38	99.54
CAT/OX	2/3	3/4	3/4	--	Mole Fract.
Mg	0.5574	0.8574	1.7613	------	X_{Fe}:
Si	0.0002	0.0031	0.9915	------	0.2173
Ti	0.9264	0.7661	0.0074	------	X_{Pt}:
Fe^{2+}	0.3643	0.9049	0.2224	------	0.7827
Fe^{3+}	0.1466	0.4616	------	------	
Ca	0.0052	0.0069	0.0183	------	
SUM	2.0001	3.0000	3.0009	------	1.0000
#	4	3	4	3	4

is the number of analyses. IL=Ilmenite. OL=Olivine. USP=Ulvospinel. LQ=Glass. Standard deviation in paretheses. Ferric iron calculated from assumed stoichiometry.

TABLE A2.7 ELECTRON MICROPROBE ANALYSES OF PHASES IN ASSEMBLAGE IL+USP+OL+LQ AT $\log fO_2$=-6.6(Cont.)

Wt%	IL	USP	OL	LQ	Pt-Fe
MgO	18.26(0.14)	19.47(0.07)	48.75(0.05)	8.78(0.58)	Wt_{Fe}%:
SiO_2	0.02(0.01)	0.08(0.01)	40.46(0.12)	18.44(1.03)	7.32(0.06)
TiO_2	57.20(0.08)	32.22(0.11)	0.36(0.01)	35.58(1.12)	Wt_{Pt}%:
FeO	18.60(0.19)	31.13(0.06)	9.24(0.08)	20.45(1.17)	92.29(0.13)
Fe_2O_3	6.84(0.24)	17.67(0.20)	------	------	
CaO	0.25(0.02)	0.20(0.02)	0.86(0.01)	16.80(0.55)	
SUM	101.17	100.77	99.67	100.10	99.71
CAT/OX	2/3	3/4	3/4	--	Mole Fract.
Mg	0.5967	0.9375	1.7963	------	X_{Fe}:
Si	0.0004	0.0026	0.9884	------	0.2172
Ti	0.9431	0.7827	0.0066	------	X_{Pt}:
Fe^{2+}	0.3411	0.8409	0.1910	------	0.7828
Fe^{3+}	0.1129	0.4296	------	------	
Ca	0.0059	0.0069	0.0227	------	
SUM	2.0001	3.0002	3.0005	------	1.0000
#	4	3	2	3	4

is the number of analyses. IL=Ilmenite. OL=Olivine. USP=Ulvospinel. LQ=Glass. Standard deviation in paretheses. Ferric iron calculated from assumed stoichiometry.

III. SUMMARY OF EXPERIMENTS

TABLE A3.1 SUMMARY OF EXPERIMENTS CONDUCTED

(ALL AT 1300°C, 1atm)

EXP.	$logfO_2$	STARTING COMPOSITIONS MgO	SiO_2	TiO_2	Fe_2O_3	CaO	PRODUCTS
101	-10.0	12.0	13.4	29.5	45.1	----	IL+USP+OL+LQ
102	-10.0	16.9	11.4	38.4	21.4	11.9	IL+USP+OL+PEROV+LQ
901	-9.0	0.0	3.3	37.7	59.0	----	IL+USP+LQ
902	-9.0	2.5	4.8	38.8	54.0	----	IL+USP+LQ
903	-9.0	5.2	5.9	37.5	51.4	----	IL+USP+LQ
904	-9.0	12.0	13.4	29.5	45.1	----	IL+USP+OL+LQ
905	-9.0	15.1	14.9	38.6	31.4	----	IL+PSB+OL+LQ
906	-9.0	21.8	30.3	24.9	22.9	----	OL+PX+PSB+LQ
907	-9.0	12.7	46.5	24.8	16.0	----	TR+PX+PSB+LQ
908	-9.0	16.8	11.2	37.7	22.7	11.6	IL+USP+OL+PEROV+LQ
801	-8.0	0.0	3.3	37.7	59.0	----	IL+USP+LQ
802	-8.0	1.2	4.0	36.8	58.0	----	IL+USP+LQ
803	-8.0	2.4	5.3	35.6	56.7	----	IL+USP+LQ
804	-8.0	3.7	5.2	36.7	54.4	----	IL+USP+LQ
805	-8.0	04.9	5.7	36.2	53.3	----	IL+USP+LQ
806	-8.0	12.0	13.4	29.5	45.1	----	IL+USP+OL+LQ
807	-8.0	15.7	14.3	27.4	41.4	01.2	IL+USP+OL+LQ
808	-8.0	16.9	14.8	27.0	38.4	02.6	IL+USP+OL+LQ
809	-8.0	19.9	14.2	30.2	32.8	02.9	IL+USP+OL+LQ
810	-8.0	20.1	14.6	30.4	30.6	04.4	IL+USP+OL+LQ
811	-8.0	22.4	14.0	31.3	28.2	04.2	IL+USP+OL+LQ
812	-8.0	16.8	11.2	37.7	22.7	11.6	IL+USP+OL+PEROV+LQ
701	-7.0	0.0	4.5	31.8	63.7	----	IL+USP+LQ
702	-7.0	1.3	5.0	32.4	61.3	----	IL+USP+LQ
703	-7.0	2.5	4.6	33.5	59.4	----	IL+USP+LQ
704	-7.0	3.7	5.2	36.7	54.4	----	IL+USP+LQ
705	-7.0	7.1	7.1	33.6	52.2	----	IL+USP+LQ
706	-7.0	13.7	14.0	26.0	46.3	----	IL+USP+OL+LQ
707	-7.0	15.8	14.2	27.4	41.4	1.2	IL+USP+OL+LQ
708	-7.0	16.9	14.8	27.0	38.4	2.6	IL+USP+OL+LQ
709	-7.0	19.9	14.2	30.2	32.8	2.9	IL+USP+OL+LQ
710	-7.0	20.1	14.6	30.4	30.6	4.4	IL+USP+OL+LQ
711	-7.0	22.4	14.0	31.3	28.2	4.2	IL+USP+OL+LQ
712	-7.0	17.9	11.5	36.4	22.6	11.6	IL+USP+OL+PEROV+LQ
601	-6.6	0.0	4.9	30.0	65.1	----	IL+USP+LQ
602	-6.6	2.3	6.1	29.6	61.9	----	IL+USP+LQ
603	-6.6	3.4	6.9	29.5	60.2	----	IL+USP+LQ
604	-6.6	5.3	6.2	31.1	57.3	----	IL+USP+LQ
605	-6.6	6.9	6.6	31.9	54.7	----	IL+USP+LQ
606	-6.6	13.7	14.0	26.0	46.3	----	IL+USP+OL LQ
607	-6.6	15.6	14.7	25.3	43.3	1.1	IL+USP+OL LQ
608	-6.6	17.5	14.4	26.1	40.2	1.8	IL+USP+OL LQ
609	-6.6	18.7	14.4	27.4	36.8	2.6	IL+USP+OL LQ
610	-6.6	20.7	14.3	28.9	32.5	3.5	IL+USP+OL LQ
611	-6.6	21.8	14.3	29.9	30.2	3.8	IL+USP+OL LQ
612	-6.6	23.2	14.4	30.5	27.5	4.4	IL+USP+OL LQ

613	-6.6	17.9	11.5	36.4	22.6	11.6	IL+USP+OL+PEROV+LQ
613	-6.1	13.1	14.4	22.1	50.4	----	IL+USP+OL+LQ
501	-5.9	13.1	14.4	22.1	50.4	----	IL+USP+OL+PSB+LQ
502	-5.3	13.1	14.4	22.1	50.4	----	IL+USP+OL+PSB+LQ